Characterization of Dephytylation and Dechelation, Two Early Steps of Chlorophyll Breakdown in Leaves and Fruits

Dissertation
zur
Erlangung der Naturwissenschaftlichen Doktorwürde
(Dr. sc. nat.)

vorgelegt der
Mathematisch-naturwissenschaftlichen Fakultät
der
Universität Zürich
von

Luzia Guyer
von
Seegräben ZH

Promotionskomitee
Prof. Dr. Stefan Hörtensteiner (Vorsitz und Leiter)
Prof. Dr. Enrico Martinoia
Prof. Dr. Magdalena Rossi
Prof. Dr. Christoph Ringli

Zürich, 2015

Table of Content

Summary

Chlorophyll is one of the most abundant pigments worldwide. Every year, chlorophyll is not only newly synthesized, but big amounts of chlorophyll are degraded during fruit ripening and in senescing leaves. The pathway of chlorophyll breakdown, the so called PAO/phyllobilin pathway, has been extensively studied over the past decades. Most of the involved genes have been cloned and characterized, except for the activity responsible for magnesium removal of chlorophyll and some of the side chain-modifying enzymes.

Pheophytinase (PPH) is one of the first enzymes involved in chlorophyll degradation, specifically hydrolyzing the ester bond between the porphyrin ring and the phytol moiety of pheophytin, but not of chlorophyll. In this work, the substrate specificity of PPH was further determined. PPH can be characterized as an esterase with tight specificity for the acid moiety, which is the porphyrin ring. The K_M for pheophytin *a* and for two other accepted substrates with similar molecular structure is in the µM range, indicating high substrate affinities. Chlorophyll is a likely inhibitor of the enzymatic activity. To reveal the substrate-binding mechanism of PPH, a crystallization approach was performed. To this end, one focus of this work was to elucidate a good purification system for PPH. However, purification and tag-separation turned out to be difficult for PPH and first potential crystallization conditions were defined with the uncleaved PPH-MBP fusion. In this work I also demonstrate that PPH is not only involved in leaf senescence, but also in chlorophyll degradation during fruit ripening. For a comparison study Tomato was chosen as a model plant. I could show that tomato PPH is an ortholog of *Arabidopsis thaliana* PPH and is responsible for phytol cleavage in senescing tomato leaves. The PAO/phyllobilin pathway is active in ripening fruits and PPH activity was found in chromoplasts. However, the absence of PPH did not impair color break in fruits, indicating that other, so far unknown, hydrolases are active in parallel. A last focus of this work was on the identification of factors responsible for magnesium dechelation from chlorophyll, the first step in the breakdown process. I obtained a first good indication that this is a non-enzymatic process, where changes in the local pH trigger the loss of magnesium. However, additional experiments will be required to corroborate this hypothesis.

Zusammenfassung

Chlorophyll ist eines der häufigsten Pigmente weltweit. Es wird nicht nur jedes Jahr neu aufgebaut, sondern grosse Mengen an Chlorophyll werden während der Fruchtreife und in seneszierenden Blättern abgebaut. Der Abbauweg von Chlorophyll, auch „PAO/phyllobilin Pathway“ genannt, wurde während der letzten Jahrzehnte intensiv untersucht. Die meisten involvierten Gene wurden kloniert und charakterisiert. Unbekannt sind noch der Faktor, der für das Ablösen des Magnesiums von Chlorophyll verantwortlich ist, und einige Enzyme, die Seitenketten modifizieren.

Die Pheophytinase (PPH) ist eines der ersten Enzyme, das im Chlorophyllabbau aktiv ist. PPH hydrolisiert die Esterbindung zwischen dem Porphyrinring und der Phytolseitenkette von Pheophytin, akzeptiert aber Chlorophyll nicht als Substrat. Die Substratspezifität von PPH wurde in dieser Arbeit weiter untersucht. PPH ist eine Esterase mit klarer Spezifität für den Säureteil ihrer Substrate, also für den Porphyrinring. Der K_M für Pheophytin *a* und für zwei weitere akzeptierte Substrate mit ähnlichen molekularen Strukturen liegt im µM-Bereich, das heisst, dass PPH eine hohe Substrataffinität hat. Chlorophyll hingegen ist ein potentieller Inhibitor der PPH. Um den Substratbindemechanismus der PPH zu verstehen, wurde versucht die PPH zu kristallisieren. Dazu war ein wichtiger Fokus dieser Arbeit, ein System zu entwickeln, um PPH aufzureinigen. Die Proteinaufreinigung von „getagter“ PPH und die Abtrennung der „Tags“ waren jedoch schwierig. Schliesslich konnten erste günstige Kristallisationsbedingungen für das PPH-MBP Fusionsprotein definiert werden. In dieser Arbeit konnte ich auch zeigen, dass die PPH nicht nur in die Blattseneszenz involviert ist, sondern auch in den Chlorophyllabbau während der Fruchtreife. Tomate wurde als Modellpflanze für eine Vergleichsstudie gewählt. Ich konnte zeigen, dass die PPH der Tomate ein Ortholog der *Arabidopsis thaliana* PPH ist. Das Tomatenenzym ist verantwortlich für die Abspaltung des Phytols während der Seneszenz von Tomatenblättern. Der „PAO/phyllobilin Pathway“ ist während der Fruchtreife aktiv und ich konnte PPH-Aktivität auch in den Chromoplasten nachweisen. Ein Fehlen der PPH verhinderte den Farbwechsel von reifenden Tomaten jedoch nicht. Dies weist darauf hin, dass noch andere, bis jetzt unbekannte Hydrolasen aktiv sein müssen. Ein letzter Fokus dieser Arbeit war die Identifizierung des Mechanismus, der zum Verlust des Magnesiums im Chlorophyll führt. Dieser Prozess ist der erste Schritt im Chlorophyllabbau. Meine Arbeit ergab erste gute Hinweise dafür, dass dies kein enzymatischer Prozess ist, sondern dass lokale pH-Veränderungen in den Chloroplasten zum Magnesiumverlust führen. Weitere Experimente sind jedoch notwendig, um diese Hypothese zu bestätigen.

1. Introduction

Chlorophyll breakdown is one of the most obvious processes during the life cycle of a plant, and every autumn it can be observed in the beautiful coloring of senescing leaves. In numbers, every year around 10^9 tonnes of chlorophyll are degraded on land and in water (Hendry et al., 1987). This number indicates how important chlorophyll breakdown is. Therefore it is surprising that the elucidation of the chlorophyll degradation pathway has only rather recently started. In leaves, chlorophyll is broken down during senescence in order to enable the retrieval and reallocation of nutrients by preventing phototoxicity of free chlorophyll (Hörtensteiner and Feller, 2002; Matile et al., 1996). The disappearance of chlorophyll unmasks other colored pigments (carotenoids and anthocyans) which cause the impressive coloring of autumnal leaves (Christ and Hörtensteiner, 2014). However, chlorophyll is not only broken down in leaves, but also in other organs such and fruits. In fleshy fruits, e.g. tomato, chlorophyll needs to be degraded in order to enable the visibility of other pigments, mainly carotenoids (Egea et al., 2010), which attract animals for seed dispersal (Goldschmidt, 2001). Still, the question arises why research on chlorophyll breakdown is of interest and high importance.

1.1 Significance of senescence-related research

With the new century the United Nations defined eight goals within the Millennium Development Goals (MDG). One of the targets is to halve the number of people suffering from hunger until 2015 in relation to 1990. Although hunger could be reduced during the past 20 years, more effort is needed in order to reach the MDG target (United Nations, 2014).

One possibility to increase crop yield is by delaying senescence, while the photosynthetic activity is maintained (Kusaba et al., 2013). Thomas and Howarth (2000) made a simple calculation, showing what effect the delay of senescence has. They state that by delaying senescence for 2 days, the total contribution of carbon to the plant by a single leaf is increased by 11%. Mutant plants which show a delay in senescence, when compared to controls, are called stay-green plants due to the retention of chlorophyll (Thomas and Howarth, 2000). There are different factors that influence the onset of senescence and could be targeted to generate stay-green plants. (i) NAC and WRKY are important transcription factors in senescence regulation. Alteration of their activities leads to stay-green phenotypes (reviewed in Kusaba et al., 2013). (ii) A stay-green phenotype is also achieved by altering the signal transduction pathways of different phytohormones (e.g. ethylene, abscisic acid, cytokinin) (reviewed in Kusaba et al., 2013). (iii) Finally, impairment of genes involved in chlorophyll breakdown also leads to stay-green phenotypes (Kusaba et al., 2013). Stay-green plants can be classified into five groups according to Thomas and Howarth (2000). In wild-type plants chlorophyll is degraded with the onset of senescence. In parallel the photosynthetic activity is decreased. (i) In plants that are classified as type A stay-greens the initiation of senescence is delayed. However, once started, the speed of chlorophyll degradation is comparable to wild type. The same is true for the photosynthetic activity and as a consequence, carbon assimilation might be enhanced in type A plants due to an extended productive period. (ii) Type B stay-greens are plants where the timing of senescence initiation is normal, but the rate of chlorophyll breakdown and of the decrease of photosynthesis is slower than in wild type. Comparable to type A plants, more carbon might get assimilated. (iii) Type C mutants are also called cosmetic stay-greens. In these plants the onset of senescence and also the decrease of the photosynthetic activity are normal. By contrast, chlorophyll is retained or not completely degraded, leading to the cosmetic stay-green phenotype. (iv) Type D stay-greenness is rather artificial and is caused by abrupt cell death (e.g freezing, drying). Photosynthetic activity is immediately stopped, but chlorophyll content remains stable. (v) Finally, type E stay-greens represent plant varieties which do not retain chlorophyll, but have a higher content. In these plants, senescence and decrease of photosynthesis process normal. However, since they contain higher levels of chlorophyll they need more time to degrade it and therefore appear green for a longer time.

Understanding the molecular mechanisms behind stay-green plants is a promising approach towards increasing crop yield (Kusaba et al., 2013). However, the elucidation of the chlorophyll breakdown pathway and the physiological analysis of mutants impaired in involved genes is a prerequisite.

1.2 Pathway of chlorophyll breakdown

The chlorophyll degradation pathway can be divided into two parts (for an overview see Figure 1) (reviewed in Christ and Hörtensteiner, 2014; Hörtensteiner and Kräutler, 2011; Kräutler and Hörtensteiner, 2013). In the first part of the pathway the central magnesium ion of chlorophyll *a* is released. Subsequently, the phytol side chain is hydrolyzed resulting in pheophorbide *a* which is releases from the thylakoid membrane. The porphyrin macrocycle of pheophorbide *a* is oxygenolytic opened and reduced to form *primary* fluorescent chlorophyll catabolites (*p*FCCs). This first part of chlorophyll breakdown is assumed to be conserved among plant species. The second part of the pathway includes different side chain modifications of *p*FCCs and the translocation of the catabolites from the chloroplast to the vacuole for their final storage. In the vacuole FCCs finally get isomerized to form nonfluorescing chlorophyll catabolites (NCCs and DNCCs). The chlorophyll degradation pathway is termed PAO/phyllobilin pathway due to the key enzyme PAO and due to the phyllobilin-type molecular structure of the catabolites (reviewed in Christ and Hörtensteiner, 2014; Hörtensteiner and Kräutler, 2011; Kräutler and Hörtensteiner, 2013).

1.2.1 Part I: Degradation of green pigments to linear tetrapyrroles

Conversion of chlorophyll *b* to chlorophyll *a*

An early step which is a prerequisite for chlorophyll degradation is the conversion of chlorophyll *b* to *a* (Ito et al., 1993). The only difference between the two chlorophylls is the methyl group at the C7 position in chlorophyll *a* which is replaced by a formyl group in chlorophyll *b* (Rüdiger, 2002). Final chlorophyll catabolites were found to have a methyl group at the C7 position, indicating that they are derived from chlorophyll *a* and not *b* (Kräutler and Matile, 1999). To date, in *Arabidopsis thaliana* (Arabidopsis) only one breakdown product was found to have a hydroxymethyl group at the C7 position. This catabolite is speculated to derive from incompletely reduced chlorophyll *b* (Müller et al., 2006). The importance of chlorophyll *b* to *a* conversion before the onset of chlorophyll degradation is determined by the tight substrate specificity of one down-stream enzyme, PAO, for the *a* form (Hörtensteiner et al., 1995).

Non-yellow coloring 1 (*NYC1*) and *NYC1-like* (*NOL*) mutants were first isolated and described in rice by Kusaba et al. (2007). *NYC1* and *NOL* are both up-regulated during senescence and encode for two short-chain dehydrogenases/reductases that catalyze the reduction of chlorophyll *b* to 7-hydroxymethyl chlorophyll *a*; however, *in vitro* activity has only been demonstrated for NOL (Kusaba et al., 2007). It has also been shown that NYC1 and NOL interact *in vitro* and might act as chlorophyll *b* reductase complex (Sato et al., 2009). In Arabidopsis, homologs of *NYC1* and *NOL* have been identified (Horie et al., 2009). Recently, the second enzyme involved in the chlorophyll *b* to *a* conversion has been characterized from Arabidopsis (Meguro et al.,

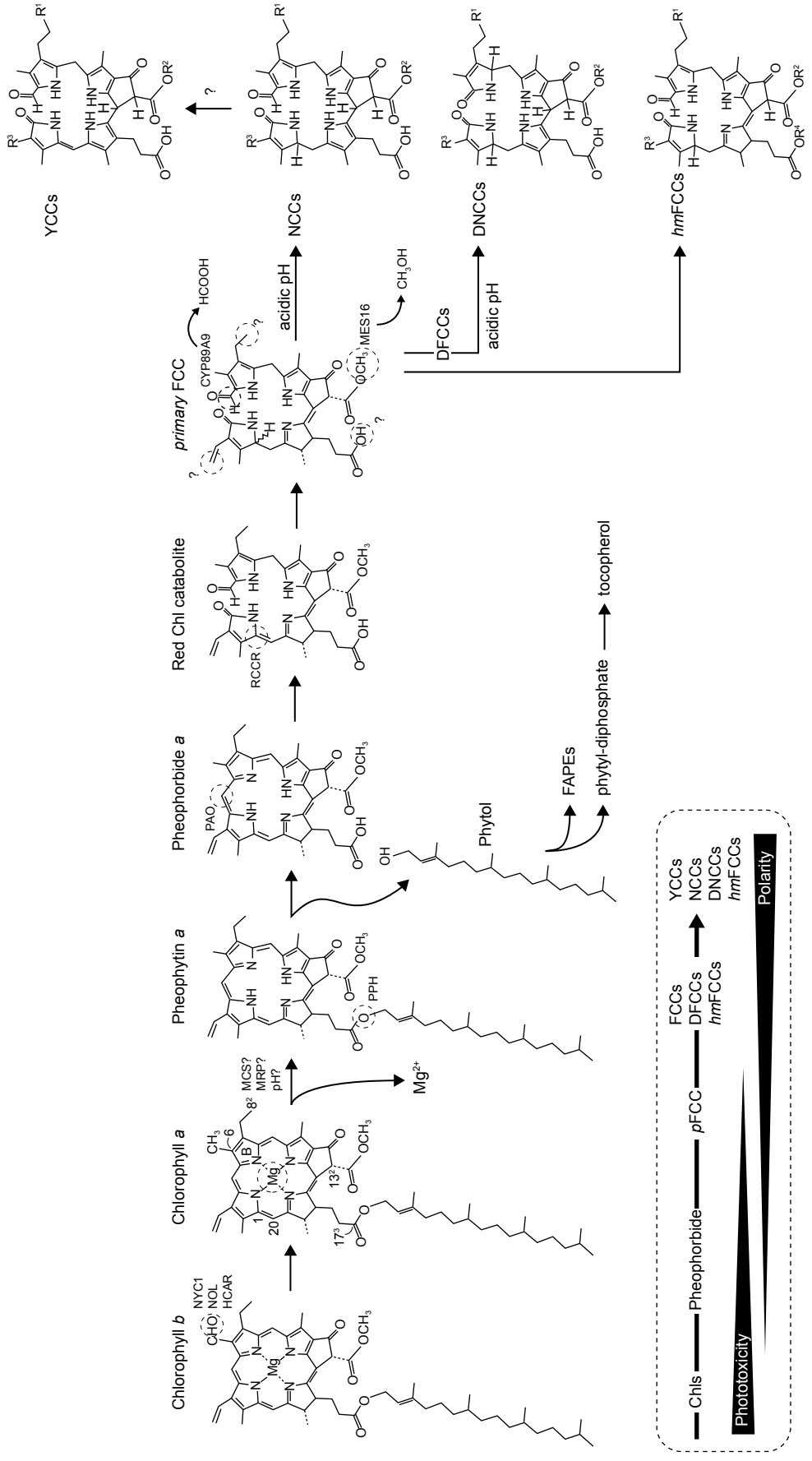

Figure 1. Overview of the PAO/phyllobilin pathway. Indicated are all so far identified activites with their site of action. Unknown enzymes are indicated with a question mark. Abbreviations in the text.
Figure from Christ and Hörtensteiner, 2014

2011). 7-hydroxymethyl chlorophyll *a* reductase (HCAR) catalyzes the second step in which the hydroxymethyl group at C7 is reduced to a methyl group using reduced ferredoxin and resulting in chlorophyll *a* (Meguro et al., 2011).

Demetalation

Demetalation is the first step of chlorophyll *a* degradation (Schelbert et al., 2009). However, for many years demetalation of chlorophyll was considered to be the second step subsequent to chlorophyll dephytylation (Hörtensteiner, 1999). In the past, many approaches have been undertaken in order to identify the mechanism underlying the loss of the central magnesium (Mg) ion. Different Mg-dechelating activities have been isolated from oilseed rape (Vicentini et al., 1995), from *Chenopodium album* (Kunieda et al., 2005; Shioi et al., 1996a; Suzuki and Shioi, 2002), from strawberries (Costa et al., 2002) and from radish cotyledons (Suzuki et al., 2005). However, the molecular identification of the responsible activity could not be achieved. Additionally, assuming that dephytylation precedes dechelation, all these studies used chlorophyllide or artificial chlorophyllin as substrates for activity assays. Recently, pheophytinase has been identified as the dephytylating enzyme involved in chlorophyll breakdown (Schelbert et al., 2009), which demonstrated that dephytylation happens after dechelation. Therefore, chlorophyll *a* should be considered to be the natural substrate of Mg-dechelation resulting in the formation of pheophytin *a* which is then further catabolized. It is also possible that another mechanism is responsible for the loss of Mg. Chlorophyll was shown to react very sensitive on pH changes and slight acidic conditions can trigger the loss of Mg (Hirai et al., 2009; Saga et al., 2013). There are first indications that Mg-dechelation is not an enzymatic reaction, but pH changes might be involved (this work chapter IV). However, the true mechanism responsible for the loss of Mg during senescence still needs to be identified.

Dephytylation

For many years chlorophyllase (CLH) was thought to catalyze the cleavage of phytol of chlorophyll, assumed to be the first step in chlorophyll breakdown (Takamiya et al., 2000). However, Schenk et al. (2007) showed that in Arabidopsis the absence of the two chlorophyllases AtCLH1 and AtCLH2 did not result in a stay-green phenotype during leaf senescence. Additionally, intracellular localization revealed their presence outside the chloroplasts (Schenk et al., 2007), more precisely at the tonoplast and the endoplasmic reticulum (ER) (Hu et al., 2015). Therefore, it can be hypothesized that in Arabidopsis CLH1 and CLH2 are not involved in chlorophyll breakdown during leaf senescence. Nevertheless, the situation might be different in other plant species or organs. In lemon (*Citrus limon*) fruits CLH is located in plastids and is most likely involved in ethylene-induced chlorophyll degradation (Azoulay Shemer et al., 2008).

Schelbert et al. (2009) confirmed that another dephytylating enzyme, distinct from CLH, is involved during chlorophyll breakdown in senescing leaves of Arabidopsis. Pheophytin pheophorbide hydrolase (pheophytinase, PPH) was shown to specifically catalyze the phytol cleavage of pheophytin, but not of chlorophyll (Schelbert et al., 2009). Today, PPH has been identified in different plant species to be the main dephytylating enzyme in senescing leaves (*Arabidopsis thaliana*: Schelbert et al., 2009; Ren et al., 2010, *Oryza sativa*: Morita et al., 2009, *Solanum lycopersicum*: Guyer et al., 2014, see chapter III). However, in fruits of tomato it was shown that PPH is not the sole dephytylating enzyme but other unknown hydrolases are active in parallel (Guyer et al., 2014, see chapter III).

AtPPH is located in the chloroplast and highly expressed in senescing leaves (Schelbert et al., 2009). Its absence results in a type C stay-green phenotype during senescence, with retention of chlorophyll and accumulation of pheophytin *a*. *AtPPH* encodes a α/β-hydrolase with a serine residue in its active centre which catalyses the hydrolytic cleavage of the phytol ester of pheophytin. Esterases are known to show substrate specificity for either the alcohol or the acid moiety of the bond (Fojan et al., 2000). AtPPH was characterized to be highly specific for the molecular structure of the porphyrin ring and enzymatic activity is not observed when the ring structure is modified. Especially the central (presence of the central Mg^{2+}-ion) and lower part of the porphyrin ring structure define the substrate acceptance (this study, chapter II). It is interesting to see if this high substrate specificity is part of the enzymatic regulation of PPH.

Dephytylation of pheophytin *a* results in pheophorbide *a*, which is further degraded (Schelbert et al., 2009), and free phytol which is highly toxic for proteins and membranes (Lippold et al., 2012). Recently the fate of free phytol was thought to be clarified. Phytol can be converted into fatty acid phytyl esters (FAPEs) (Lippold et al., 2012) or it is phosphorylated to phytyl-diphosphate (phytyl-PP). Phytyl-PP serves as a precursor of tocopherol biosynthesis (Ischebeck et al., 2006; Valentin et al., 2006). However, analysis of seeds of Arabidopsis *pph-1* and *pph-1/clh1/clh2* lines revealed that tocopherol content was not different from wild type (Zhang et al., 2014). Hence, it remains unclear if chlorophyll-derived phytol is incorporated into tocopherol in seeds. It is also possible that PPH and CLHs are not involved in dephytylation during seed maturation and that other hydrolases catalyze phytol cleavage (Zhang et al., 2014). These data are in good agreement with results from ripening tomato fruits, where it was shown that PPH is only partially involved in dephytylation (Guyer et al., 2014). Therefore, alternative dephytylating enzymes need to be characterized in reproductive organs. Nevertheless, it also remains to be clarified during leaf senescence if the salvage process for phytol is really conversion to tocopherol.

Oxidative ring opening and reduction to *p*FCC

The last step of the first part of chlorophyll degradation is the conversion of pheophorbide *a* to *primary* fluorescent chlorophyll catabolites (*p*FCCs). Two enzymes are involved in this important step which leads to color-free non-phototoxic intermediates: pheophorbide *a* oxygenase (PAO) which catalyzes the oxidative ring opening, and the subsequent reduction by red chlorophyll catabolite reductase (RCCR) (Hörtensteiner, 2006).

Oxygenolytic opening of the porphyrin macrocycle was characterized as a reaction catalyzed by an iron-containing enzyme (Hörtensteiner et al., 1995). Pružinská et al. (2003) identified PAO to be a Rieske-type iron-sulfur protein that uses reduced ferredoxin as electron donor and pheophorbide *a* and molecular oxygen as substrates. PAO is highly specific for pheophorbide *a*, not accepting pheophorbide *b* (Hörtensteiner et al., 1995). The expression of *PAO* increases during senescence and its absence in respective mutants leads to pheophorbide *a* accumulation resulting in a stay-green phenotype. Strikingly, these mutants also show cell-death phenotype in senescing leaves when exposed to light due to the phototoxicity of the accumulating pheophorbide *a* (Pružinská et al., 2003, 2005). Today, PAO is considered to be the key enzyme in the chlorophyll degradation pathway leading to the defined phyllobilin structure of final catabolites (Hörtensteiner, 2013).

PAO activity leads to the formation of red chlorophyll catabolite (RCC), a linear tetrapyrrole. However, RCC never accumulates but is immediately reduced at the C20/C1 double bond to *p*FCC. This reaction is catalyzed by a soluble enzyme, termed RCCR (Rodoni et al., 1997a). RCCR activity is detectable during all developmental stages of barley plants, but its activity is highest in senescing leaves (Rodoni et al., 1997b). Wüthrich et al. (2000) purified and partially cloned RCCR from barley and characterized mature RCCR as a soluble 31 kDa protein requiring reduced ferredoxin for the reduction of the double bond of RCC. The homologous gene from Arabidopsis was cloned and expressed in a heterologous system in order to confirm RCCR activity (Wüthrich et al., 2000). Arabidopsis RCCR forms homodimers in its native conformation (Sugishima et al., 2009). The a*ccelerated cell death 2* (*acd2*) mutant of Arabidopsis was shown to be deficient in RCCR, thus the *ACD2* locus was confirmed to encode RCCR (Mach et al., 2001). RCCR/ACD2 localizes to the chloroplast; however, with low abundance it is also present in mitochondria of young seedlings. *acd2* mutants show accumulation of RCC and reveal a cell death lesion phenotype which is caused by the accumulation of phototoxic porphyrin molecules (Mach et al., 2001; Pattanayak et al., 2012).

1.2.2 Part II: Modification and transport of *p*FCCs

The second part of the degradation pathway of chlorophyll includes modifications of different side chains of *p*FCCs. The modified fluorescent chlorophyll catabolites (*m*FCCs) are finally transported and stored in the vacuole as nonfluorescent chlorophyll catabolites (NCCs) or as dioxobilin-type nonfluorescent chlorophyll catabolites (DNCCs). Recently two other tetrapyrrole species have been identified: yellow chlorophyll catabolites (YCCs) and *hypermodified* FCCs (*hm*FCCs) (Christ and Hörtensteiner, 2014) (Figure 1). The conversion of *m*FCCs into NCCs and of dioxobilin-type FCCs (DFCCs) into nonfluorescing DNCCs takes place in the acidic environment of the vacuoles by non-enzymatic izomerization (Christ et al., 2013; Oberhuber et al., 2003). To date five different NCCs and one DNCC have been identified in Arabidopsis (Christ and Hörtensteiner, 2014). Except of one NCC (Müller et al., 2006) all final catabolites derive from chlorophyll *a* (Kräutler and Matile, 1999).

While the first part of the degradation pathway, until the oxygenolytic ring opening, is conserved among plant species, the side chain modifications are species-specific (for an overview of identified catabolites see Christ and Hörtensteiner, 2014). However, a first difference among species is already found in the isomeric structures of *p*FCCs which are caused by the stereospecific activity of RCCRs from different plants (Rodoni et al., 1997b).

Hydroxylation

C8^2-hydroxylated *p*FCCs are found in all plant species from which catabolites have been identified so far (Christ and Hörtensteiner, 2014). The mechanism underlying this modification was speculated to result from cytochrome P450 monooxygenase activity. However, this assumption was refuted since the treatment of senescing leaves with carbon monoxide did not prevent hydroxylation (Christ and Hörtensteiner, 2014). Recently, the enzyme responsible for this C8^2-modification was identified in Arabidopsis (M. Hauenstein and S. Hörtensteiner, unpublished results). TIC55 is a Rieske-type iron-sulfur protein, belonging to the same protein family as PAO. Plants deficient in TIC55 do not accumulate NCCs that are hydroxylated at the C8^2-position. The subcellular localization of TIC55 revealed its presence in the envelope of chloroplasts. Therefore, *p*FCC hydroxylation occurs prior to the export to the cytosol and, thus, is the first *p*FCC-modifying activity (M. Hauenstein and S. Hörtensteiner, unpublished results).

Deformylation

Only recently, DNCCs were identified to account for 90% of total chlorophyll catabolites in Arabidopsis (Christ et al., 2013). The cytochrome P450 monooxygenase CYP89A9 was identified to be responsible for the conversion of FCCs into DFCCs which finally isomerize to DNCCs. CYP89A9 does not localize to the chloroplasts, but is present in the cytosol associated with the endoplasmic reticulum (ER). The deformylation activity of CYP89A9 at the C5 position

of FCCs was confirmed with protein expressed in a heterologous system. Deformylation and demethylation by MES16 (see below) take place in the cytosol. However, investigations in plants where MES16 was mistargeted to the chloroplasts, clearly showed that CYP89A9 is not active on demethylated FCCs and therefore precedes MES16 activity in the cytosol. *cyp89a9* mutants did not accumulate DNCCs, but respective increased amounts of NCCs. Nevertheless, an obvious phenotype is not observed in *cyp89a9* mutants. Thus, the biological function of DNCC formation needs to be shown (Christ et al., 2013).

Demethylation

NCCs from Arabidopsis have a demethylated C13^2-carboxymethyl group at the isocyclic ring. METHYL ESTERASE 16 (MES16) was characterized to catalyze this conversion (Christ et al., 2012). MES16 belongs to the family of α/β-hydrolyses and the expression of its gene expression is specifically upregulated in senescing leaves. The localization of MES16 to the cytosol clarified that *p*FCCs are the sole chlorophyll catabolites serving as substrate. Thus, MES16 does not demethylate pheophorbide *a* as originally suggested (Shioi et al., 1996b). Interestingly, *mes16* mutants accumulate significantly more FCCs than NCCs in the vacuole, leading to a high UV-fluorescence of senescing leaves. Christ et al. (2012) could show that the intact C13^2-carboxymethyl group of *mes16*-FCCs has a big impact on the speed of acid-catalyzed isomerization. Therefore non-isomerized FCCs accumulate during senescence. However, *mes16* plants do not show an obvious phenotype during normal growth. Also the senescence-specific fluorescence phenotype is limited to the accumulation of FCCs. The biological function of demethylation remains unclear. One approach to clarify this question may be the investigation of Arabidopsis Landsberg *erecta* (Ler) ecotype, which is a natural *mes16* mutant (Christ et al., 2012).

Glycosylation

Little is known about the glycosylation which follows hydroxylation at the C8^2-position. To date, the responsible protein has not yet been identified. However, there are some indications that a UDP-dependent glycosyltransferase (UGT) might possibly catalyze the glycosylation of hydroxylated FCCs (Christ and Hörtensteiner, 2014). A broad analysis of chlorophyll catabolites of different Arabidopsis ecotypes with liquid chromatography-mass spectrometry (LC-MS), revealed a natural occurring mutant deficient in glycosylation of FCCs (M. Hauenstein and S. Hörtensteiner, unpublished results). These findings might be helpful in identifying the responsible gene.

Other modifications

The recently identified yellow chlorophyll catabolites (YCCs) are oxidized NCCs found in the vacuole. So far, only two YCCs from two plant species have been identified (Christ and Hörtensteiner, 2014). *Hypermodified* FCCs (*hm*FCCs) derive from *m*FCCs by additional modification at the C17 propionic acid chain. *hmFCCs* are not isomerized to respective NCCs, resulting in the persistence of fluorescing end-catabolites. The vacuolar localization of *hm*FCCs needs to be shown (Christ and Hörtensteiner, 2014).

Transport of chlorophyll catabolites

The fact that final chlorophyll catabolites are stored in the vacuole demands for two transport mechanisms: first, hydroxylated *p*FCC needs to be transported across the chloroplast envelope into the cytosol and finally, after undergoing modifications, they are imported across the tonoplast into the vacuole. First evidence for a vacuolar localization of NCCs was already found almost 30 years ago (Matile et al., 1988). However, until today the two underlying transport mechanisms remain unclear. There is strong evidence that an active transporter is involved in the transport across the envelope (Christ and Hörtensteiner, 2014; Hörtensteiner, 2006; Hörtensteiner and Kräutler, 2011). ABC transporters are likely involved; however, an experimental proof is missing. Though, experimental proof might be difficult due to high redundancy. It is also possible that different transport mechanisms are involved (Christ and Hörtensteiner, 2014).

The situation is similar for the transport across the tonoplast. Until today, there is no proof of involved transporters. There is some evidence that two members of the AtABCC transporter family are involved. Expression of AtABCC2 and AtABCC3 in yeast led to the uptake of a oilseed rape NCC (Lu et al., 1998; Tommasini et al., 1998); however, today it is known that the transport across the tonoplast takes place at the level of FCCs. *In vivo* participation of AtABCC2 and AtABCC3 needs to be shown. A task which might be hindered by functional redundancy (Christ and Hörtensteiner, 2014; Hörtensteiner and Kräutler, 2011).

1.3 SGR and the organisation of chlorophyll catabolic enzymes (CCE)

In summary, chlorophyll is broken down in a multistep pathway. Its degradation is initiated while still being embedded in the thylakoid membrane. After Mg dechelation and dephytylation intermediate chlorophyll breakdown products are finally converted to linear tetrapyrroles. Only after the ring opening by PAO and the subsequent reduction photoactivity is lost. Thus, this multistep degradation process needs tight coordination of the different enzymes in order to

prevent accumulation of phototoxic intermediates that may cause production of reactive oxygen species. Therefore, chlorophyll degradation can also be seen as a detoxification process (Matile et al., 1996)

STAY-GREEN (*SGR*) (also termed *nonyellowing 1* [*NYE1*] in Arabidopsis) codes for a protein involved in chlorophyll breakdown (Ren et al., 2007); however, an enzymatic function has not been described. *sgr/nye1* mutants from different species retain big amounts of chlorophyll during senescence, resulting in a non-functional type C stay-green phenotype (Aubry et al., 2008; Park et al., 2007; Ren et al., 2007). Analysis of Arabidopsis *nye1* plants indicated that SGR changes PAO activity (Ren et al., 2007). On the one hand, silencing of *SGR* in *pao* mutants led to less pheophorbide *a* accumulation, thereby preventing plants from cell death (Aubry et al., 2008). On the other hand, overexpression of *SGR* enhanced the rate of chlorophyll degradation (Kusaba et al., 2013). Different studies suggested that SGR has a regulatory function. Interaction of SGR with light-harvesting complex II (LHCII) has been shown for rice SGR (Park et al., 2007). The authors suggest that SGR triggers disassembly of LHCII, thus promoting chlorophyll degradation. A recent study confirmed physical interaction of SGR with different chlorophyll catabolic enzymes (CCEs) at LHCII and it was assumed that CCEs together with SGR form a multiprotein complex to metabolically channel intermediates of chlorophyll degradation (Sakuraba et al., 2012). Therefore, a regulatory and enzyme recruiting function of SGR is very likely.

1.4 Significance of chlorophyll breakdown

1.4.1 Reallocation of nutrients during senescence

Senescence is a well-ordered process which is linked to the remobilization of nutrients (Hörtensteiner and Feller, 2002). However, the fact that chlorophyll catabolites are not degraded beyond the level of linear tetrapyrroles, indicates that the four nitrogen atoms of the chlorophyll molecule are not recycled (Matile et al., 1996). Nevertheless, more than 70% of mesophyll nitrogen is present in chloroplasts. On the one hand, a significant part of nitrogen is present in Rubisco (Hörtensteiner and Feller, 2002) and on the other hand, chlorophyll apoproteins contain around 20% of cellular nitrogen (Hörtensteiner, 2006).

A good indication that chlorophyll degradation is coupled to the degradation of apoproteins is derived from the characterization of stay-green mutants. In these plants, apoproteins (e.g. LHCII) remain complexed and stabilized with chlorophyll and are not targeted by proteases

(Hörtensteiner and Feller, 2002; Matile et al., 1996). The reason for chlorophyll breakdown during nutrient retrieval from apoproteins can rather be defined as a detoxification process (Matile et al., 1996) since chlorophyll and its degradation products above the level of FCCs are photoactive (Christ and Hörtensteiner, 2014). This photoactivity needs to be reduced in coordination with the dismantling of the photosynthetic machinery and membranes (Matile et al., 1996).

1.4.2 Defense mechanism against pathogens

Chlorophyll and its breakdown products above pFCCs absorb light energy. However, if proper acceptors are missing, the absorbed energy might be transmitted to molecular oxygen resulting in the formation of toxic reactive oxygen species (ROS) (Mach et al., 2001). As an example, *pao* and *acd2* mutants accumulate pheophorbide *a* and RCCs, respectively, which are two phototoxic chlorophyll intermediates causing cell death due to the production of ROS (Mach et al., 2001; Pružinská et al., 2005). ROS are critical for plants, but can also be used in pathogen defense. Thus, ROS may trigger the hypersensitive response (HR) or they are directly targeted to defeat pathogens (Kariola et al., 2005).

Different studies have reported an involvement of chlorophyll catabolites in pathogen defense (Kariola et al., 2005; Mach et al., 2001; Mur et al., 2010). Kariola et al. (2005) suggested that AtCLH1 plays a crucial role in activating and regulating the different defense pathways. Recently, it was also shown that chlorophyll catabolites might have an influence in the defense against herbivores (Hu et al., 2015). The results of the study led to the conclusion that upon tissue damage, caused by chewing herbivores, chlorophyllide is produced by AtCLH1. The accumulating chlorophyllide had a toxic effect on *Spodoptera litura* larvae (Hu et al., 2015). Interestingly, chlorophyll catabolites can even have an interspecific defense effect (Vencl et al., 2009). Pheophorbide *a* was found in the fecal shield on the back of *Chelymorpha alternans* larvae, preventing predator attacks (Vencl et al., 2009). A first study on chlorophyll degradation in the gut of Lepidopteran caterpillars was recently published. Thus, Lepidoptera were able to degrade chlorophyll to pheophorbide (Badgaa et al., 2014).

1.4.3 Chlorophyll breakdown during fruit ripening

In contrast to chlorophyll breakdown in leaves, the major reason for chlorophyll degradation in fleshy fruits (e.g. tomato, pepper) is not nutrient remobilization but rather the unmasking of other colored pigments in order to attract animals for seed dispersal (Goldschmidt, 2001). Chlorophyll is degraded during the transition from chloroplasts to chromoplasts in fruits (Barsan

et al., 2012). Nevertheless, not all fleshy fruits degrade chlorophyll during ripening (e.g. kiwi). One question that arises is why fleshy fruits contain chlorophyll during their maturation phase. One hypothesis is that ripe fleshy fruits have high respiratory costs which can only be maintained by photosynthetic activity in fruits. Therefore, it is likely that plants have to find the balance between animal attraction and photosynthesis (Goldschmidt, 2001).

To date, it has not been completely proven whether chlorophyll is degraded via the PAO/phyllobilin pathway (Käutler and Hörtensteiner, 2013) or if the pathway differs in fruits from leaves. However, a broad proteomic study with tomato chromoplasts revealed that PPH, PAO and SGR are present in chromoplasts (Barsan et al., 2010). The tomato *green-flesh* and the pepper *chlorophyll-retainer* mutants are characterized by their brownish color caused by the simultaneous accumulation of chlorophyll and carotenoids in ripe fruits. *SGR*, whose expression is induced during fruit ripening, has been identified to be mutated in these two lines (Barry et al., 2008). These findings indicate the involvement of the PAO/phyllobilin pathway in fruit ripening. In a later study, the expression of different CCEs was confirmed in ripening tomato fruits. However, dephytylation seems to be different in fruits compared to leaves. Although PPH is involved in chlorophyll degradation in fruits, there must be other, so far unknown, hydrolases that are active on chlorophyll or pheophytin (Guyer et al., 2014, see chapter III). Analyzing tomato mutants that show differences in color break might reveal the fruit-specific dephytylating enzyme.

Aim of the Thesis

Pheophytinase (PPH) is one of the first enzymes involved in chlorophyll degradation and it was shown that PPH specifically hydrolyses phytol from pheophytin, while activity on chlorophyll is not observed.

(i) The first focus of this work was to further define biochemical properties of *Arabidopsis thaliana* (Arabidopsis) PPH. One priority was elucidating whether the substrate specificity is defined by the alcohol or the acid moiety of the ester bond. For this, various substrates that show small differences in the molecular structure to pheophytin were tested. K_M values for accepted substrates were calculated and chlorophyll was examined as potential inhibitor of the enzymatic activity. In order to understand the binding mechanism, a protein crystallization approach was undertaken. Potential crystallization conditions were investigated and first crystals were analyzed for diffraction.

(ii) The second focus of this work was a comparison study of dephytylating enzymes involved in leaf senescence and fruit ripening. This work was started by a former group member. Here, it is proven, that PPH is required for chlorophyll breakdown in senescing tomato leaves. A major goal was to enlighten the involvement of PPH in color break of ripening tomato fruits.

(iii) The third focus of this work considers the first step of chlorophyll breakdown, i.e. the loss of magnesium (Mg). The goal was to test Arabidopsis mutants which, according to the literature, were candidates for Mg-dechelatase deficiency. Another hypothesis, i.e. that a non-enzymatic process is responsible for Mg-removal, was also followed. To test this, chloroplastic pH changes were measured during senescence and the effect of plastidic pH changes on chlorophyll degradation was investigated.

(iv) The last focus of this work was to establish a purification method to achieve highly pure AtPPH protein that is suitable for protein crystallization. Different expression vectors and affinity tags were examined.

2. *Biochemical Characterization of Arabidopsis PHEOPHYTINASE*

Arabidopsis Pheophytinase (PPH) was identified as esterase dephytylating pheophytin during chlorophyll breakdown in leaves. It was shown that its activity is specific for pheophytin while chlorophyll is not accepted as substrate. From these findings it can be assumed that the substrate specificity might play an important role in the regulation of chlorophyll breakdown. However, the structural characteristics of PPH, causing this high specificity, need to be demonstrated. In this study I elucidated biochemical properties of recombinant PPH, expressed as ΔPPH-MBP fusion protein. On the one hand, I found that the length of the esterified side chain did not influence enzyme activity. On the other hand, modifications of the porphyrin ring, especially in the central and lower part of the molecular structure, had a strong effect and dephytylation was no longer observed. Therefore it could be concluded that the substrate specificity of PPH is determined by the tetrapyrrole ring structure, which is the acid moiety of the ester bond between the porphyrin ring and phytol. The K_M value for the native substrate pheophytin *a* was found at 10.3 μM and was similar for pheophorbide *a* methyl ester and bacteriopheophytin *a*. Although PPH does not dephytylate chlorophyll *a*, it was able to bind this pigment which led to a competitive inhibition of enzymatic activity. In order to understand the binding mechanism of PPH a protein crystallization approach was undertaken. Details on the attempt of PPH purification are presented in chapter V of this work. I found conditions which led to protein crystal formation of the PPH-MBP fusion protein; however, a refinement screen will be necessary to further improve crystal quality.

2.1 Introduction

Chlorophyll breakdown is one of the very obvious processes in a plant's life cycle. More than 70% of mesophyll nitrogen is present in chloroplasts and yellowing of leaves is an apparent sign of nitrogen mobilization, two processes which correlate (Thomas et al., 2002; Hörtensteiner and Feller, 2002). Therefore, leaf senescence is an important step in plant development. Chlorophyll is broken down via the PAO/phyllobilin pathway (Hörtensteiner and Kräutler, 2011). One of the early steps in the pathway is the dephytylation of pheophytin, which is Mg-free chlorophyll. The hydrolysis of the phytol chain releases the pigment from the thylakoid membrane and thereby increases its polarity and water solubility (Thomas et al., 1989). These characteristics are important for all downstream processes and therefore this step can be considered as one of the key reactions in chlorophyll breakdown. The importance of dephytylation is seen in the stay-green phenotype of plants lacking this hydrolytic activity (Schelbert et al., 2009).

PHEOPHYTINASE (PPH) has been described to be the specific enzyme catalyzing the dephytylation of pheophytin (Schelbert et al., 2009). It was shown that PPH acts specifically on pheophytin *a* and *b*. Although pheophytin differs from chlorophyll only by having lost the central Mg^{2+}-ion, PPH is unable to hydrolyze chlorophylls (Schelbert et al., 2009). The importance of this high enzyme specificity remains to be investigated. Due to the remaining photoactivity of free chlorophyll derivates its rapid degradation is crucial (Takamiya et al., 2000) in order to prevent formation of reactive oxygen species (Kariola et al., 2005). Nevertheless, during chlorophyll breakdown the pigment is released from the thylakoid membrane. Since the porphyrin ring remains unchanged until the oxidation by PAO, the pigment remains photoactive and is able to cause cell death (Pružinská et al., 2003). Recently, Hu et al. (2015) showed that by mistargeting CHLOROPHYLLASE (CLH) to the chloroplast, chlorophyll is unspecifically hydrolyzed and released from the thylakoid membrane which finally led to cell death. This indicates that chlorophyll needs to be broken down in a highly coordinated process. Sakuraba et al. (2012) showed that different chlorophyll catabolic enzymes form together with stay-green (SGR) a multiprotein complex in order to metabolically channel the degradation process. Plants have developed different strategies in order to prevent unspecific enzyme activity. (i) Enzymes are expressed only during specific developmental stages, as for example PPH, which is only expressed during senescence (Schelbert et al., 2009). (ii) Enzymes are locally separated from their substrate, as seen for Arabidopsis CLH (Hu et al., 2015; Schenk et al., 2007). (iii) Enzymes are post-translationally modified, which has been observed for citrus CLH (Azoulay-Shemer et al., 2011) and PAO (Pružinská et al., 2003). (iv) Enzymes can also show high substrate specificity which prevents non-targeted reactions as it has been shown for PAO, which specifically oxidizes pheophorbide *a* but not pheophorbide *b* (Hörtensteiner et al., 1995).

PPH is most likely regulated at different levels. Several studies (Schelbert et al., 2009; Guyer et al., 2014) have shown that PPH is not expressed in green leaves, but highly up-regulated in senescent leaves. However, although PPH is localized in chloroplasts no unspecific

pheophorbide formation has been observed. The described substrate specificity might act as an additional regulatory mechanism. PPH is known to belong to the family of α/β-hydrolases with a serine residue in its active site (Schelbert et al., 2009). α/β hydrolases are a broad and rapidly growing enzyme family including esterases and lipases. They consist of eight parallel β-sheets and contain a conserved catalytic triad in their active site (Schrag and Cygler, 1997). Esterases are further specified to hydrolyze the bond between an acid and an alcohol, with specificity for one of the two moieties (Fojan et al., 2000).

The goal of this study was to characterize Arabidopsis PHEOPHYTINASE (PPH) biochemically. I was interested in determining its substrate specificity by testing different tetrapyrrole derivates with modifications at different positions of the chemical structure. I defined K_M values for the native substrate pheophytin *a* and for pheophorbide *a* methyl ester and bacteriopheophytin *a*, two substrates which were also hydrolyzed by PPH. Although chlorophyll is not accepted as substrate, I was able to identify chlorophyll *a* as a potential competitive inhibitor of PPH. To elucidate the structural features responsible for the high substrate specificity, I identified potential crystallization conditions in order to define the crystal structure of PPH.

2.2 RESULTS

2.2.1 PPH is expressed in pMCSG29 as ΔPPH-MBP fusion protein and is active on pheophytin *a*

The coding sequence of PPH from Arabidopsis, lacking the predicted chloroplast transit peptide (ΔPPH), was cloned into pMCSG29 (Eschenfeldt et al., 2010) in order to express the protein as ΔPPH-MBP (maltose-binding protein) fusion protein in *Escherichia coli* (*E. coli*). The fusion protein was well expressed after overnight induction at 20 °C and ΔPPH-MBP was present in the soluble fraction after cell lysis. The soluble fraction was used for protein activity

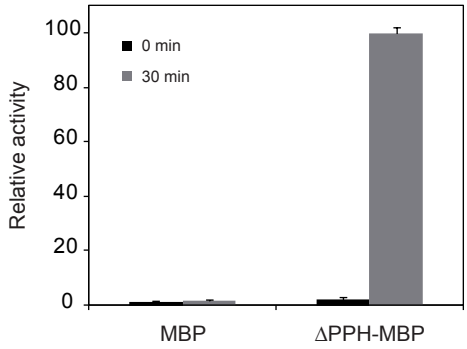

Figure 1. Activity of ΔPPH-MBP fusion protein. Activity measurement of ΔPPH-MBP and MBP. Both proteins were incubated for 30 min at 34 °C in the presence of pheophytin *a*. Only the fusion protein ΔPPH-MBP was able to convert pheophytin *a* to the dephytylated form pheophorbide *a*.

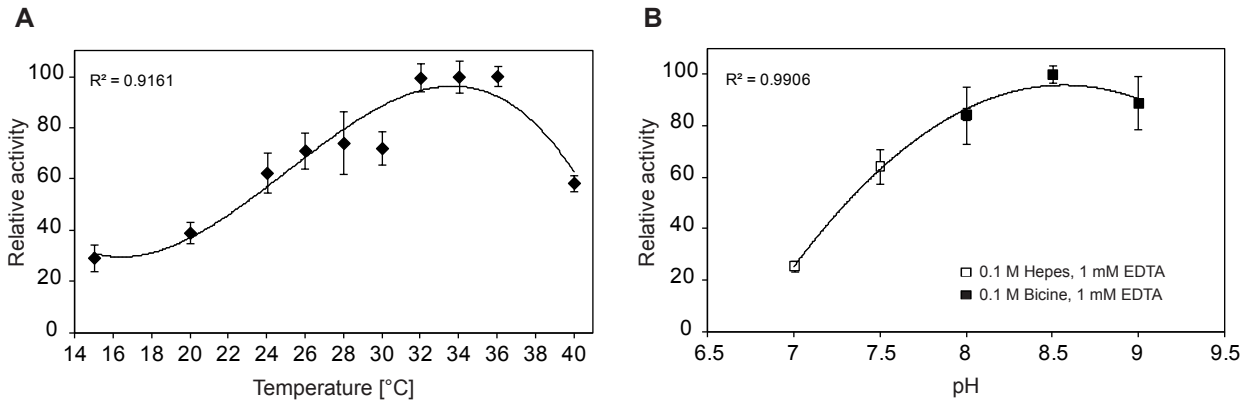

Figure 2. Temperature and pH optimum of ΔPPH-MBP. A, The temperature optimum for ΔPPH-MBP was found at 34 °C. However, ΔPPH-MBP showed more than 80% activity over a broad band of temperatures, ranging from 28 °C to 37 °C. **B,** The pH optimum was found to be at pH 8.5 with a steep drop of activity at conditions with a pH below 8.

assays. ΔPPH-MBP showed high activity on pheophytin *a* and was able to convert the substrate into the dephytylated form pheophorbide *a*, whereas MBP was not able to catalyze the cleavage of the phytol of pheophytin *a* (Figure 1).

2.2.2 pH and temperature optima of ΔPPH-MBP

pH and temperature optima were determined for ΔPPH-MBP. ΔPPH-MBP showed more than 80% activity over a broad range of temperatures, ranging from 28 °C to 37 °C. The temperature optimum was determined to be 34 °C (Figure 2A). The same temperature optimum for PPH was already defined in an earlier study by Schelbert (2010).

In the study of Schelbert (2010) the pH optimum was found to be pH 8. Though, here I found the pH optimum for ΔPPH-MBP at pH 8.5 (Figure 2B), therefore slightly higher than shown for a purified MBP-tag-free PPH. Nevertheless, comparable to the earlier observation (Schelbert, 2010), the activity of ΔPPH-MBP dropped quite fast below a pH of 8. At pH 7 only 20% of the maximum activity remained.

2.2.3 ΔPPH-MBP is specifically active on pheophytin, but chlorophyll *a* is a putative inhibitor

It was shown before that PPH is an enzyme with high substrate specificity for pheophytin (Schelbert et al., 2009). This could be confirmed in this study for PPH expressed as ΔPPH-MBP fusion protein (Figure 3A and B). Pheophytin *a* or chlorophyll *a*, respectively, were incubated at 34 °C for 60 min and assay products were analyzed by HPLC. Pheophytin *a* was converted to pheophorbide *a* (Figure 3A), while chlorophyll *a* was not accepted as substrate (Figure 3B).

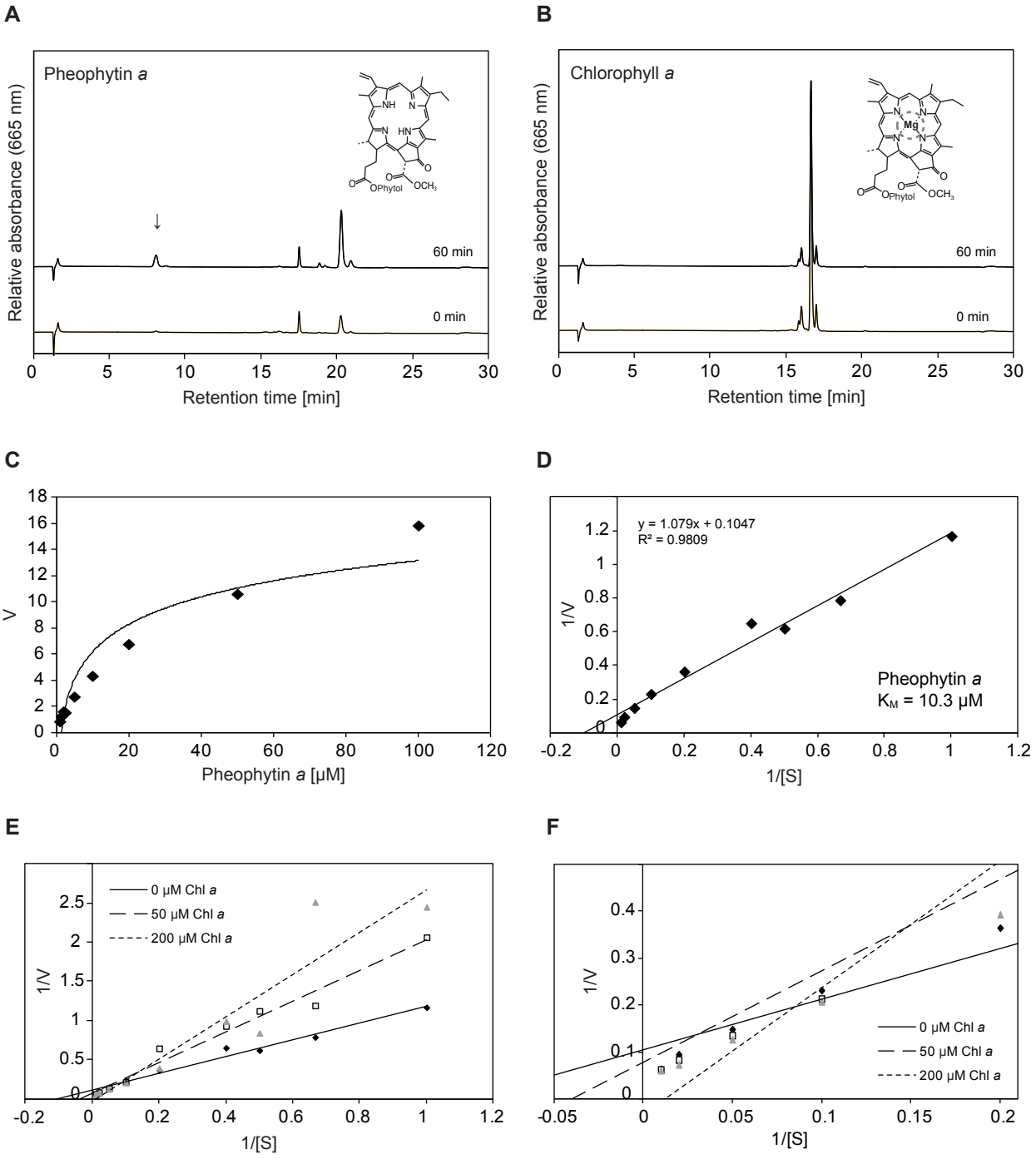

Figure 3. Kinetic properties of ΔPPH-MBP. A and B, HPLC analysis of activity assays of ΔPPH-MBP with pheophytin *a* and chlorophyll *a*, respectively. Arrow indicates dephytylated pheophytin *a* that is pheophorbide *a*. Note that only pheophytin *a* is dephytylated but not chlorophyll *a*. The difference in the structure of chlorophyll *a* from pheophytin *a* is indicated with a grey circle. **C,** Dependence of the enzymatic reaction velocity on substrate concentration. **D,** Determination of K_M value for pheophytin *a* in a Lineweaver-Burk plot. The K_M was found to be 10.3 µM. **E,** Lineweaver-Burk plot of the reaction velocity of ΔPPH-MBP with pheophytin *a* as substrate and chlorophyll *a* as potential inhibitor. Note that the slope of the regression curve increases with higher chlorophyll *a* concentration with remaining xy-intercept, indicating that chlorophyll *a* is a competitive inhibitor of ΔPPH-MBP. **F,** Close-up of the xy-intercept of the Lineweaver-Burk plot in panel E.

The enzyme kinetic of ΔPPH-MBP followed the Michaelis-Menten model (Figure 3C) and by plotting the enzyme velocity and substrate concentration in a double reciprocal plot, according to Lineweaver and Burk (Lineweaver and Burk, 1934), the K_M was calculated to be 10.3 µM (Figure 3D). This value is in good agreement with the K_M value calculated by Schelbert (2010). As can be seen in the structures of pheophytin *a* and chlorophyll *a* (Figure 3A and B), the only difference between the two pigments is the central Mg^{2+}-ion. In order to investigate whether chlorophyll *a* is able to bind to the enzyme and might act as an inhibitor, an inhibition study was performed. ΔPPH-MBP was incubated for 30 min with different concentrations of pheophytin *a* together with either 50 µM or 200 µM chlorophyll *a*. Formed pheophorbide *a* was analyzed by HPLC and plotted against substrate concentration in a double reciprocal plot according to Lineweaver and Burk (Lineweaver and Burk, 1934). It could be observed, that the slopes of the resulting regression curves increased with higher chlorophyll *a* concentrations (Figure 3E and F). However, the xy-axes intercept remained rather stable and therefore it can be assumed that chlorophyll *a* is a potential competitive inhibitor of ΔPPH-MBP.

2.2.4 Substrate specificity of ΔPPH-MBP is determined by the structure of the porphyrin ring

It is well known that esterases show a substrate specificity, which is defined either by the alcohol or the acid moiety of the ester bond (Fojan et al., 2000). Since PPH does not accept chlorophyll as substrate, it can be assumed that the porphyrin ring, which is the acid moiety, is responsible for the substrate specificity of PPH. In order to further identify the structural characteristics which determine the acceptance of a certain substrate by ΔPPH-MBP, different porphyrins were tested by performing activity assays. For this, ΔPPH-MBP was incubated with 200 µM of the substrates for 60 min and the resulting pigment compositions were analyzed by HPLC (Figure 4). I found that modifications of the length of the esterified alcohol did not hinder the hydrolytic activity of ΔPPH-MBP. Thus, replacing the phytol chain by a methyl group (pheophorbide *a* methyl ester) resulted in accumulation of pheophorbide *a* after 60 min (Figure 4A). However, with Zn^{2+}-ion as central metal atom (Zn(II) pheophorbide *a* methyl ester), enzymatic activity was completely absent (Figure 4B). I was also interested if ΔPPH-MBP was able to dephytylate bacteriochlorophyll *a* or bacteriopheophytin *a*. The two substrates differ from

Figure 4. Substrate specificity of ΔPPH-MBP. The activity of ΔPPH-MBP on different substrates was tested by incubating the protein with the substrates for 60 min. Resulting products were analyzed by HPLC. Differences between the substrates and pheophytin *a* are indicated with grey circles. **A,** With pheophorbide *a* methyl ester, conversion to pheophorbide *a* was observed. Here, the phytol chain of pheophytin *a* is replaced by a methyl group. **B,** With Zn(II) pheophorbide *a* methyl ester, no activity was observed. The phytol chain of pheophytin *a* is replaced by a methyl group, the porphyrin ring contains a central Zn^{2+}-ion. **C,** With bacteriochlorophyll *a*, no activity was observed. The porphyrin ring contains a central Mg^{2+}-ion, additionally bacteriochlorophyll *a* has a reduced double bond in the pyrrole ring B

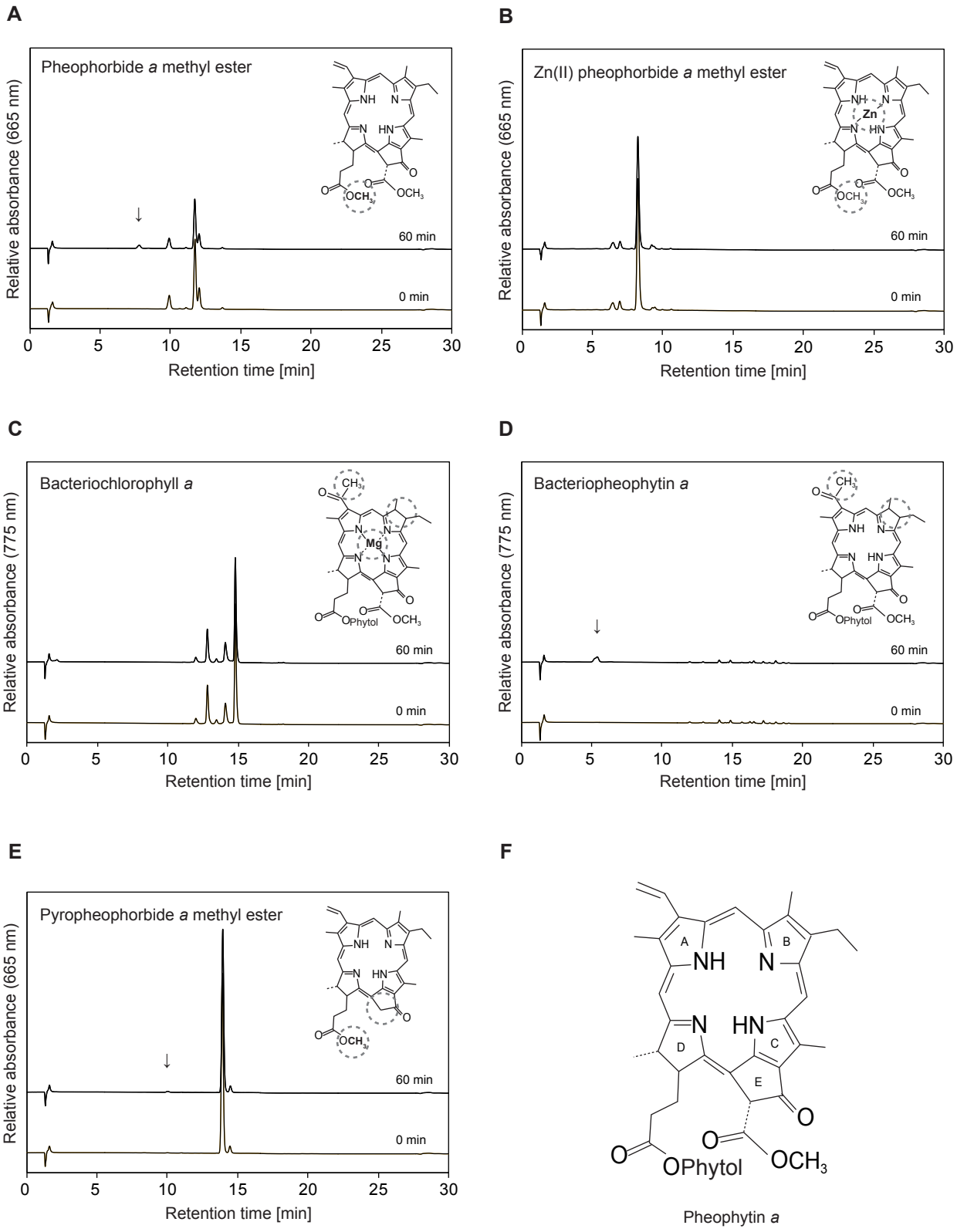

and an acetyl group in the pyrrole ring A**. D,** With bacteriopheophytin *a*, enzymatic activity could be observed. The structure has a reduced double bond in pyrrole ring B and an acetyl group in pyrrole ring A. **E,** With pyropheophorbide *a* methyl ester, only marginal activity was observed. The phytol chain of pheophytin *a* is replaced by a methyl group and isocyclic ring E contains a carboxy methyl ester. **F,** Chemical structure of pheophytin *a*. Note that all chromatograms are representatives of three replicates.

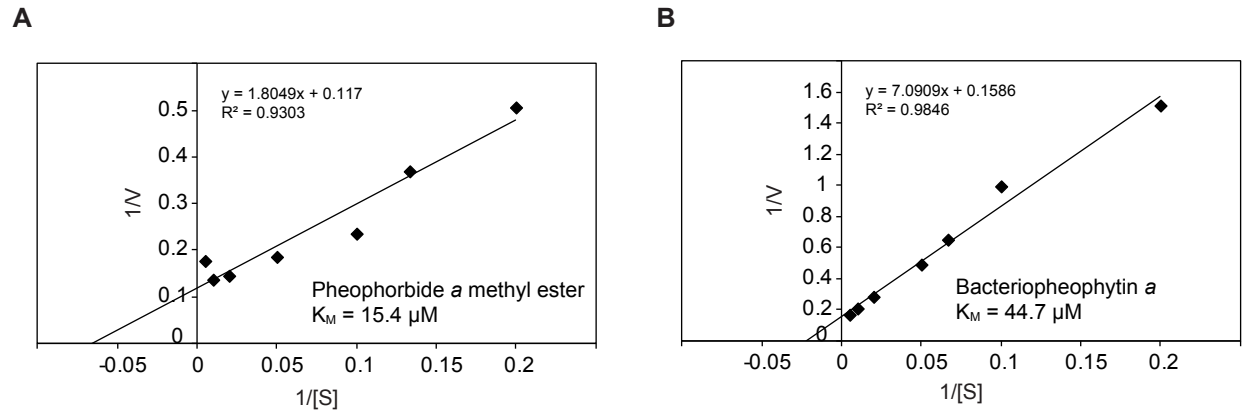

Figure 5. Determination of K_M for pheophorbide *a* methyl ester and bacteriopheophytin *a*. A, Determination of K_M value for pheophorbide *a* methyl ester with a Lineweaver-Burk plot. The K_M was found to be 15.4 µM. **B,** Determination of K_M value for bacteriopheophytin *a* with a Lineweaver-Burk plot. The K_M was found to be 44.7 µM.

pheophytin *a* only in slight modifications of the upper two pyrrole rings A and B. As expected, bacteriochlorophyll *a* was not accepted as substrate, most likely because of the central Mg^{2+}-ion (Figure 4C). Yet, bacteriopheophytin *a* was accepted and converted into a more polar product, assumed to be bacteriopheophorbide *a* (Figure 4D). As a last substrate pyropheophorbide *a* methyl ester was tested. Pyropheophorbide *a* methyl ester has a methyl group instead of phytol and misses a carboxy methyl ester at the isocyclic ring E. Although a very small peak could be detected on the HPLC chromatogram after 60 min, the activity was only marginal (Figure 4E) and pyropheophorbide *a* methyl ester most likely is not accepted as substrate.

In summary I can conclude that the substrate specificity of ΔPPH-MBP is determined by the porphyrin ring. On the one hand, it is irrevocable that the centre of the ring structure must be metal-free. On the other hand, it seems that modifications of the pyrrole rings A and B do not hinder protein activity, therefore bacteriopheophytin *a* was accepted as substrate. This was also shown by Schelbert et al. (2009), where they tested PPH activity on pheophytin *a* and *b*. PPH accepted both pigments as substrates, regardless of the differences in the molecular structure at the C7 position. However, the modification of the isocyclic ring E in pyropheophorbide *a* methyl ester influences the acceptance of the substrate (Figure 4). The hydrolytic activity of ΔPPH-MBP on pyropheophorbide *a* methyl ester was only marginal. Interestingly, the length of the esterified alcohol (phytol or methyl group) does not influence the activity, as seen for pheophorbide *a* methyl ester.

2.2.5 Pheophorbide *a* methyl ester and bacteriopheophytin *a* have similar K_M values as determined for pheophytin *a*

As shown in Figure 4, ΔPPH-MBP hydrolyzed pheophorbide *a* methyl ester and bacteriopheophytin *a*. The K_M values for both substrates were determined. ΔPPH-MBP was incubated with different concentrations of the substrates for 30 min, and the K_M was calculated by plotting 1/V against 1/[S] as described by Lineweaver and Burk (Lineweaver and Burk, 1934). The K_M was found to be 15.4 µM for pheophorbide *a* methyl ester (Figure 5A) and 44.7 µM for bacteriopheophytin *a* (Figure 5B). Both calculated K_M values fell into the same range as the K_M for the native substrate pheophytin *a* (Figure 3D). Also the K_M value calculated for chlorophyll *b* by Schelbert (2010) was similar. I therefore conclude that the modifications in the alcohol part (methyl group of pheophorbide *a* methyl ester) and the slight modifications of the upper part of the porphyrin ring in bacteriopheophytin *a* do not have a great impact on the protein kinetics.

2.2.6 Crystallization conditions for ΔPPH-MBP

In this study I could show that PPH has a strong specificity for the acid moiety of pheophytin, i.e. the porphyrin ring structure. More precisely, I found that especially modifications in the centre and the lower part of the porphyrin inhibited enzymatic activity (Figure 4). However, PPH was able to bind chlorophyll *a*, but its conversion into chlorophyllide *a* was not possible. Thus, it acted as a competitive inhibitor (Figure 3). In order to elucidate the mechanism of substrate binding by PPH, a crystallization approach was undertaken. The ΔPPH-MBP fusion

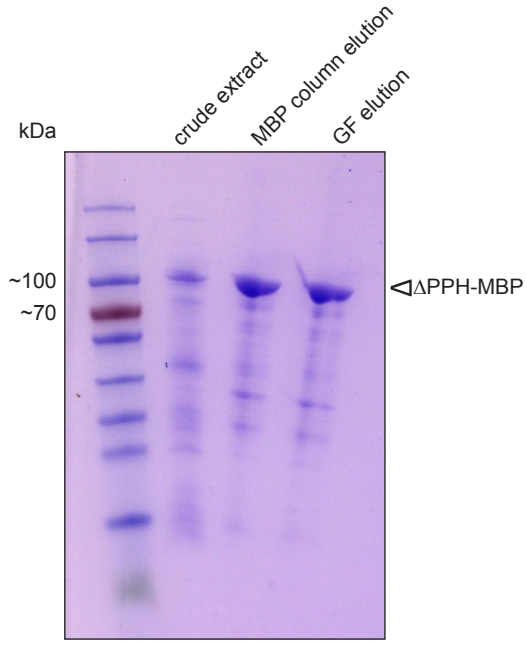

Figure 6. Purification of ΔPPH-MBP. Protein fractions of the purification process were separated on SDS-PAGE and stained with coomassie. Crude extract: soluble protein fraction after cell lysis. MBP column elution: eluted protein purified with an MBP-affinity column. GF elution: protein eluted from a size-exclusion chromatography column. In each lane 3 µg of protein were loaded.

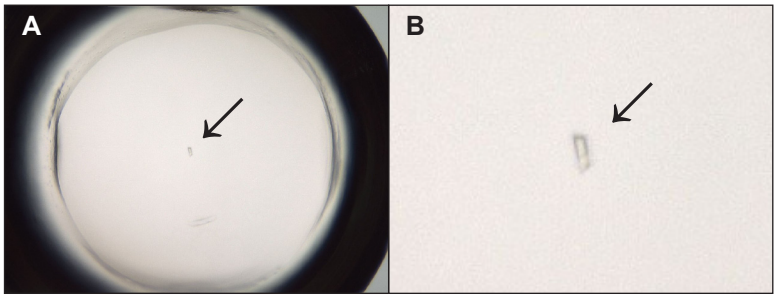

Figure 7. ΔPPH-MBP protein crystal. The crystal grew during the first few hours of incubation at 20 °C. The crystallization mother liquor contained 0.1 M Tris(HOAc), pH 8.5 and 40% 2-methyl-2,4-pentanediol (MPD). Protein concentration was 7.5 mg ml^{-1}. ML:P = 1:2. Size of crystal ~ 45 µm. **A,** Overview of the protein drop with the crystal. **B,** Close-up of the crystal.

protein was purified by a MBP-affinity column and subsequent size-exclusion chromatography. The resulting significantly purified protein (Figure 6) was buffer exchanged into 10 mM Tris-HCl pH 8 and used for crystallization studies. To indentify suitable crystallization conditions, eight different screens with 96 different conditions each were tested (see Material and Methods). For each condition three different mother liquor to protein ratios (ML:P) were chosen and the protein concentration was either 15 mg ml^{-1} or 7.5 mg ml^{-1}. Each plate was set up twice and incubated at 20 °C or 4 °C. In this initial screen, 9216 different conditions were tested.

2.2.7 Crystallization of ΔPPH-MBP

First crystals appeared after a few hours or days. 20 crystals which grew under 6 different conditions (Table 1) were tested for diffraction. All crystals grew at 20 °C. For most of the conditions several crystals were analyzed with varying protein concentration and/or ML:P ratios (Table 1). For crystals that grew under conditions with: pH 8.5, 0.085 M Tris-HCl, 15% glycerol, 25.5% polyethylene glycol (PEG) 4000 and 0.17 M Li-sulfate, fishing was not possible and crystals were not analyzed. By analyzing diffraction of the crystals, it was possible to assign if it was a salt or a protein crystal. Most of the crystals were assumed to be salt crystals due to their diffraction with large separation. Only one crystal (Figure 7) did not show diffraction and it is very likely that this is a protein crystal. This crystal grew at 20 °C, pH 8.5, 0.1 M Tris(HOAc) and 40% 2-methyl-2,4-pentanediol (MPD). The protein concentration was 7.5 mg ml^{-1} and the ML:P ratio was 1:2 (Table 1). However, further analysis and a refinement screen will be required in order to confirm this result.

Crystal growth is still under investigation and more crystals are growing. In Table 2 an overview of interesting crystallization conditions is listed (list of crystals might not be complete). For these conditions first crystals started to appear. It can be well observed that crystallization

Table 1. Overview of tested crystals. Crystals were grown under different conditions with pH ranging from 7.5 to 8.5. Buffer, precipitant and salt additives varied among tested conditions. Types of crystals were assigned according to diffraction results. Salt crystals showed diffraction with large separation, while the protein crystal did not diffract. The crystal grown at pH 8.5, 0.1 M Tris(HOAc), 40 % MPD did not show diffraction, therefore a protein crystal is very likely. PEG, polyethylene glycol; MME, monomethyl ether; MPD, 2-methyl-2,4-pentanediol

pH	Buffer	Precipitant	Salt	T [°C]	Protein [mg ml^{-1}]	Ration ML:P	# tested crystals	crystal type
7.5	0.1 M Bis Tris propane	20% PEG 3350	0.2 M Sodium citrate	20	15	1:2	2	salt
8.5	0.1M Tris(HOAc)	8% PEG 20K; 8% PEG 550MME	0.2 M Ca-acetate	20	15	1:1	2	salt
				20	15	1:2	1	salt
8.5	0.1M Tris(HOAc)	10% PEG 8000; 10% PEG 1000	0.2 M Ca-acetate	20	15	1:2	2	salt
8.5	0.1M Tris(HOAc)	15% PEG 4000	0.2 M Ca-acetate	20	15	2:1	2	salt
				20	15	1:1	3	salt
				20	7.5	1:1	1	salt
				20	15	1:2	2	salt
8.5	0.1 M Tris	40% PEG 400	0.2 M Li-sulfate	20	15	2:1	1	salt
				20	15	1:1	1	salt
				20	15	1:2	1	salt
8.5	0.1M Tris(HOAc)	40% MPD		20	7.5	1:1	1	salt
				20	7.5	1:2	1	protein

Table 2. Overview of interesting crystallization conditions. Listed are crystallization conditions which were tested and which showed first crystal formations. List might not be complete. Crystals have not yet been tested for their diffraction. PEG, polyethylene glycol; MPD, 2-methyl-2,4-pentanediol

pH	Buffer	Precipitant	Salt	T [°C]	Protein [mg ml^{-1}]	Ratio ML:P	crystal shape
5.5	0.1 M Na-Acetate	40 % MPD		4	15	2:1; 1:1; 1;2	small crystalline spots
					7.5	1:1; 1;2	small crystalline spots
6.5	0.1 M Cacodylate	40 % MPD		4	15	2:1; 1:1; 1;2	small crystalline spots
					7.5	1:1; 1;2	small crystalline spots
7.5	0.1 M Tris(HOAc)	40 % MPD		4	15	1:1; 1;2	small crystalline spots
6.5	0.1 M Bis-Tris	0.5 M Magnesium formate dihydrate		20	15	2:1; 1:1; 1;2	round crystals ~30 µm
					7.5	1:1	small bar 55 µm
7.5	0.1 M Hepes	0.5 M Magnesium formate dihydrate		20	15	2:1; 1:1; 1;2	needles or round crystals ~30 µm
					7.5	2:1	round crystals
8.5	0.1 M Tris	0.3 M Magnesium formate dihydrate		20	15	2:1; 1:1; 1;2	
					7.5	1:1; 1;2	round crystals
7	0.1 M MOPS	25 % PEG 400		20	7.5	2:1; 1:1; 1;2	needles 50-90 µm
9	0.1 M Tris	25 % PEG 400		20	7.5	2:1; 1:1; 1;2	needles 50-90 µm
9	0.1 M Tris	25 % Ammonium sulfate		20	7.5	2:1; 1:2	small needles
7.5	0.1 M Tris(HOAc)		0.8 M Li-sulfate	20	15	2:1; 1:1; 1;2	very small needles
8.5	0.1 M Tris(HOAc)		0.8 M Li-sulfate	20	15	2:1; 1:1; 1;2	needles ~30 µm
					7.5	2:1; 1:1; 1;2	needles
8.5	0.1 M Tris(HOAc)		1.8 M Li-sulfate	20	15	1:2	small crystalline spots
					7.5	2:1; 1:1; 1;2	small crystalline spots
7.5	0.075 M Hepes Na-salt	25 % Glycerol	1.125 M Li-sulfate	20	15	2:1; 1:1; 1;2	small needles
					7.5	1:1; 1;2	small crystalline spots
8.5	0.085 M Tris-HCl	15 % Glycerol; 25.5 % PEG 4000	0.17 M Li-sulfate	4	15	2:1; 1:1; 1;2	needles
				20	15	2:1; 1:1; 1;2	small plates 20-40 µm
				20	7.5	2:1; 1:2	small needles
		15 % PEG 3350	0.1 M Magnesium formate dihydrate	20	15	2:1; 1:1; 1;2	round aggregated crystals
					7.5	1:2	round aggregated crystals
7	0.1 M Hepes	20 % PEG 6000	0.01 M Zinc chloride	20	15	2:1; 1:1; 1;2	cubes 20-50 µm
					7.5	1:2	small crystalline spots
8.5	0.1 M Tris(HOAc)	20 % PEG 4K	0.005 M Cadmium chloride	20	15	2:1; 1:1; 1;2	small crystalline spots
8.5	0.1 M Tris	1 M Li-sulfate monohydrate	0.01 M Nickel(II) chloride hexahydrate	20	15	2:1; 1:1; 1;2	needles 20-50 µm
					7.5	2:1; 1:1; 1;2	small needles

is possible under a wide range of pH (pH 5.5 to pH 9). Therefore it can be assumed that pH is not critical. A second interesting observation is that on the one hand many crystals are growing under conditions without salt additives. On the other hand, Li-sulfate as a salt additive seems to trigger crystal growth (Table 2). However, the first diffraction analysis of crystals showed that all crystal grown under Li-sulfate conditions were salt crystals (Table 1). It is therefore well possible that the crystals found under Li-sulfate conditions are not protein but salt crystals. Nevertheless, growing crystals will be further observed and analyzed for diffraction.

2.3 Discussion

PPH is the core dephytylating enzyme during leaf senescence and it is also involved in color break during fruit ripening (Guyer et al., 2014; Schelbert et al., 2009). PPH encodes a α/β-hydrolase which cleaves the ester bond between the porphyrin ring and the phytol moiety of pheophytin *a*. It has been shown that PPH is highly specific for pheophytin and does not accept chlorophyll as substrate (Schelbert et al., 2009). In this study, Arabidopsis PPH was expressed as recombinant protein fused to a maltose-binding protein (MBP) tag (ΔPPH-MBP) in order to further specify its biochemical properties. ΔPPH-MBP showed a temperature optimum of 34 °C and its highest activity was found at pH 8.5 (Figure 2). If the optimal growth temperature for Arabidopsis is considered to be at around 20 °C the determined temperature optimum is rather high. However, at 20 °C more than 30% enzyme activity were still present. Since the K_M of ΔPPH-MBP was found to be 10.3 µM (Figure 3) the lack of activity at 20 °C might be compensated by the high affinity of PPH to pheophytin *a*. As already shown in other studies chlorophyll *a* was not accepted as substrate (Schelbert et al., 2009). Nevertheless, an inhibition study showed that PPH was able to bind chlorophyll *a* and it could inhibit enzyme activity towards pheophytin *a*. By testing different chlorophyll *a* concentrations as inhibitors, it was revealed that chlorophyll *a* most likely acted as a competitive inhibitor. These findings led to the assumption that the binding-site of PPH is not substrate specific; however, its active site only recognizes Mg-free porphyrin derivates. In order to confirm this assumption different porphyrins were tested as possible substrates. Results showed that enzyme activity was not influenced by the length of the esterified side chain. Pheophorbide *a* methyl ester which has a methyl group instead of phytol, was hydrolyzed with a similar K_M as determined for pheophytin *a*. Also bacteriopheophytin *a* (Figure 4 and 5) was accepted as substrate, as well as pheophytin *b* (Schelbert et al., 2009), with similar K_M values as calculated for pheophytin *a* (Figure 5, Schelbert, 2010). Other substrates (bacteriochlorophyll *a* and pyropheophorbide *a* methyl ester) with modifications in the porphyrin ring were not dephytylated. From these findings I conclude that PPH is an esterase with specificity for the acid moiety (Fojan et al., 2000). However, only modifications in the lower and central part of the tetrapyrrole inhibited enzyme activity. It would be interesting

to understand how the binding mechanism of PPH works and what the biological function of the very defined substrate acceptance may be. Revealing the crystal structure of PPH would shed light on these properties. For this I started a crystallization experiment. First conditions which triggered crystal formation were found. At pH 8.5 and 40% MPD protein crystals grew within one day. However, crystallization conditions need further improvement in order to obtain high quality protein crystals. As a general conclusion from the first crystallization approach it seems that pH is not critical and salt is not required as precipitant. However, finding the right precipitant at the correct concentration is important.

Further experiments will include the final elucidation of the crystal structure of PPH. Since PPH binds chlorophyll *a*, but does not convert it into chlorophyllide *a*, it might be possible to use chlorophyll for crystallizing PPH as an enzyme-pigment complex. Alternatively, a PPH variety that is mutated in the active site serine residue (PPH_{S221A}) and that does not show enzymatic activity (Schelbert et al., 2009) could be used. However, it needs to be shown if PPH_{S221A} is able to bind substrates and could therefore be used for a co-crystallization.

2.4 Material and Methods

2.4.1 Cloning of ΔPPH-MBP

For generating a ΔPPH-MBP fusion construct, a truncated PPH fragment, lacking the first 138 bp encoding the chloroplast transit peptide (ΔPPH), was amplified with Phusion polymerase (New England Biolabs) using the two primers PPH_LIC_fw (GTCTCTCCCatgagtggaaattccgatggttatg) and PPH_LIC_rv (GGTTCTCCCCagctgcagacttccctccaaacac). pMCSG29 (Eschenfeldt et al., 2010) was digested with *Sma*I and subsequently the vector and the PCR product were both gel purified with Wizard® SV Gel and PCR Clean-Up System (Promega). Ligation-independent cloning (LIC) was performed according to published protocols (Eschenfeldt et al., 2009; De Rybel et al., 2011) with adaptations. The T4 treatment was performed with T4 polymerase (New England Biolabs). The PCR reaction was supplemented with dTTP and the vector reaction with dATP, respectively. Both reactions were incubated at 22 °C for 90 min and stopped by incubating at 75 °C for 15 min. Annealing was performed by mixing the vector and the PCR product and incubating at 22 °C for 40 min. The annealed construct was transformed into NEB 10-beta competent *E. coli* (High Efficiency) cells (New England Biolabs). Sequence accuracy was verified by sequencing. The final construct was transformed into *E. coli* BL21(DE3).

2.4.2 Expression and purification of ΔPPH-MBP

E. coli BL21 (DE3*)* harboring pMCSG29_PPH were grown at 37 °C to an optical density at 600 nm of 0.5-0.6. Protein expression was induced by adding 1 mM isopropyl β-D-1-thiogalactopyranoside (IPTG) and expression was performed at 20 °C over night. Bacterial cells were harvested, resuspended and lysed by using a French Press (Constant Cell Disruption System; Constant Systems) at 150 MPa and subsequently centrifuged for 45 min, 20'000 g. The supernatant was used to proceed. Total protein concentration in the supernatant was set to 0.5 mg ml^{-1} and the cell lysate was filtered through a 22 µm filter. The cell lysate was finally loaded on a MBP-affinity column (MBPTrap, GE Healthcare) with a constant flow of 0.25-0.5 ml min^{-1}. Subsequently, the column was washed with MBP buffer (20 mM Tris-HCl pH 8, 200 mM NaCl). Bound protein was eluted by adding 10 mM maltose to the MBP buffer. Eluted purified protein was loaded on a gel-filtration column (HiLoad 16/600 Superdex 200 pg, GE Healthcare) and eluted with 20 mM Tris-HCl pH 8, 50 mM NaCl. The buffer of the eluted protein was exchanged to 10 mM Tris-HCl pH 8 using an Amicon Ultra-15 centrifugal filter unit with ultracel-50 membrane (Merck Millipore) and concentrated to 15 mg ml^{-1}. All purification steps were carried out on ice or at 4 °C. Protein purification was monitored by protein analysis on SDS-PAGE. All protein quantifications were performed by Bradford assay (BioRad). Purified protein was used for protein crystallization.

2.4.3 Biochemical properties of ΔPPH-MBP

Activity of expressed protein

After protein expression bacterial cells were resuspended in buffer containing 200 mM NaCl and 20 mM Tris-HCl pH 8 and lysed using a French Press as described above. The protein concentration in the supernatant was set to 3 mg ml^{-1} for both, empty vector pMCSG29 and pMCSG29 harboring ΔPPH, and the buffer was supplemented with 10% glycerol. The prepared protein was frozen in liquid N_2 and stored at -80 °C until usage for all following activity assays. Note that all determinations of biochemical properties were performed with non-purified ΔPPH-MBP fusion protein. In order to confirm the activity of ΔPPH-MBP 5 µl protein (15 µg) were mixed with 10 µl pheophytin *a* (~100 µM) dissolved in acetone (final acetone concentration in the assay 10%) and with 85 µl 0.1 M Hepes-KOH, 1 mM EDTA, pH 8 and incubated for 30 min at 34 °C. Reactions were stopped by adding 2 volumes of 100% acetone. The mixture was centrifuged and analyzed by HPLC according to Das and Guyer et al. (submitted).

Determination of temperature and pH optima

In order to determine the temperature optimum of ΔPPH-MBP, assays were performed by incubating 5 µl pheophytin *a* (~100 µM) (dissolved in acetone, 10% final acetone concentration in the assays) with 2.5 µl protein (7.5µg) and 42.5 µl 0.1 M Bicine, 1 mM EDTA, pH 8.5 at different temperatures for 60 min. Reactions were stopped and analyzed as described above.

To determine the pH optimum of ΔPPH-MBP, assays were performed by incubating 5 µl pheophytin *a* (~100 µM) (dissolved in acetone, 10% final acetone concentration in the assays) with 2.5 µg protein (7.5 µg) and 42.5 µl of two different buffers with different pH (0.1 M Hepes, 1 mM EDTA, pH 7.5, pH 8 and pH 8.5 or 0.1 M Bicine, 1 mM EDTA, pH 8, pH 8.5 and pH 9) for 60 min at 34 °C. Reactions were stopped and analyzed as described above.

Activity measurement of different substrates

The different substrates were obtained as follows: chlorophyll *a,* bacteriochlorophyll *a* and pyropheophorbide *a* methyl ester (Livchem Logistics GmbH), pheophorbide *a* methyl ester and Zn(II) pheophorbide *a* methyl ester were gifts from Bernhard Kräutler, University Innsbruck, Austria. Pheophytin *a* and bacteriopheophytin *a* were prepared by supplementing chlorophyll *a* or bacteriochlorophyll *a*, respectively, with 20 mM HCl for 2 min, followed by neutralizing by adding 20 mM NaOH.

Activity assays were performed by incubating 10 µl substrate (200 µM, 10% acetone in the assays) and 5 µl protein (15 µg) in 85 µl assay buffer (0.1 M Bicine, 1 mM EDTA, pH 8.5) for 60 min. Reactions were stopped and analyzed as described above.

Determination of K_M and inhibition study

For determining the K_M of pheophytin *a*, 10 µl protein (30 µg) were incubated with 20 µl pheophytin *a* at different concentrations (1 to 100 µM) and 170 µl assay buffer at 34 °C for 30 min. Total acetone concentration in the assays was 10%. Reactions were stopped and analyzed as described above.

For the inhibition study with chlorophyll *a*, the assays contained 5 µl protein (15 µg), 5 µl pheophytin *a* (concentrations ranging from 1 to 100 µM), 5 µl chlorophyll *a* (50 or 200 µM) and 85 µl assay buffer. Both pigments were dissolved in acetone and the final acetone concentration in the assays was 10%. Assays were incubated at 34 °C for 30 min. Reactions were stopped and analyzed as described above.

The K_M values of pheophorbide *a* methyl ester and bacteriopheophytin *a* were determined by incubating 5 µl protein (15 µg) with 10 µl substrate at different concentrations (pheophorbide *a* methyl ester 2 to 200 µM and bacteriopheophytin *a* 5 to 200 µM) and 85 µl assay buffer at 34 °C for 30 min. Both pigments were dissolved in acetone and the final acetone concentration in the assays was 10%. Reactions were stopped and analyzed as described above.

2.4.4 Crystallization

The concentration of purified protein (ΔPPH-MBP) in 10 mM Tris-HCl pH 8 was set to 15 or 7.5 mg ml^{-1}. The following crystallization screens were applied: Clear Strategy™ Screens I pH 5.5, 6.5, 7.5, 8.5 (Molecular Dimensions), Clear Strategy™ Screens II pH 5.5, 6.5, 7.5, 8.5 (Molecular Dimensions), Crystallization Cryo Kit for Proteins (Sigma), Crystallization Low Ionic Strength Kit for Proteins (Sigma), JCSG+ Suite (Qiagen) or JCSG-*plus*™ (Molecular Dimensions), PACT *premier*™ (Molecular Dimensions), Crystal Screen (Hampton Research), Crystal Screen 2 (Hampton Research), Index HT (Hampton Research) and a screen using different ammonium sulfate, 2-methyl-2,4-pentanediol (MPD), polyethylene glycol (PEG) 400 or PEG 6000 concentrations as precipitants against different pH (malonic acid pH 3, citric acid pH 5, MOPS pH 7, Tris pH 9). Each screen was performed with 15 and 7.5 mg ml^{-1} protein. For each tested condition three different mother liquor to protein ratios (ML:P) were applied: 2:1, 1:1 and 1:2. For the 15 mg ml^{-1} protein concentration the final drop volume was 400 nl for the 2:1 and 1:2 ratios and 300 nl for the 1:1 ratio. For the 7.5 mg ml^{-1} protein concentration the final drop volume was 300 nl for the 2:1 and 1:2 ratios and 200 nl for the 1:1 ratio. Mother liquors were transferred to crystallization plates using Aquarius (Tecan) pipetting robot. Crystallization was set up as vapor diffusion experiment at room temperature or at 4 °C in Intelli-Plate R96-3 LV (Art Robbins) using Phoenix or Gryphon-LCP (Art Robbins Instruments) nano-drop liquid handlers. All plates were set up twice and incubated at 20 °C or 4 °C in a Rock Imager 1000 (Formulatrix) for automated imaging.

2.4.5 Diffraction measurements of crystals

Crystals were saturated with cryobuffer (mother liquor containing 20% glycerol [v/v]) and frozen in liquid nitrogen. Diffraction of crystals was measured using X-rays (wavelength = 1.0 Å) generated by a synchrotron (Swiss Light Source, Paul Scherrer Institut, Villigen). Data was collected by Peer Mittl (Department of Biochemistry, University of Zurich).

2.5 Acknowledgment and Contribution

All experimental work, except the analysis of crystal diffraction, was carried out by me. I would like to thank Peer Mittl (Department of Biochemistry, University of Zurich) for his very helpful input and especially for performing the crystal measurements. I would also like to thank Beat Blattmann and Céline Stutz-Ducommun (Protein Crystallization Centre, Department of Biochemistry, University of Zurich) for their help with setting up the crystallization plates and for all the helpful inputs.

3. *Dephytylation during Fruit Ripening*

3.1 Publication: Guyer et al., 2014

Different mechanisms are responsible for chlorophyll dephytylation during fruit ripening in leaf senescence in tomato

Luzia Guyer*, Silvia Schelbert Hofstetter*, Bastien Christ, Bruno Silvestre Lira, Magdalena Rossi and Stefan Hörtensteiner

Plant Physiology 166: 44-56

* Equal contribution

Different Mechanisms Are Responsible for Chlorophyll Dephytylation during Fruit Ripening and Leaf Senescence in Tomato[1][W][OPEN]

Luzia Guyer[2], Silvia Schelbert Hofstetter[2], Bastien Christ, Bruno Silvestre Lira, Magdalena Rossi, and Stefan Hörtensteiner*

Institute of Plant Biology, University of Zurich, CH-8008 Zurich, Switzerland (L.G., S.S.H., B.C., S.H.); and Departemento de Botânica, Instituto de Biociências, Universidade de São Paulo, CEP05508–090 Sao Paulo, Brazil (B.S.L., M.R.)

Chlorophyll breakdown occurs in different green plant tissues (e.g. during leaf senescence and in ripening fruits). For different plant species, the PHEOPHORBIDE *A* OXYGENASE (PAO)/phyllobilin pathway has been described to be the major chlorophyll catabolic pathway. In this pathway, pheophorbide (i.e. magnesium- and phytol-free chlorophyll) occurs as a core intermediate. Most of the enzymes involved in the PAO/phyllobilin pathway are known; however, the mechanism of dephytylation remains uncertain. During Arabidopsis (*Arabidopsis thaliana*) leaf senescence, phytol hydrolysis is catalyzed by PHEOPHYTINASE (PPH), which is specific for pheophytin (i.e. magnesium-free chlorophyll). By contrast, in fruits of different *Citrus* spp., chlorophyllase, hydrolyzing phytol from chlorophyll, was shown to be active. Here, we enlighten the process of chlorophyll breakdown in tomato (*Solanum lycopersicum*), both in leaves and fruits. We demonstrate the activity of the PAO/phyllobilin pathway and identify tomato PPH (SlPPH), which, like its Arabidopsis ortholog, was specifically active on pheophytin. SlPPH localized to chloroplasts and was transcriptionally up-regulated during leaf senescence and fruit ripening. *SlPPH*-silencing tomato lines were impaired in chlorophyll breakdown and accumulated pheophytin during leaf senescence. However, although pheophytin transiently accumulated in ripening fruits of *SlPPH*-silencing lines, ultimately these fruits were able to degrade chlorophyll like the wild type. We conclude that PPH is the core phytol-hydrolytic enzyme during leaf senescence in different plant species; however, fruit ripening involves other hydrolases, which are active in parallel to PPH or are the core hydrolases in fruits. These hydrolases remain unidentified, and we discuss the question of whether chlorophyllases might be involved.

Chlorophyll breakdown is an important physiological process in plants that occurs during different phases of plant development. Most obvious and eye-catching is the loss of green pigment color during autumnal leaf senescence in deciduous trees, but also the ripening phase of many fruits such as banana (*Musa acuminata*) and tomato (*Solanum lycopersicum*) includes massive degradation of chlorophyll.

For many years, chlorophyll degradation was considered a biological enigma (Hendry et al., 1987). Only the identification and structure determination of a first colorless nonfluorescent chlorophyll catabolite from senescing barley (*Hordeum vulgare*) as a (final) breakdown product (Kräutler et al., 1991) paved the way for the step-wise elucidation of a pathway of chlorophyll degradation (for review, see Hörtensteiner and Kräutler, 2011; Kräutler and Hörtensteiner, 2013; Christ and Hörtensteiner, 2014). This pathway leads to the ultimate degradation of chlorophyll to a group of colorless, linear tetrapyrroles, termed phyllobilins (Kräutler and Hörtensteiner, 2013).

The pathway can be divided into two parts. Early reactions take place within senescing chloroplasts and result in the formation of a colorless primary fluorescent chlorophyll catabolite (*p*FCC; Fig. 1; Mühlecker et al., 1997). The reactions catalyzing the chlorophyll-to-*p*FCC conversion are commonly present in land plants (Hörtensteiner, 2013) and, therefore, represent the core part of the pathway. The second part of the chlorophyll degradation pathway is characterized by largely species-specific modifications at different peripheral positions within *p*FCC (indicated in Fig. 1 with R^1–R^4) and ultimate conversion to respective nonfluorescent phyllobilins that represent the end products of chlorophyll breakdown in most species and are stored in the vacuole (Kräutler and Hörtensteiner, 2013).

To date, a total of four steps are known to be required for the conversion of chlorophyll *a* to *p*FCC. Except for the activity that is responsible for magnesium dechelation, genes encoding these catalytic activities have been identified in Arabidopsis (*Arabidopsis thaliana*) and other species. Since all except one of the phyllobilins that have

[1] This work was supported by the Swiss National Science Foundation (grant no. 31003A–132603 to S.H.).

[2] These authors contributed equally to the article.

* Address correspondence to shorten@botinst.uzh.ch.

The author responsible for distribution of materials integral to the findings presented in this article in accordance with the policy described in the Instructions for Authors (www.plantphysiol.org) is: Stefan Hörtensteiner (shorten@botinst.uzh.ch).

[W] The online version of this article contains Web-only data.

[OPEN] Articles can be viewed online without a subscription.

www.plantphysiol.org/cgi/doi/10.1104/pp.114.239541

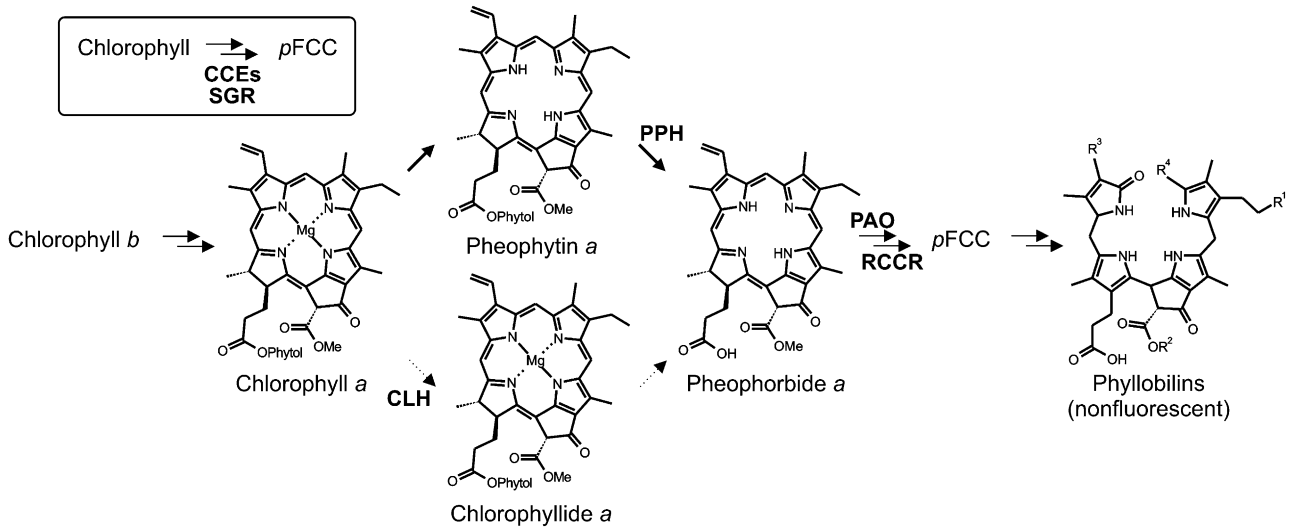

Figure 1. Structural outline of the PAO/phyllobilin pathway of chlorophyll breakdown showing the chemical constitutions of chlorophyll *a* and of selected chlorophyll catabolites that are relevant for this work. R^1 to R^4 indicate sites of modifications that are found in nonfluorescent phyllobilins of different plant species (Kräutler and Hörtensteiner, 2013). Relevant reactions (PPH, CLH, PAO, and RCCR) are indicated. Note that dephytylation by PPH was shown to be the major reaction of pheophorbide *a* formation during leaf senescence in Arabidopsis (Schelbert et al., 2009). The inset indicates that conversion of chlorophyll to *p*FCC requires the concerted action of different CCEs and of SGR.

been characterized structurally are derived from chlorophyll *a* (Hörtensteiner and Kräutler, 2011), the reductive part of the chlorophyll cycle that converts chlorophyll *b* into chlorophyll *a* has been considered an integral part of senescence-related chlorophyll breakdown (Tanaka et al., 2011).

The magnesium- and phytol-free intermediate of chlorophyll *a*, pheophorbide *a*, is a genuine breakdown product of chlorophyll (Langmeier et al., 1993). However, the means of pheophorbide formation during leaf senescence was (and still is) controversial, because the order of reactions—that is, dechelation versus dephytylation—was unclear (Amir-Shapira et al., 1987), although the favored hypothesis was that dephytylation by CHLOROPHYLLASE (CLH) would precede magnesium dechelation (Tanaka and Tanaka, 2006). We recently showed that the two CLHs of Arabidopsis are dispensable for leaf senescence (Schenk et al., 2007). Instead, we and others identified a novel esterase, PHEOPHYTINASE (PPH), which specifically dephytylates pheophytin, but not chlorophyll, and is required for chlorophyll breakdown in Arabidopsis and rice (*Oryza sativa*; Morita et al., 2009; Schelbert et al., 2009; Ren et al., 2010). Thus, *PPH*-deficient mutants exhibit a stay-green phenotype, which is characterized by a high retention of chlorophyll together with the accumulation of significant amounts of pheophytin during leaf senescence. This indicates that dechelation precedes dephytylation, at least during leaf senescence. By contrast, CLHs have been implicated in the postharvest senescence of broccoli (*Brassica oleracea* var *italica*) and citrus (*Citrus* spp.) fruit ripening (Jacob-Wilk et al., 1999; Azoulay Shemer et al., 2008; Chen et al., 2008; see below). Pheophorbide *a*, the last chlorin-type intermediate of chlorophyll breakdown, is oxygenolytically opened by PHEOPHORBIDE *A* OXYGENASE (PAO) to yield a red chlorophyll catabolite, which is further reduced to *p*FCC by RED CHLOROPHYLL CATABOLITE REDUCTASE (RCCR; Rodoni et al., 1997). PAO is responsible for the open tetrapyrrolic backbone of the phyllobilins. For this reason, the pathway described above is now termed the PAO/phyllobilin pathway of chlorophyll breakdown (Kräutler and Hörtensteiner, 2013).

Recently, it was shown that the chloroplast-localized chlorophyll catabolic enzymes (CCEs) physically interact at the thylakoid membrane, most likely to allow metabolic channeling of the breakdown intermediates upstream of *p*FCC that are potentially phototoxic (Sakuraba et al., 2012). STAY-GREEN (SGR), a chloroplast-localized protein (Hörtensteiner, 2009), is critical for these interactions; *nonyellowing1-1*, an Arabidopsis *SGR* mutant (Ren et al., 2007), is defective in CCE protein interaction (Sakuraba et al., 2012). This indicates that, rather being biochemically active itself, SGR may function as a scaffold protein to recruit CCEs for protein complex formation during chlorophyll breakdown. As a consequence, mutants that are deficient in SGR exhibit a stay-green phenotype (Barry, 2009; Hörtensteiner, 2009). In addition, SGR (negatively) regulates carotenoid biosynthesis during tomato fruit ripening (Luo et al., 2013) and (positively) regulates root nodule senescence in *Medicago truncatula* (Zhou et al., 2011), implying that SGR has diverse functions that are not restricted to chlorophyll degradation.

The PAO/phyllobilin pathway has largely been elucidated through investigations that focused on leaf

senescence. Nevertheless, chlorophyll breakdown during fruit ripening was considered to be identical to the mechanism occurring during leaf senescence (Hörtensteiner and Kräutler, 2011). Deficiency of SGR, as for example in the tomato *green flesh* (*gf*) and the red pepper (*Capsicum annuum*) *chlorophyll retainer* mutants, causes a stay-green phenotype of these mutants in leaves and fruits (Barry et al., 2008; Borovsky and Paran, 2008), indicating that SGR is required for chlorophyll breakdown in both tissues. Similarly, PAO and RCCR were found to be active in chromoplast membranes isolated from tomato and red pepper fruits (Moser and Matile, 1997; Akhtar et al., 1999), and recently, different fluorescent and nonfluorescent phyllobilins were shown to occur in ripening apple (*Malus domestica*), pear (*Pyrus communis*), and banana (Kräutler, 2008; Moser et al., 2009). Finally, SGR and PAO have been identified in a recent proteome analysis of tomato chromoplasts (Barsan et al., 2010). In summary, these data indicate that the pathways of chlorophyll breakdown during fruit ripening and leaf senescence are identical. Yet, the identification of PPH as the major dephytylating enzyme of leaf senescence (Schelbert et al., 2009) challenges this view, because, contrary to the situation in leaves, CLH was shown to be involved during ethylene-induced ripening of citrus fruits (Jacob-Wilk et al., 1999; Harpaz-Saad et al., 2007; Azoulay Shemer et al., 2008).

The aim of this work, therefore, was to investigate whether PPH, besides its requirement for leaf senescence, is also involved in chlorophyll breakdown during fruit ripening. Using tomato as a model, we show that the PAO/phyllobilin pathway is active both during fruit ripening and leaf senescence, because genes encoding CCEs and SGR are transcriptionally up-regulated in both ripening fruits and senescing leaves. However, lines silenced in tomato *PPH* (*SlPPH*) were specifically deficient in leaf senescence-related chlorophyll breakdown, while the involvement of PPH in fruit ripening-related breakdown seems to be less important. Although our data show a transient delay of chlorophyll breakdown in the absence of PPH, *SlPPH*-silencing fruits ultimately degrade chlorophyll like the wild type. Pheophytin-specific phytol hydrolysis was reduced in chromoplasts of *SlPPH*-silencing lines, but substantial enzyme activity remained in these lines, which leads us to speculate that other hydrolases are important (in addition to PPH). The identity of these activities remains elusive.

RESULTS

The PAO/Phyllobilin Pathway Is Active during Chlorophyll Degradation in Tomato Leaves and Fruits

To enlighten whether the PAO/phyllobilin pathway is responsible for the loss of chlorophyll in tomato, CCE gene expression was analyzed during leaf senescence and fruit ripening. Yellowing was observed during the progression of natural senescence of tomato leaves starting at 60 d after germination (Fig. 2A), and within 23 d, the content of chlorophyll *a* and *b* decreased to around 30% of the initial amount (Fig. 2C). As shown in Figure 2, B and D, the chlorophyll content of tomato fruits at the breaker stage was reduced within 4 d of ripening, and red and yellow pigments, mainly carotenoids (Egea et al., 2010), became visible. Gene expression levels of *SlSGR* and *SlPAO*, as analyzed by semiquantitative reverse transcription (RT)-PCR, increased during both leaf senescence and fruit ripening (Fig. 2, E and F).

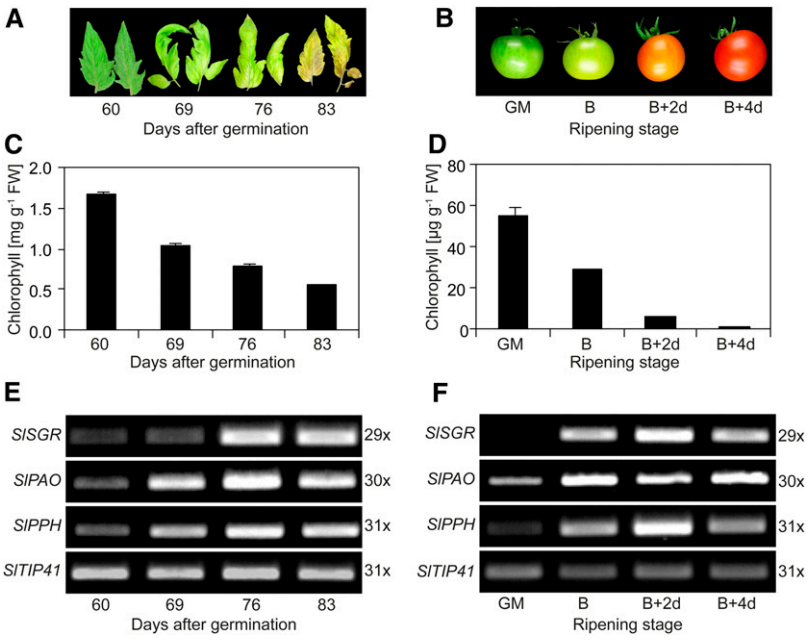

Figure 2. The PAO/phyllobilin pathway is active during chlorophyll degradation in tomato leaves and fruits. A, Phenotypic appearance of the first true leaves from wild-type tomato during natural senescence starting from 60 d after germination. B, Phenotypes of fruits during ripening. GM, Green mature; B, breaker. C and D, Quantification of total chlorophyll during natural leaf senescence (C) and fruit ripening (D). Total leaves and fruit exocarp and mesocarp tissues at the indicated times were used for chlorophyll quantification. Data represent means of three technical replicates ± SD. FW, Fresh weight. E and F, Analysis of gene expression during natural leaf senescence (E) and fruit ripening (F). *SlTIP41* was used as a control (Expósito-Rodríguez et al., 2008). Expression was analyzed with the number of PCR cycles as indicated. PCR products were separated on agarose gels and visualized with ethidium bromide.

These results confirmed published quantitative PCR (qPCR) data on CCE gene expression (Lira et al., 2014) and indicated that the PAO/phyllobilin pathway is activated during chlorophyll breakdown in tomato and that chlorophyll is degraded in a similar manner in tomato leaves and fruits. Nevertheless, it remained to be demonstrated whether the core phytol hydrolytic enzyme during chlorophyll degradation is PPH, as demonstrated in Arabidopsis leaves (Schelbert et al., 2009).

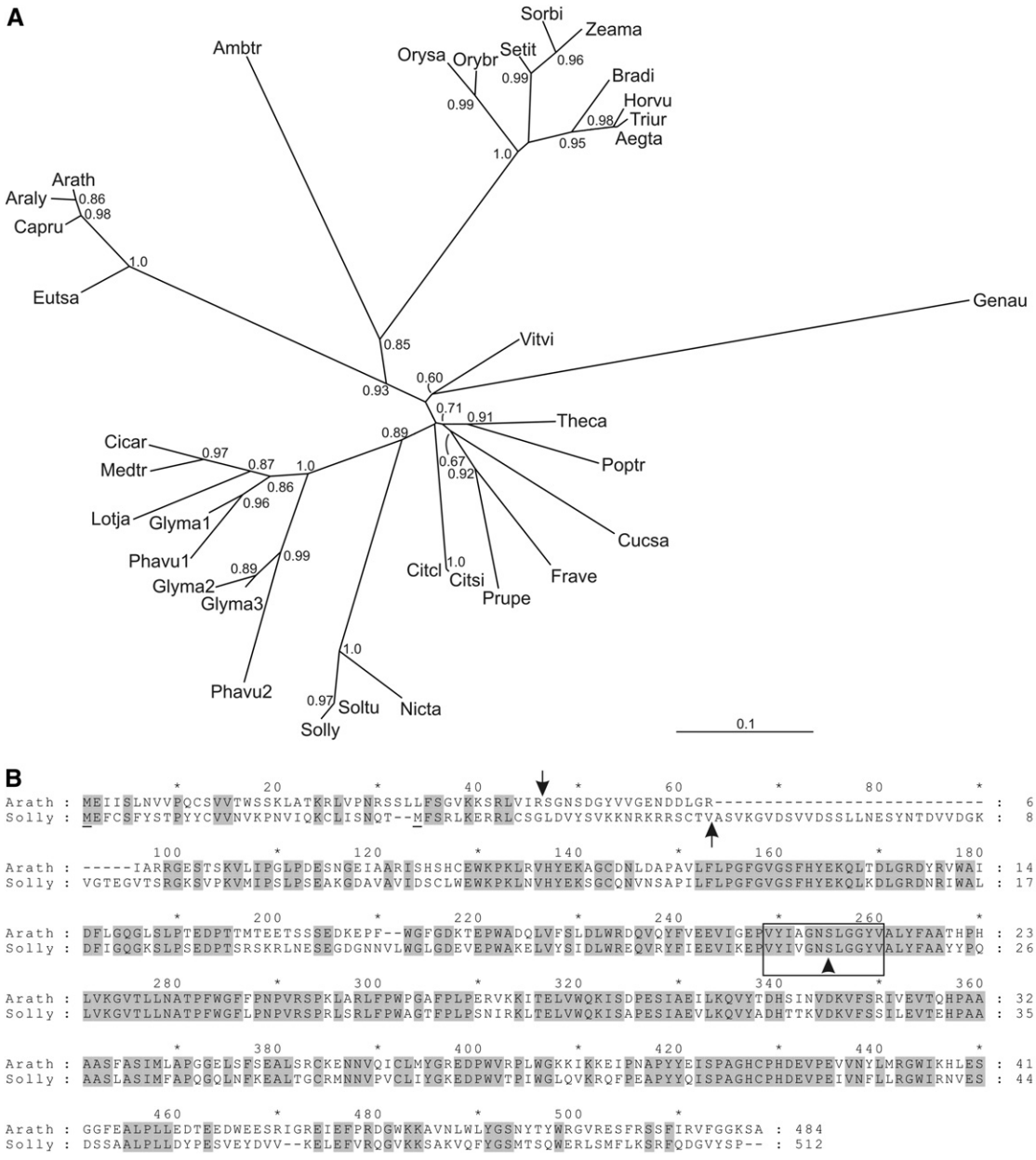

Figure 3. Analysis of PPH proteins from different plant species. A, Maximum likelihood phylogenetic tree of PPH proteins from different higher plant species. Branch support values are based on 100 bootstrap replicates and are indicated when higher than 0.6. Aegta, *Aegilops tauschii*; Ambtr, *Amborella trichopoda*; Araly, *Arabidopsis lyrata*; Arath, Arabidopsis; Bradi, *Brachypodium distachyon*; Capru, *Capsella rubella*; Cicar, *Cicer arietinum*; Citcl, *Citrus clementina*; Citsi, *Citrus sinensis*; Cucsa, *Cucumis sativus*; Eutsa, *Eutrema salsugineum*; Frave, *Fragaria vesca*; Genau, *Genlisea aurea*; Glyma, soybean; Horvu, barley; Lotja, *Lotus japonicus*; Medtr, *Medicago truncatula*; Nicta, *Nicotiana tabacum*; Orybr, *Oryza brachyantha*; Orysa, rice; Phavu, common bean; Poptr, *Populus trichocarpa*; Prupe, *Prunus persica*; Setit, *Setaria italica*; Solly, tomato; Soltu, *Solanum tuberosum*; Sorbi, *Sorghum bicolor*; Theca, *Theobroma cacao*; Triur, *Triticum urartu*; Vitvi, *Vitis vinifera*; Zeama, *Zea mays*. B, Alignment of PPH proteins from Arabidopsis (Arath) and tomato (Solly). Two potential start Met residues are underlined. Cleavage sites of the chloroplast transit peptide sequences as predicted by ChloroP (Emanuelsson et al., 1999) are indicated with arrows. The PPH motif (Schelbert et al., 2009) containing the active-site Ser residue (arrowhead) is boxed. Identical amino acids are shaded in gray.

SlPPH Is Expressed in Tomato and Localizes to Chloroplasts

BLASTP searches (Altschul et al., 1997) for PPH protein homologs in tomato identified SlPPH (Solyc01g088090). Highly homologous PPH proteins were present in all sequenced plant genomes as single proteins, except for soybean (*Glycine max*) and common bean (*Phaseolus vulgaris*), with three and two PPHs, respectively (Fig. 3A). PPHs of species within different plant families, including Fabaceae, Brassicaceae, Solanaceae, and Gramineae, clustered into separate clades. Overall protein sequence identity within families was between 65% and 96%, and even the most divergent PPH from *Genlisea aurea* was more than 58% identical to the other protein sequences. An alignment of SlPPH and AtPPH, which exhibits 62.8% sequence identity, is shown in Figure 3B. The conserved PPH domain (Schelbert et al., 2009) with its proposed active-site Ser residue (boxed in Fig. 3B) was present in all PPH proteins included in the phylogenetic tree of Figure 3A. Expression of *SlPPH*, as analyzed by semiquantitative RT-PCR, increased with the onset of leaf senescence and fruit ripening and correlated with the transcript levels of *SlPAO* and *SlSGR* (Fig. 2, E and F). From these results, we concluded that SlPPH is involved in chlorophyll breakdown and likely acts as the phytol hydrolytic enzyme in leaves and fruits. In order to analyze the subcellular localization of SlPPH, which based on its proposed function was expected to localize to plastids, we constructed C-terminal GFP fusions (SlPPH-GFP). The sequence of the predicted *SlPPH* complementary DNA (cDNA) contained two possible in-frame start codons (underlined Met residues in Fig. 3B); however, none of these encoded a PPH version that would contain an N-terminal chloroplast transit peptide according to the prediction by ChloroP (Emanuelsson et al., 1999). Therefore, both varieties, SlPPH(long) and SlPPH(short), were cloned. The fusion proteins were transiently expressed in senescing Arabidopsis mesophyll protoplasts and analyzed by confocal laser-scanning microscopy. As shown in Figure 4, the overlay of GFP fluorescence and chlorophyll autofluorescence indicated that the long SlPPH version localized to the chloroplast, while the GFP signal of the short version was detected in the cytosol. From these results, we conclude that SlPPH is indeed located in the chloroplast and that SlPPH(long) represents the full-length SlPPH version, with a likely 61-amino acid chloroplast transit peptide as predicted by ChloroP (Emanuelsson et al., 1999; Fig. 3B).

SlPPH Is a Genuine PPH

Phylogenetic analysis and sequence alignment of PPH homologs revealed the PPH motif including the proposed active-site Ser residue to be present in SlPPH (Fig. 3B). This indicated that SlPPH is a genuine PPH and, thus, an ortholog of Arabidopsis PPH (Schelbert et al., 2009). To confirm this, the Arabidopsis *pph-1* mutant was complemented with an *SlPPH* cDNA construct (long version) under the control of the cauliflower mosaic virus (CaMV) 35S promoter. As shown earlier, *pph-1* is impaired in chlorophyll breakdown and shows a stay-green phenotype (Schelbert et al., 2009). To induce senescence, detached T1 leaves of three independent complementation lines (*pph-1/35S::SlPPH_1*, *pph-1/35S::SlPPH_2*, and *pph-1/35S::SlPPH_10*) were dark incubated for 7 d. Indeed, ectopic expression of SlPPH complemented the *pph-1* phenotype, and leaves of all three tested lines showed leaf yellowing comparable to the wild type (Fig. 5A). To further verify the function of SlPPH as PPH, we examined the enzymatic activity of a recombinant truncated version of SlPPH devoid of the predicted chloroplast transit peptide (ΔSlPPH). ΔSlPPH was expressed in *Escherichia coli* as an N-terminal maltose-binding protein fusion (MBP-ΔSlPPH). The recombinant fusion protein was highly stable and largely located in the soluble bacterial cell fraction (Fig. 5B). Using chlorophyll *a* or pheophytin *a*, or mixtures of both as substrate, we could confirm SlPPH to be highly specific for pheophytin *a* (Fig. 5, C and D), comparable to its Arabidopsis ortholog (Schelbert et al., 2009). These

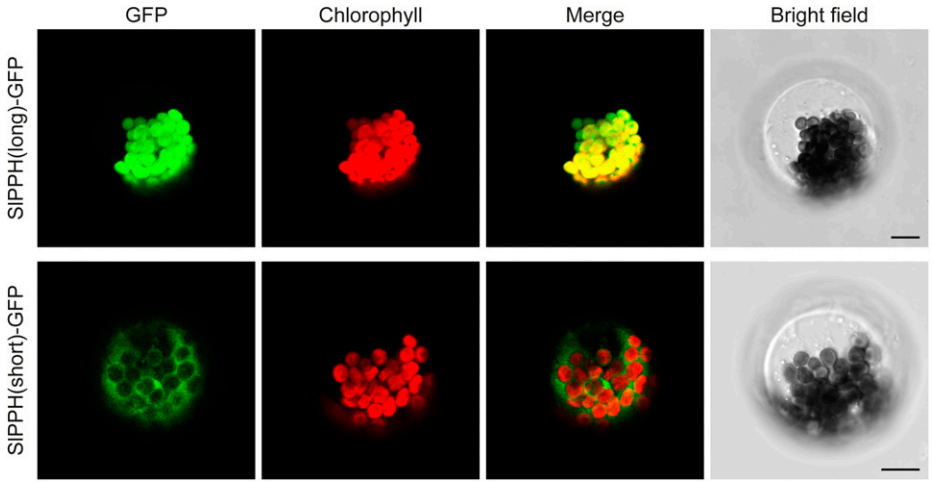

Figure 4. Subcellular localization of SlPPH. Two SlPPH varieties, SlPPH(long) and SlPPH(short), were transiently expressed as GFP fusions in Arabidopsis protoplasts isolated from senescent leaves. GFP fluorescence (GFP) and chlorophyll autofluorescence (chlorophyll) were examined by confocal laser-scanning microscopy. Merged images show the overlay of GFP and autofluorescence. Bars = 10 μm.

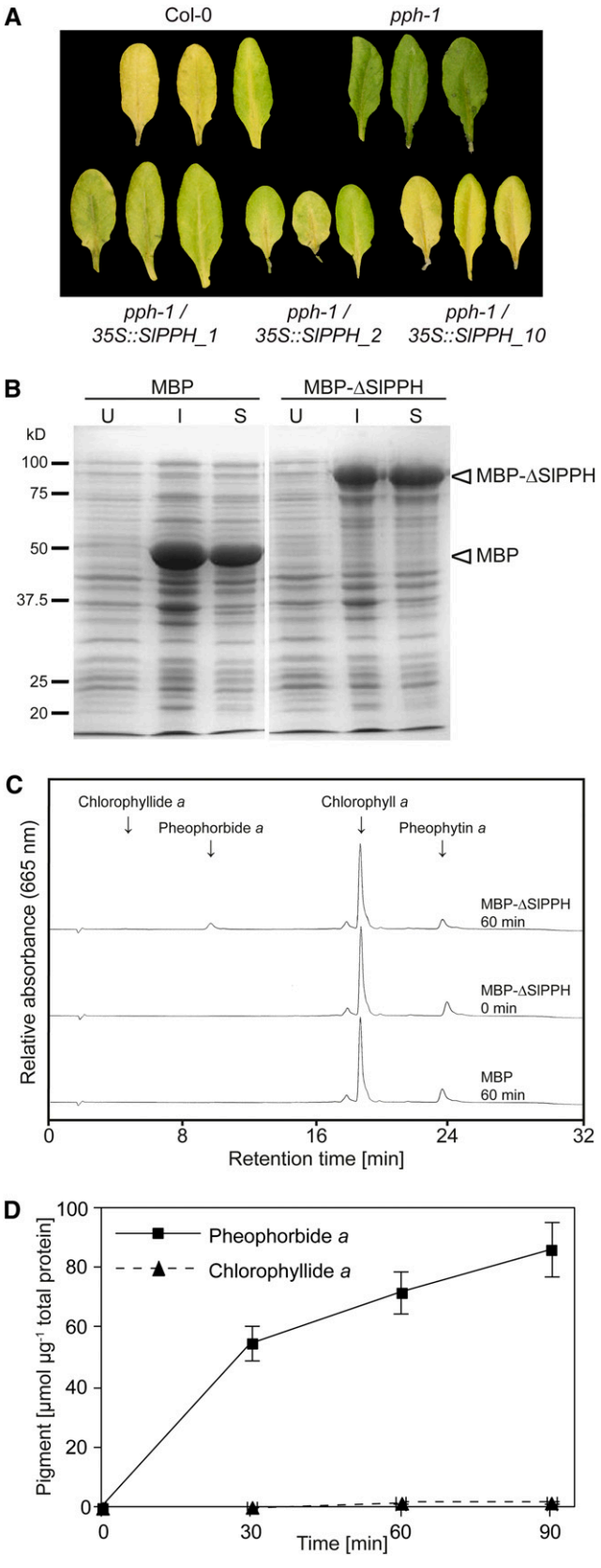

Figure 5. Confirmation of SlPPH as a genuine PPH. A, Complementation of Arabidopsis *pph-1* with SlPPH. Detached leaves of 4-week-old plants of three independent transformants (*pph-1/35S::SlPPH_1*, *pph-1/35S::SlPPH_2*, and *pph-1/35S::SlPPH_10*) in the T1 generation were dark incubated for 7 d. Col-0, Columbia-0. B to D, Analysis of recombinant SlPPH. B, Heterologous expression of MBP and MBP-ΔSlPPH fusion proteins in *E. coli*. U, Cells before induction with isopropylthio-β-galactoside; I, cells after isopropylthio-β-galactoside induction for 3 h; S, soluble cell fraction after lysis. Note that MBP-ΔSlPPH was largely retained in the soluble cell fraction. Molecular size markers (kD) are indicated on the left. C, HPLC analysis of 60-min assays employing soluble *E. coli* lysates expressing MBP-ΔSlPPH or MBP alone with mixtures of chlorophyll *a* and pheophytin *a* as substrate. Note that SlPPH specifically hydrolyzed pheophytin *a* to pheophorbide *a*, although chlorophyll *a* was present in excess. Arrows indicate HPLC retention times of substrates and the respective dephytylated products. D, Time-dependent formation of pheophorbide *a* and chlorophyllide *a* from pheophytin *a* and chlorophyll *a*, respectively, in assays with MBP-ΔSlPPH. Note that the activity of MBP-ΔSlPPH with chlorophyll *a* as substrate is marginal. Data are means ± SD of three assays.

data strongly support the assumption that SlPPH acts as genuine PPH.

SlPPH Catalyzes the Cleavage of Phytol in Senescing Tomato Leaves

To analyze whether SlPPH is required for in vivo chlorophyll breakdown in tomato, transgenic tomato plants were generated that harbored an *SlPPH*-silencing construct expressed under the control of the CaMV 35S promoter (*SlPPHi*). Levels of *SlPPH* expression of several independent transgenic tomato lines were determined in leaf and fruit tissues by semiquantitative RT-PCR and qPCR (Supplemental Fig. S1). Several independent RNA interference (RNAi) lines displayed strongly reduced *SlPPH* expression as compared with the wild type, and lines *SlPPHi_17* and *SlPPHi_27*, with expression levels of less than 16% and 7%, respectively, in leaves and fruits at breaker + 1 d were chosen for further analysis.

To elucidate whether the absence of SlPPH causes a stay-green phenotype during chlorophyll breakdown in leaves as described for Arabidopsis (Schelbert et al., 2009), senescence was initiated in detached leaves of the wild type, *gf*, *SlPPHi_17*, and *SlPPHi_27* by dark incubation for up to 10 d in the presence of 1 mM ethephon, a precursor of ethylene. After 6 d, visual yellowing (Fig. 6A) and decrease of chlorophyll *a* and *b* (Fig. 6B) were observed in wild-type leaves, while leaves of *gf* and the two silencing lines still appeared green and chlorophyll degradation was significantly delayed. Thus, after 10 d, chlorophyll content was decreased to less than 50% in the wild type, whereas in *gf*, *SlPPHi_17*, and *SlPPHi_27*, approximately 70% of the initial chlorophyll was still present. In addition, HPLC analysis of pigment extracts showed that pheophytin accumulated in both analyzed RNAi lines after 6 and 10 d of dark incubation (Fig. 6C). By contrast, pheophytin was detected in only marginal amounts in wild-type and *gf* leaves. This was in agreement with the in vitro substrate specificity of SlPPH for

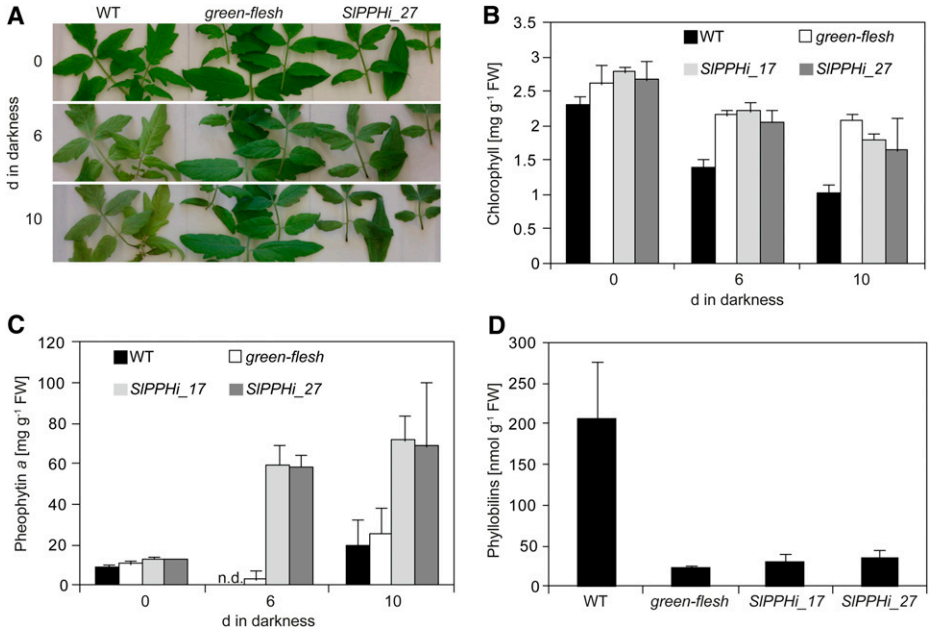

Figure 6. Silencing of *SlPPH* results in a stay-green phenotype in senescing tomato leaves. A, Leaf phenotype after 0, 6, and 10 d of ethylene-induced senescence in the dark. B to D, Pigment composition in senescing tomato leaves. B, Quantification of total chlorophyll. C, Quantification of pheophytin *a*. Note that pheophytin *a* was not detected (n.d.) in the wild type (WT) after 6 d of dark incubation. D, Quantification of phyllobilins after 10 d of dark incubation. All data are means of three biological replicates ± SD. FW, Fresh weight.

pheophytin (Fig. 5) and comparable to the effect in the Arabidopsis *pph-1* mutant (Schelbert et al., 2009).

In Arabidopsis and many other species, nonfluorescent phyllobilins have been shown to constitute final catabolites of chlorophyll breakdown (Hörtensteiner and Kräutler, 2011; Kräutler and Hörtensteiner, 2013). Tomato wild-type leaves accumulated large quantities of phyllobilins after 10 d of dark incubation (Fig. 6D). By contrast, in *SlPPHi_17* and *SlPPHi_27* as well as in *gf*, phyllobilins did not accumulate to the same extent (Fig. 6D), confirming the impairment of chlorophyll degradation in these lines. In summary, we conclude that SlPPH is the core hydrolytic enzyme during chlorophyll breakdown in tomato leaves and that its absence blocks the overall process of chlorophyll degradation. As a consequence, chlorophyll is retained, pheophytin accumulates, and phyllobilin abundance is largely diminished.

SlPPH Is Active during Fruit Ripening, But Other Unknown Hydrolases Are Active in Parallel

As shown in Figure 2, chlorophyll breakdown in tomato occurs during both leaf senescence and fruit ripening. Hence, we were interested in whether dephytylation in tomato fruits was also catalyzed by SlPPH, as shown for tomato leaves (Fig. 6). For this, we analyzed pigment composition in fruits of the wild type, *gf*, and the two RNAi lines *SlPPHi_17* and *SlPPHi_27* during the process of ripening at four different ripening stages: green mature, breaker, breaker + 2 d, and breaker + 4 d (Fig. 7). When compared with the wild type, the two *SlPPH*-silencing lines were retarded in chlorophyll breakdown and showed higher chlorophyll levels at the onset of ripening (breaker) and the half-ripe stage (breaker + 2 d). However, at the full-ripe stage (breaker + 4 d), the RNAi lines had lost chlorophyll comparable to the wild type. This indicated that the absence of SlPPH caused a transient retention of chlorophyll during fruit ripening but did not result in a true stay-green phenotype, as in *gf* fruits (Fig. 7A; Barry et al., 2008). The transient retardation of chlorophyll degradation in the silencing lines was accompanied by a transient accumulation of pheophytin *a*, the substrate of SlPPH, while wild-type and *gf* fruits did not accumulate pheophytin *a* at any stage of ripening (Fig. 7B). Thus, the RNAi lines accumulated up to 13-fold levels of pheophytin *a* at the breaker stage as compared with the controls. However, pheophytin *a* quantities were largely reduced at the breaker + 4 d stage in *SlPPH*-silencing fruits and were comparable to the wild type and *gf* (Fig. 7B). This transient accumulation of pheophytin *a* during the fruit ripening process implied an involvement of SlPPH in chlorophyll breakdown also during fruit ripening on the one hand; on the other hand, however, it indicated that other phytol hydrolytic activities may be involved and may compensate for the absence of PPH in the silencing lines. To address this, we performed in vitro activity assays using chromoplasts of wild-type and RNAi lines at the breaker + 2 d stage, thereby comparing pheophytin-specific activities in solubilized and non-solubilized chromoplast membranes. For different plant species, including citrus fruits, membrane solubilization has been shown to be a prerequisite for the activation of CLHs (and possibly other dephytylating activities), which are present in membranes in a latent form (Amir-Shapira et al., 1986; Matile et al., 1999). Dephytylation of pheophytin was significantly reduced by about 25% in non-solubilized chromoplasts of *SlPPHi_17* and *SlPPHi_27* when compared with the wild type (Fig. 7C). These differences likely reflect the absence of SlPPH in the RNAi lines; in addition, other dephytylating activities are present in chromoplasts. Furthermore, after solubilization,

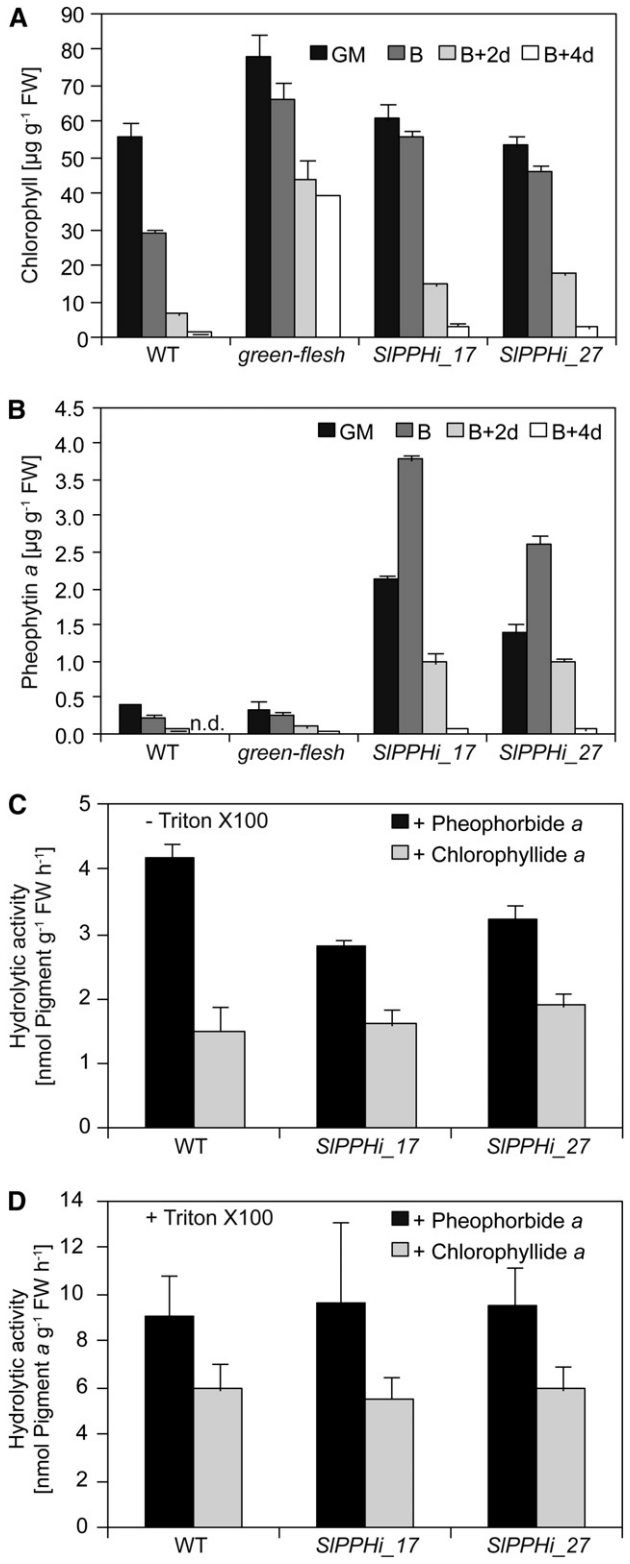

Figure 7. Analysis of SlPPH during fruit ripening. A and B, Analysis of pigment composition during fruit ripening in *SlPPH*-silencing lines. A, Quantification of total chlorophyll. Note that silencing of *SlPPH* causes a transient delay of chlorophyll degradation. B, Quantification of pheophytin *a*. Note that *SlPPH*-silencing lines transiently accumulate pheophytin *a*. GM, Green mature; B, breaker. C and D, Phytol hydrolytic activities of tomato chromoplasts at the breaker + 2 d stage. Pheophytin *a* + *b* or chlorophyll *a* + *b* was used as substrate, and the formation of the respective products (pheophorbide *a* or chlorophyllide a) was analyzed by HPLC. Note that, because the b forms of substrates were present in only small quantities in the assays, their products were not quantified. C, Hydrolytic activities in nonsolubilized chromoplasts (−Triton X-100). D, Total hydrolytic activities in solubilized chromoplasts (+Triton X-100). Data are means of three biological replicates ± SD. FW, Fresh weight; WT, wild type.

overall activity in the wild type was about twice that compared with nonsolubilized chromoplasts, but it was not different between the wild type and the silencing lines for both chlorophyll and pheophytin (Fig. 7D). This indeed supports the assumption that, besides PPH, major additional activities are present in ripening tomato fruit chromoplasts that are capable of dephytylation of either chlorophyll or pheophytin.

To test whether CLHs could be important, we analyzed tomato *CLH* (*SlCLH*) expression during leaf senescence and fruit ripening. The tomato genome contains four *CLH* genes. The deduced proteins of two of them (Solyc06g053980 = SlCLH1 and Solyc09g082600 = SlCLH3) clustered with Arabidopsis CLH2 in a phylogenetic tree, while Solyc09g06520 (SlCLH2) and Solyc12g005300 (SlCLH4) were more similar to AtCLH1 (Supplemental Fig. S2A; Lira et al., 2014). With the exception of a slight up-regulation of *SlCLH1* during leaf senescence, the expression of none of the *SlCLHs* as analyzed by semiquantitative RT-PCR correlated with the progression of leaf senescence (Supplemental Fig. S2B) or fruit ripening (Fig. 8). Transcripts for *SlCLH3* were hardly detectable. This confirmed published qPCR data on *SlCLH* expression (Lira et al., 2014). It is interesting that these results reflect the situation in Arabidopsis, where *CLH1* expression decreases during leaf senescence (Zimmermann et al., 2004; Winter et al., 2007) and PPH represents the major dephytylating activity (Schelbert et al., 2009).

DISCUSSION

The identification of pheophorbide *a* as an intermediate of chlorophyll breakdown (Hörtensteiner et al., 1995) demonstrated that dephytylation is an early step of breakdown and occurs within plastids. Phytol removal is important for two reasons: (1) it renders chlorophyll breakdown products water soluble (that is, a prerequisite for their ultimate storage in the vacuole as phyllobilins; Matile et al., 1988; Kräutler and Hörtensteiner, 2013); and (2) removal of phytol is regarded as a prerequisite for the degradation of chlorophyll-binding proteins during senescence. Thus, mutants that are incapable of phytol hydrolysis, such as Arabidopsis *pph-1* and rice *nonyellow coloring3* (*nyc3*), exhibit a stay-green phenotype during leaf senescence and retain large quantities of light-harvesting complex subunits (Morita et al., 2009; Schelbert et al., 2009). Likewise, mutations in

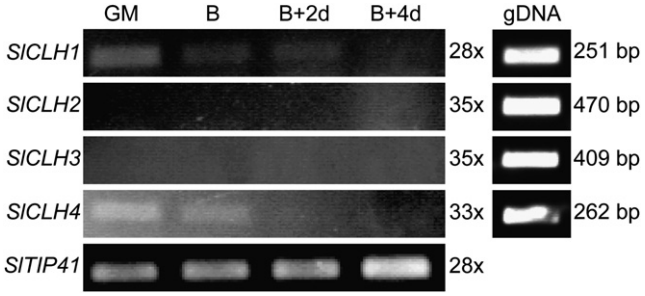

Figure 8. Gene expression analyses of *SlCLH1* to *SlCLH4* during fruit ripening in wild-type tomato. *SlTIP41* was used as a control (Expósito-Rodríguez et al., 2008). Expression was analyzed with the number of PCR cycles as indicated. PCR products were separated on agarose gels and visualized with ethidium bromide. PCR on genomic DNA (gDNA) was performed to test the efficacy of the primers used for gene expression analyses. The sizes of the fragments amplified with genomic DNA are indicated on the right. GM, Green mature; B, breaker.

steps upstream of dephytylation, such as SGR and NYC1 (that is, a CCE involved in chlorophyll *b*-to-chlorophyll *a* reduction), also result in stay-greenness coupled to apoprotein retention (Kusaba et al., 2007; Park et al., 2007; Aubry et al., 2008; Barry et al., 2008; Horie et al., 2009).

Pigment dephytylation was considered for more than a century to be catalyzed by CLHs (Willstätter and Stoll, 1913) that are able to hydrolyze both chlorophyll and pheophytin (Schelbert et al., 2009). However, their molecular identification in 1999 (Jacob-Wilk et al., 1999; Tsuchiya et al., 1999) was puzzling, since, in contrast with the predicted localization within plastid membranes, some of the cloned CLHs were suggested to localize extraplastidically and all of the identified genes encoded predicted soluble rather than membrane-localizing proteins (Takamiya et al., 2000; Hörtensteiner, 2006). Several reports that address the subcellular localization of CLHs have been published with conflicting results. Thus, the two Arabidopsis CLHs were shown to reside in the cytosol (Schenk et al., 2007), while the CLHs of citrus and *Ginkgo biloba* localize within plastids (Okazawa et al., 2006; Azoulay Shemer et al., 2008). The conflicting subcellular localization of CLHs prompted the hypothesis that additional extraplastidial breakdown pathways for chlorophyll may exist (Takamiya et al., 2000). However, demonstration that chloroplast-localized PAO, acting downstream of dephytylation, is involved in chlorophyll breakdown (Hörtensteiner et al., 1995; Sakuraba et al., 2012) and the finding that the absence of both Arabidopsis CLHs had only a marginal effect on chlorophyll breakdown (Schenk et al., 2007) challenged this idea and questioned whether CLHs are involved at all. The identification of PPH as a pheophytin-specific phytol hydrolase (Schelbert et al., 2009) supported this view, and now it is commonly accepted that PPHs rather than CLHs are responsible for leaf senescence-related chlorophyll breakdown (Tanaka et al., 2011), at least in Arabidopsis and rice. The results of this study extend this assumption to tomato, because, as in Arabidopsis *pph* mutants (Schelbert et al., 2009), leaf yellowing was largely blocked in *SlPPH*-silencing lines and significant amounts of pheophytin *a* accumulated upon senescence induction in the dark (Fig. 6). Furthermore, genes encoding highly conserved PPHs are commonly present in higher plants (Fig. 3), allowing the extrapolation that pheophytin-specific dephytylation by PPHs may be a common feature of chlorophyll breakdown during leaf senescence.

Chlorophyll breakdown, however, not only occurs during leaf senescence but also, for example, during leaf desiccation in resurrection plants (*Craterostigma pumilum* and *Xerophyta viscosa*), during fruit ripening and seed maturation (Armstead et al., 2007; Delmas et al., 2013; Christ et al., 2014). Analysis of the dephytylation step in ripening fruits has been limited nearly exclusively to *Citrus* spp. (Amir-Shapira et al., 1987; Trebitsh et al., 1993; Jacob-Wilk et al., 1999; Azoulay Shemer et al., 2008), where leaf senescence-related chlorophyll breakdown has not been studied in detail (Katz et al., 2005). We chose tomato as a model because, besides a rather short life cycle, it offers established genetic tools as well as well-defined methods for fruit ripening and leaf senescence analysis (Akhtar et al., 1999; Barry et al., 2008) and, thus, allowed the simultaneous analysis of dephytylation during leaf senescence and fruit ripening (Figs. 6 and 7). With the *SlPPH*-silencing lines produced here, we are able to demonstrate that PPH surely participates in chlorophyll breakdown also during tomato fruit ripening, but its contribution is limited. Based on activity measurements on isolated chromoplast membranes (Fig. 7), we conclude that other phytol hydrolytic activities are present in ripening tomato fruits that either naturally participate in dephytylation as well or compensate for the absence of PPH in the silencing lines. The nature of these activities remains elusive; however, CLHs appeared as possible candidates. CLHs have been shown to dephytylate chlorophyll and pheophytin in vitro (Schelbert et al., 2009). Furthermore, CLHs exhibit an intriguing latency, which requires their in vitro activation by detergents or high concentrations of solvents (Amir-Shapira et al., 1986; Matile et al., 1999). In our assays, solubilization of chromoplasts with Triton X-100 increased the overall pheophytin hydrolytic activity by about 2-fold, indicating that CLHs contribute to the overall activity. This view that tomato CLHs may participate in dephytylation and/or may substitute for PPH seems to be in agreement with studies in citrus, where CLH was shown to play a major role in fruit ripening (Trebitsh et al., 1993; Brandis et al., 1996; Jacob-Wilk et al., 1999). Thus, citrus CLH was detected in chloroplasts by in situ immunofluorescence labeling. Furthermore, the enzyme is proteolytically processed at the N- and C termini, posttranslational modifications that are unrelated to chloroplast targeting but were shown to be important for activity (Harpaz-Saad et al., 2007; Azoulay Shemer et al., 2008; Azoulay-Shemer et al., 2011). Finally, citrus *CLH* is transcriptionally up-regulated during ethylene-induced citrus ripening (Jacob-Wilk et al., 1999). Because of the

presence of four *CLH* genes in the tomato genome, analysis of CLH function during fruit ripening was beyond the scope of this work and needs to be addressed in a separate study in the future. Nevertheless, we analyzed *CLH* expression, but in contrast to *PPH* expression (Fig. 2), *CLH* transcript levels were rather low and did not correlate with the progression of fruit ripening or leaf senescence (Fig. 8; Supplemental Fig. S2B). We cannot exclude, however, the possibility that, also in tomato, CLHs may be regulated posttranscriptionally rather than at the expression level. Nevertheless, it is interesting that CLHs have not been identified in proteome analyses of tomato chromoplasts, in contrast to many CCEs, such as PPH, SGR, PAO and RCCR (Barsan et al., 2010, 2012; Wang et al., 2013), pointing to their presence, if at all, in rather low abundance.

Thus, despite the implication that CLHs may contribute to the overall phytol hydrolytic activity observed in tomato fruit chromoplasts, other explanations are possible as well. The genome of tomato, like other species (Schelbert et al., 2009), encodes several hundred α/β-hydrolases, many of which are predicted to localize to plastids. The common feature of such hydrolases is the presence of a catalytic triad with a conserved Ser residue (Tsuchiya et al., 2003), but they group into distinct protein families based on sequence similarity. As an example, both tomato PPH and CLHs belong to the α/β-hydrolases, but their overall sequence identity is below 27%. It is possible that one or several other, so far unidentified, plastid-localizing hydrolases are involved in dephytylation during chlorophyll breakdown in tomato fruits. These activities may also contribute to the remaining chlorophyll degradation activities observed in leaves of *SlPPH*-silencing lines (Fig. 6B) and Arabidopsis *pph* mutants (Schelbert et al., 2009).

This view is supported from investigations in Arabidopsis, where VITAMIN E5 (VTE5) has been shown to be responsible for the biosynthesis of 80% of α-tocopherol present in seeds (Valentin et al., 2006). VTE5 catalyzes the phosphorylation of phytol to phytyl phosphate (i.e. the first of two phosphorylation steps required to synthesize phytyl pyrophosphate for salvage into tocopherol; DellaPenna and Last, 2006; Ischebeck et al., 2006). It is commonly accepted that phytol hydrolysis of chlorophyll is a major source of phytol for tocopherol biosynthesis. Surprisingly, however, the absence of PPH, the two CLHs, or all three genes in a triple mutant does not affect seed tocopherol content in Arabidopsis (Zhang et al., 2014), pointing to a different phytol hydrolytic activity. Furthermore, triple *pph-1 clh1 clh2* mutants do not show an embryo stay-green phenotype (Zhang et al., 2014), contrary to mutants deficient in SGR or NYC1 (Nakajima et al., 2012; Delmas et al., 2013). Thus, it appears that SGR and some CCEs, such as NYC1 and PAO, are commonly active during chlorophyll degradation in different plant tissues, while PPH is active in leaf senescence but plays only a minor role during fruit ripening and seed development.

MATERIALS AND METHODS

Plant Material and Senescence Induction

Seeds of tomato (*Solanum lycopersicum*) ecotype Ailsa Craig wild type and *gf* were obtained from Yoram Eyal (Volcani Center). For analysis of fruit ripening, plants were grown in soil under nutrient-sufficient conditions; plants were kept in small pots with limited nutrient supply to induce timely leaf senescence. Growth was under long-day conditions in a greenhouse with fluence rates of 100 to 200 μmol photons m^{-2} s^{-1} at 25°C and 60% humidity. Alternatively, sterilized seeds were placed on one-half-strength Murashige and Skoog (MS) medium (2.2 g L^{-1} MS basal salt mixture, 10 g L^{-1} Suc, and 0.6% [w/v] phyotagar), and plants were grown for 4 to 6 weeks at 80 μmol photons m^{-2} s^{-1} at 21°C. Plants were subsequently transferred to soil and grown for another 5 to 6 weeks in a phytotron (12-h/12-h light/dark cycle [40 to 50 μmol photons m^{-2} s^{-1}], 60% humidity, and 22°C). For induction of senescence with ethylene, leaves of phytotron-grown plants were placed on filter paper soaked with 1 mM ethephon and incubated in the dark at room temperature. Likewise, leaves of Arabidopsis (*Arabidopsis thaliana*) Columbia-0 and *pph-1* (Schelbert et al., 2009) were placed on wet filter paper and incubated in the dark.

Analysis of Chlorophyll and Catabolites

For the determination of chlorophyll and pheophytin concentrations, pigments were extracted from tomato leaf tissue and flavedo of fruits by homogenization in liquid nitrogen and subsequent extraction into 90% (v/v) acetone and 10% (v/v) 0.2 M Tris-HCl, pH 8 (Schelbert et al., 2009; Christ et al., 2012). After centrifugation (2 min, 16,000*g*, and 4°C), supernatants were used for spectrophotometric analysis (Strain et al., 1971) or for reverse-phase HPLC (C18 Hypersil ODS column [125 × 4.0 mm, 5 μm], Linear 206 PHD-diode array detector [365–700 nm], and ChromQuest version 2.51 software [Thermo Fisher Scientific]) as described (Langmeier et al., 1993). Phyllobilins were extracted and analyzed by HPLC as described (Christ et al., 2012).

Biocomputational Methods and Phylogenetic Analysis

SlPPH (Solyc01g088090.2) and SlCLHs (SlCLH1, Solyc06g053980.2; SlCLH2, Solyc09g065620.2; SlCLH4, Solyc12g005300.1; and SlCLH3, Solyc09g082600.1) were identified by BLASTP searches (Altschul et al., 1997) with the Sol Genomics Network database (http://solgenomics.net/) using Arabidopsis PPH (AtPPH) and CLH1 (AtCLH1), respectively, as queries. Full-length protein sequences of PPH homologs from other species were identified by BLASTP searches at the National Center for Biotechnology Information (http://ncbi.nlm.nih.gov/). Phylogenetic trees (Fig. 3A; Supplemental Fig. S2A) were estimated using the maximum likelihood method (http://phylogeny.fr; Dereeper et al., 2008). Branch support values of the phylogram are based on 100 nonparametric bootstrap replicates. The sequence alignment between SlPPH and AtPPH (Fig. 3B) was performed using the program DIALIGN (http://bibiserv.techfak.uni-bielefeld.de/dialign/submission.html; Morgenstern, 2004).

Generation of Transgenic Tomato Lines and *pph-1* Complementation

cDNA derived from mature green tomato fruits was obtained from Yoram Eyal and was used to clone the full-length sequence of *SlPPH* [*SlPPH*(long)]. For silencing of *SlPPH* by RNAi, a 400-bp cDNA sense and antisense fragment of *SlPPH* was amplified using Pfu polymerase (Promega) with gene-specific primers as listed in Supplemental Table S1 and cloned in the silencing vector pHannibal (Wesley et al., 2001). A *Not*I fragment containing the silencing construct between the CaMV 35S promoter and an OCTOPINE SYNTHASE terminator was excised and subcloned into pGreen0029 (Hellens et al., 2000). For ectopic complementation of *pph-1*, full-*SlPPH*(long) was cloned in a pGreen0029-derived vector (pGr-At-RCCR; Pružinská et al., 2007) that harbors a CaMV 35S promoter and a CaMV poly(A) terminator. For that, the *Nde*I/*Eco*RI insert of pGr-At-RCCR was replaced with a PCR-amplified (for primers, see Supplemental Table S1), *Nde*I/*Eco*RI-restricted fragment containing *SlPPH*(long). After verifying the inserts by sequencing, both constructs were transformed into *Agrobacterium tumefaciens* strain GV3101 together with pSOUP (Hellens et al., 2000). Arabidopsis *pph-1* mutants were transformed by the floral dip method (Clough and Bent, 1998). Transformants were selected on kanamycin, and plants of the T1 generation were used for further experiments.

To generate *SlPPH*-silencing tomato lines, seeds were sterilized with 1.2% (v/v) sodium hypochlorite for 15 min. Seeds were rinsed three times with sterile water

and placed on medium (one-half-strength MS, 1.5% [w/v] Suc, and 0.8% [w/v] phytagar) in 10-cm-high sterile glass pots. After 9 to 12 d of growth under long-day conditions in a culture room at 80 μmol photons m^{-2} s^{-1} at 21°C, cotyledons were excised by removing 2 to 3 mm of the leaf blades from both the proximal and distal ends. Cotyledons were placed upside down in petri dishes containing D1 medium (4.4 g L^{-1} MS salts including B5 vitamins, 30 g L^{-1} Glc, 1 mg L^{-1} zeatin, 0.1 mg L^{-1} naphthyl acetic acid, 1 mg L^{-1} folic acid, 2 mM MES-KOH, pH 5.6–5.7, and 8 g L^{-1} phytagar) and incubated in the culture room for 2 d. *A. tumefaciens* cells harboring the silencing construct were grown overnight at 28°C. Cells of a 20-mL culture were collected by centrifugation (6,000*g* for 15 min), and the pellet was resuspended in MSO-KOH, pH 5.6 (4.4 g L^{-1} MS salts including B5 vitamins and 20 g L^{-1} Suc) to an optical density at 600 nm of 0.4 to 0.5. Acetosyringone (100 μM) was added, and the culture was grown for another 2 h at 28°C. For transformation, cotyledons were incubated with the bacterial culture for 2 h in the dark. After another 2 to 3 d of cultivation on D1 medium, the cotyledons were transferred to D1 medium containing kanamycin (75 mg L^{-1}) and timenten (100 mg L^{-1}). Shoot regeneration was detected after about 30 d, and respective plantlets were then transferred to DL medium (4.4 g L^{-1} MS salts including B5 vitamins, 20 g L^{-1} Glc, 2 mg L^{-1} indole-3-butyric acid, 1 mg L^{-1} folic acid, 2 mM MES-KOH, pH 5.6–5.7, and 8 g L^{-1} agar) for root induction. Rescued transformants were transferred to soil.

GFP Fusion Protein Analysis

Both *SlPPH* cDNA varieties, *SlPPH*(long) and *SlPPH*(short), were amplified using PCR Extender polymerase (5Prime) with the gene-specific primers listed in Supplemental Table S1. After restriction digestion with *Xma*I, the fragment was cloned into the corresponding site of pUC18-spGFP6 (Meyer et al., 2006), thereby producing C-terminal fusions of SlPPH with GFP (SlPPH-GFP). Sequence accuracy was confirmed by sequencing. Mesophyll protoplasts were isolated from leaves of Arabidopsis (Columbia-0) grown under short-day conditions according to published procedures (Endler et al., 2006). Leaves were incubated in the dark for 3 d prior to protoplast isolation. Cell numbers were quantified with a Neubauer chamber, and density was adjusted to 2×10^6 protoplasts mL^{-1}. Transformation of protoplasts was performed with 20% (w/v) polyethylene glycol as published (Meyer et al., 2006). Transformed protoplasts were incubated in the dark at room temperature for 24 to 48 h prior to confocal laser-scanning microscopic analysis (Leica TCS SP5; Leica Microsystems). GFP fluorescence was imaged at an excitation wavelength of 488 nm, and the emission signal was detected between 495 and 530 nm for GFP and between 643 and 730 nm for chlorophyll autofluorescence.

RNA Isolation, Semiquantitative RT-PCR, and qPCR

For semiquantitative RT-PCR, total RNA was extracted from leaf tissues or the flavedo of fruits using TRIzol according to the manufacturer's instructions (Life Technologies). Polyvinylpolypyrrolidone was added to ground tissue for extraction. After DNA digestion with RQ1 DNase (Promega), first-strand cDNA was synthesized from total RNA using either the RETROscript kit (Life Technologies) or Moloney murine leukemia virus reverse transcriptase (Promega) and oligo$(dT)_{15}$ primers (Promega). PCR was performed with gene-specific primers as listed in Supplemental Table S1. To control primer suitability for RT-PCR analysis, PCR was run with genomic DNA extracted from tomato fruits. Tomato *type 2A-interacting protein41* (*SlTIP41*) (Solyc10g049850.1) was used as the control gene (Expósito-Rodríguez et al., 2008).

RNA extraction for qPCR analysis and qPCR were performed as described (Quadrana et al., 2013). The PCR primers used are listed in Supplemental Table S1. All reactions were performed with two technical replicates and at least three biological replicates. mRNA levels were quantified using the 7500 Real-Time PCR system (Applied Biosystems) and SYBR Green Master Mix (Applied Biosystems). Data were analyzed with LinRegPCR software (Ruijter et al., 2009) to obtain cycle threshold values and to calculate primer efficiency. Expression values were normalized to the mean of two constitutively expressed genes, *TIP41* and *EXPRESSED* (Solyc07g025390.2.1; Expósito-Rodríguez et al., 2008). A permutation test, which lacks sample distribution assumptions (Pfaffl et al., 2002), was used to detect statistical ($P < 0.05$) differences in expression levels between samples using the algorithms in the fgStatistics software (http://sites.google.com/site/fgStatistics/).

Analysis of Recombinant SlPPH

For heterologous expression of SlPPH in *Escherichia coli*, a truncated cDNA fragment, lacking the 61 5′-terminal amino acids encoding the likely chloroplast transit peptide, was produced by PCR using Extender polymerase (5Prime) with primers as listed in Supplemental Table S1. After restriction digestion with *Eco*RI, the fragment was cloned into pMal_c2 (New England Biolabs), producing a truncated MBP-SlPPH fusion (MBP-ΔSlPPH). After verifying the insert by sequencing, the construct was transformed into *E. coli* BL21(DE3). Recombinant SlPPH protein was expressed and cells were lysed as described (Schelbert et al., 2009). PPH activity assays (300 μL) were performed with 15 μL of crude protein extract (approximately 130 μg of soluble protein), 0.1 mM pheophytin *a* and/or chlorophyll *a* (final acetone concentration, 6.7% [v/v]), and 0.1 M HEPES-KOH, pH 8, containing 1 mM EDTA. In assays with substrate mixtures, pheophytin *a* and chlorophyll *a* were present at concentrations of 35 and 65 μM, respectively. After incubation at 34°C for various time periods, reactions were stopped by adding 2 volumes of acetone and analyzed by reverse-phase HPLC as described (Schelbert et al., 2009). Pheophytin *a* was produced from pure chlorophyll *a* (LivChem) by acidification as described (Schelbert et al., 2009).

Chromoplast Isolation and Activity Measurements

Chromoplasts of tomato mesocarp tissue at the breaker + 2 d stage were isolated as published for red pepper (*Capsicum annuum*; Christ et al., 2012) with some modifications. Mesocarp tissue was blended in a Sorvall mixer three times for 5 s with isolation buffer (1 mL g^{-1} fresh weight) containing 400 mM Suc, 50 mM Tris-MES, pH 8, 2 mM EDTA, 10 mM polyethylene glycol 4000, 5 mM dithiothreitol, and 5 mM L(+)-ascorbic acid. Subsequently, the suspension was filtered through two layers of gauze and centrifuged (10 min at 12,000*g*). The pellet was carefully resuspended in isolation buffer (1 mL g^{-1} fresh weight). After repeating the centrifugation step, chromoplasts were resuspended in Tris-MES buffer (0.05 mL g^{-1} fresh weight) containing 25 mM Tris-MES, pH 8, and 5 mM L(+)-ascorbic acid. Isolated chromoplasts were divided into two fractions and either supplemented with 0.1 volume of Tris-MES buffer containing 10% (v/v) Triton X-100 to obtain a final Triton X-100 concentration of 1% (v/v) (+Triton X-100) or chromoplasts were supplemented with 0.1 volume of Tris-MES buffer (−Triton X-100). Both chromoplast fractions were incubated with rotation in the dark at 4°C for 30 min. Aliquots of isolated chromoplasts were frozen in liquid nitrogen and stored at −80°C. Phytol hydrolysis assays (total volume of 100 μL) consisted of 10 μL of chromoplasts (corresponding to 0.2 g fresh weight), 70 μM pheophytin *a*/*b* or chlorophyll *a*/*b*, with about 10-fold excess of the *a* pigment in both cases (3% [v/v] final acetone concentration) and reaction buffer (0.1 M HEPES-KOH, pH 8, and 1 mM EDTA). After incubation at 34°C for 45 min, reactions were stopped by adding 2 volumes of acetone. After centrifugation (16,000*g* for 2 min), samples were analyzed by reverse-phase HPLC as described (Langmeier et al., 1993). Substrate production and quantification were performed as described (Schelbert et al., 2009).

GenBank or Sol Genomics Network (http://solgenomics.net/) identification numbers for the DNA/protein sequences used in this work are as follows. PPH sequences: *Aegilops tauschii*, 475611823; *Amborella trichopoda*, 548840076; *Arabidopsis lyrata*, 297811489; Arabidopsis, 15240707 (AtPPH, At5g13800); *Brachypodium distachyon*, 357123819; *Capsella rubella*, 565459260; *Cicer arietinum*, 502127590; *Citrus clementina*, 567892823; *Citrus sinensis*, 568858818; *Cucumis sativus*, 449436343; *Eutrema salsugineum*, 567173584; *Fragaria vesca*, 470134497; *Genlisea aurea*, 527208569; soybean, 356539136 (Glyma1), 356531629 (Glyma2), 356542875 (Glyma3); barley, 326498881; *Lotus japonicus*, 388497996; *Medicago truncatula*, 357458507; *Nicotiana tabacum*, 156763846; *Oryza brachyantha*, 573959173; rice, 115467988; common bean, 561022305 (Phavu1), 561004436 (Phavu2); *Populus trichocarpa*, 224106163; *Prunus persica*, 462415467; *Setaria italica*, 514804304; tomato, 460367643 (SlPPH, Solyc01g088090.2); *Solanum tuberosum*, 565357100; *Sorghum bicolor*, 242060434; *Theobroma cacao*, 508704687; *Triticum urartu*, 473998920; *Vitis vinifera*, 225449963; and *Zea mays*, 226530215. Additional sequences for Arabidopsis: AtCLH1, 30912637 (At1g19670); AtCLH2, 30912739 (At5g43860); SGR, 75100772 (At4g22920); and PAO, 41688605 (At3g44880). Additional sequences for tomato: SlCLH1, 460390857 (Solyc06g053980.2); SlCLH2, 460403437 (Solyc09g065620.2); SlCLH4, 460412186 (Solyc12g005300.1); SlCLH3 (Solyc09g082600.1); SlTIP41, 460406627 (Solyc10g049850.1); and EXPRESSED, 460394765 (Solyc07g025390.2.1).

Supplemental Data

The following materials are available in the online version of this article.

Supplemental Figure S1. Expression analysis of *SlPPH* in *SlPPH*-silencing lines.

Supplemental Figure S2. Analysis of tomato CLHs.

Supplemental Table S1. List of primers used in this study.

ACKNOWLEDGMENTS

We thank Yoram Eyal for providing tomato seeds and cDNA, and gardeners Christian Frey and Kari Huwiler, for taking care of the plants.

Received March 14, 2014; accepted July 3, 2014; published July 17, 2014.

LITERATURE CITED

Akhtar MS, Goldschmidt EE, John I, Rodoni S, Matile P, Grierson D (1999) Altered patterns of senescence and ripening in *gf*, a stay-green mutant of tomato (*Lycopersicon esculentum* Mill.). J Exp Bot **50:** 1115–1122

Altschul SF, Madden TL, Schaffer AA, Zhang JH, Zhang Z, Miller W, Lipman DJ (1997) Gapped BLAST and PSI-BLAST: a new generation of protein database search programs. Nucl Acids Res **25:** 3389–3402

Amir-Shapira D, Goldschmidt E, Altman A (1986) Autolysis of chlorophyll in aqueous and detergent suspensions of chloroplast fragments. Plant Sci **43:** 201–206

Amir-Shapira D, Goldschmidt EE, Altman A (1987) Chlorophyll catabolism in senescing plant tissues: *in vivo* breakdown intermediates suggest different degradative pathways for *Citrus* fruit and parsley leaves. Proc Natl Acad Sci USA **84:** 1901–1905

Armstead I, Donnison I, Aubry S, Harper J, Hörtensteiner S, James C, Mani J, Moffet M, Ougham H, Roberts L, et al (2007) Cross-species identification of Mendel's *I* locus. Science **315:** 73

Aubry S, Mani J, Hörtensteiner S (2008) Stay-green protein, defective in Mendel's green cotyledon mutant, acts independent and upstream of pheophorbide *a* oxygenase in the chlorophyll catabolic pathway. Plant Mol Biol **67:** 243–256

Azoulay Shemer T, Harpaz-Saad S, Belausov E, Lovat N, Krokhin O, Spicer V, Standing KG, Goldschmidt EE, Eyal Y (2008) Citrus chlorophyllase dynamics at ethylene-induced fruit color-break: a study of chlorophyllase expression, posttranslational processing kinetics, and in situ intracellular localization. Plant Physiol **148:** 108–118

Azoulay-Shemer T, Harpaz-Saad S, Cohen-Peer R, Mett A, Spicer V, Lovat N, Krokhin O, Brand A, Gidoni D, Standing KG, et al (2011) Dual N- and C-terminal processing of citrus chlorophyllase precursor within the plastid membranes leads to the mature enzyme. Plant Cell Physiol **52:** 70–83

Barry CS (2009) The stay-green revolution: recent progress in deciphering the mechanisms of chlorophyll degradation in higher plants. Plant Sci **176:** 325–333

Barry CS, McQuinn RP, Chung MY, Besuden A, Giovannoni JJ (2008) Amino acid substitutions in homologs of the STAY-GREEN protein are responsible for the *green-flesh* and *chlorophyll retainer* mutations of tomato and pepper. Plant Physiol **147:** 179–187

Barsan C, Sanchez-Bel P, Rombaldi C, Egea I, Rossignol M, Kuntz M, Zouine M, Latché A, Bouzayen M, Pech JC (2010) Characteristics of the tomato chromoplast revealed by proteomic analysis. J Exp Bot **61:** 2413–2431

Barsan C, Zouine M, Maza E, Bian W, Egea I, Rossignol M, Bouyssie D, Pichereaux C, Purgatto E, Bouzayen M, et al (2012) Proteomic analysis of chloroplast-to-chromoplast transition in tomato reveals metabolic shifts coupled with disrupted thylakoid biogenesis machinery and elevated energy-production components. Plant Physiol **160:** 708–725

Borovsky Y, Paran I (2008) Chlorophyll breakdown during pepper fruit ripening in the *chlorophyll retainer* mutation is impaired at the homolog of the senescence-inducible stay-green gene. Theor Appl Genet **117:** 235–240

Brandis A, Vainstein A, Goldschmidt EE (1996) Distribution of chlorophyllase among components of chloroplast membranes in *Citrus sinensis* organs. Plant Physiol Biochem **34:** 49–54

Chen LFO, Lin CH, Kelkar SM, Chang YM, Shaw JF (2008) Transgenic broccoli (*Brassica oleracea* var. *italicia*) with antisense chlorophyllase (*BoCLH1*) delays postharvest yellowing. Plant Sci **174:** 25–31

Christ B, Egert A, Süssenbacher I, Kräutler B, Bartels D, Peters S, Hörtensteiner S (2014) Water deficit induces chlorophyll degradation via the 'PAO/phyllobilin' pathway in leaves of homoio- (*Craterostigma pumilum*) and poikilochlorophyllous (*Xerophyta viscosa*) resurrection plants. Plant Cell Environ (in press)

Christ B, Hörtensteiner S (2014) Mechanism and significance of chlorophyll breakdown. J Plant Growth Regul **33:** 4–20

Christ B, Schelbert S, Aubry S, Süssenbacher I, Müller T, Kräutler B, Hörtensteiner S (2012) MES16, a member of the methylesterase protein family, specifically demethylates fluorescent chlorophyll catabolites during chlorophyll breakdown in Arabidopsis. Plant Physiol **158:** 628–641

Clough SJ, Bent AF (1998) Floral dip: a simplified method for *Agrobacterium*-mediated transformation of *Arabidopsis thaliana*. Plant J **16:** 735–743

DellaPenna D, Last RL (2006) Progress in the dissection and manipulation of plant vitamin E biosynthesis. Physiol Plant **126:** 356–368

Delmas F, Sankaranarayanan S, Deb S, Widdup E, Bournonville C, Bollier N, Northey JG, McCourt P, Samuel MA (2013) ABI3 controls embryo degreening through Mendel's I locus. Proc Natl Acad Sci USA **110:** E3888–E3894

Dereeper A, Guignon V, Blanc G, Audic S, Buffet S, Chevenet F, Dufayard J-F, Guindon S, Lefort V, Lescot M, et al (2008) Phylogeny.fr: robust phylogenetic analysis for the non-specialist. Nucl Acids Res **36:** W465–469

Egea I, Barsan C, Bian W, Purgatto E, Latché A, Chervin C, Bouzayen M, Pech J-C (2010) Chromoplast differentiation: current status and perspectives. Plant Cell Physiol **51:** 1601–1611

Emanuelsson O, Nielsen H, von Heijne G (1999) ChloroP, a neural network-based method for predicting chloroplast transit peptides and their cleavage sites. Protein Sci **8:** 978–984

Endler A, Meyer S, Schelbert S, Schneider T, Weschke W, Peters SW, Keller F, Baginsky S, Martinoia E, Schmidt UG (2006) Identification of a vacuolar sucrose transporter in barley and Arabidopsis mesophyll cells by a tonoplast proteomic approach. Plant Physiol **141:** 196–207

Expósito-Rodríguez M, Borges AA, Borges-Pérez A, Pérez JA (2008) Selection of internal control genes for quantitative real-time RT-PCR studies during tomato development process. BMC Plant Biol **8:** 131

Harpaz-Saad S, Azoulay T, Arazi T, Ben-Yaakov E, Mett A, Shiboleth YM, Hörtensteiner S, Gidoni D, Gal-On A, Goldschmidt EE, et al (2007) Chlorophyllase is a rate-limiting enzyme in chlorophyll catabolism and is post-translationally regulated. Plant Cell **19:** 1007–1022

Hellens R, Edwards EA, Leyland NR, Bean S, Mullineaux PM (2000) pGreen: a versatile and flexible binary Ti vector for *Agrobacterium*-mediated plant transformation. Plant Mol Biol **42:** 819–832

Hendry GAF, Houghton JD, Brown SB (1987) The degradation of chlorophyll: a biological enigma. New Phytol **107:** 255–302

Horie Y, Ito H, Kusaba M, Tanaka R, Tanaka A (2009) Participation of chlorophyll *b* reductase in the initial step of the degradation of light-harvesting chlorophyll *a*/*b*-protein complexes in *Arabidopsis*. J Biol Chem **284:** 17449–17456

Hörtensteiner S (2006) Chlorophyll degradation during senescence. Annu Rev Plant Biol **57:** 55–77

Hörtensteiner S (2009) Stay-green regulates chlorophyll and chlorophyll-binding protein degradation during senescence. Trends Plant Sci **14:** 155–162

Hörtensteiner S (2013) Update on the biochemistry of chlorophyll breakdown. Plant Mol Biol **82:** 505–517

Hörtensteiner S, Kräutler B (2011) Chlorophyll breakdown in higher plants. Biochim Biophys Acta **1807:** 977–988

Hörtensteiner S, Vicentini F, Matile P (1995) Chlorophyll breakdown in senescent cotyledons of rape, *Brassica napus* L.: enzymatic cleavage of phaeophorbide *a in vitro*. New Phytol **129:** 237–246

Ischebeck T, Zbierzak AM, Kanwischer M, Dörmann P (2006) A salvage pathway for phytol metabolism in *Arabidopsis*. J Biol Chem **281:** 2470–2477

Jacob-Wilk D, Holland D, Goldschmidt EE, Riov J, Eyal Y (1999) Chlorophyll breakdown by chlorophyllase: isolation and functional expression of the *Chlase1* gene from ethylene-treated *Citrus* fruit and its regulation during development. Plant J **20:** 653–661

Katz E, Riov J, Weiss D, Goldschmidt EE (2005) The climacteric-like behaviour of young, mature and wounded citrus leaves. J Exp Bot **56:** 1359–1367

Kräutler B (2008) Chlorophyll breakdown and chlorophyll catabolites in leaves and fruit. Photochem Photobiol Sci **7:** 1114–1120

Kräutler B, Hörtensteiner S (2013) Chlorophyll breakdown: chemistry, biochemistry and biology. *In* GC Ferreira, KM Kadish, KM Smith, R Guilard, eds, Handbook of Porphyrin Science, Vol 28. World Scientific Publishing, Hackensack, NJ, pp 117–185

Kräutler B, Jaun B, Bortlik KH, Schellenberg M, Matile P (1991) On the enigma of chlorophyll degradation: the constitution of a secoporphinoid catabolite. Angew Chem Int Ed Engl **30:** 1315–1318

Kusaba M, Ito H, Morita R, Iida S, Sato Y, Fujimoto M, Kawasaki S, Tanaka R, Hirochika H, Nishimura M, et al (2007) Rice NON-YELLOW COLORING1 is involved in light-harvesting complex II and grana degradation during leaf senescence. Plant Cell **19:** 1362–1375

Langmeier M, Ginsburg S, Matile P (1993) Chlorophyll breakdown in senescent leaves: demonstration of Mg-dechelatase activity. Physiol Plant **89:** 347–353

Lira BS, de Setta N, Rosado D, Almeida J, Freschi L, Rossi M (2014) Plant degreening: evolution and expression of tomato (*Solanum lycopersicum*) dephytylation enzymes. Gene **546:** 359–366

Luo ZD, Zhang JH, Li JH, Yang CX, Wang TT, Ouyang B, Li HX, Giovannoni J, Ye ZB (2013) A STAY-GREEN protein SlSGR1 regulates lycopene and beta-carotene accumulation by interacting directly with SlPSY1 during ripening processes in tomato. New Phytologist **198:** 442–452

Matile P, Ginsburg S, Schellenberg M, Thomas H (1988) Catabolites of chlorophyll in senescing barley leaves are localized in the vacuoles of mesophyll cells. Proc Natl Acad Sci USA **85:** 9529–9532

Matile P, Hörtensteiner S, Thomas H (1999) Chlorophyll degradation. Annu Rev Plant Physiol Plant Mol Biol **50:** 67–95

Meyer A, Eskandari S, Grallath S, Rentsch D (2006) AtGAT1, a high affinity transporter for g-aminobutyric acid in *Arabidopsis thaliana*. J Biol Chem **281:** 7197–7204

Morgenstern B (2004) DIALIGN: multiple DNA and protein sequence alignment at BiBiServ. Nucleic Acids Res **32:** W33–W36

Morita R, Sato Y, Masuda Y, Nishimura M, Kusaba M (2009) Defect in non-yellow coloring 3, an α/β hydrolase-fold family protein, causes a stay-green phenotype during leaf senescence in rice. Plant J **59:** 940–952

Moser D, Matile P (1997) Chlorophyll breakdown in ripening fruits of *Capsicum annuum*. J Plant Physiol **150:** 759–761

Moser S, Müller T, Holzinger A, Lütz C, Jockusch S, Turro NJ, Kräutler B (2009) Fluorescent chlorophyll catabolites in bananas light up blue halos of cell death. Proc Natl Acad Sci USA **106:** 15538–15543

Mühlecker W, Ongania KH, Kräutler B, Matile P, Hörtensteiner S (1997) Tracking down chlorophyll breakdown in plants: elucidation of the constitution of a 'fluorescent' chlorophyll catabolite. Angew Chem Int Ed Engl **36:** 401–404

Nakajima S, Ito H, Tanaka R, Tanaka A (2012) Chlorophyll *b* reductase plays an essential role in maturation and storability of Arabidopsis seeds. Plant Physiol **160:** 261–273

Okazawa A, Tango L, Itoh Y, Fukusaki E, Kobayashi A (2006) Characterization and subcellular localization of chlorophyllase from *Ginkgo biloba*. Z Naturforsch C **61:** 111–117

Park SY, Yu JW, Park JS, Li J, Yoo SC, Lee NY, Lee SK, Jeong SW, Seo HS, Koh HJ, et al (2007) The senescence-induced staygreen protein regulates chlorophyll degradation. Plant Cell **19:** 1649–1664

Pfaffl MW, Horgan GW, Dempfle L (2002) Relative expression software tool (REST) for group-wise comparison and statistical analysis of relative expression results in real-time PCR. Nucleic Acids Res **30:** e36

Pruzinská A, Anders I, Aubry S, Schenk N, Tapernoux-Lüthi E, Müller T, Kräutler B, Hörtensteiner S (2007) In vivo participation of red chlorophyll catabolite reductase in chlorophyll breakdown. Plant Cell **19:** 369–387

Quadrana L, Almeida J, Otaiza SN, Duffy T, Corrêa da Silva JV, de Godoy F, Asís R, Bermúdez L, Fernie AR, Carrari F, et al (2013) Transcriptional regulation of tocopherol biosynthesis in tomato. Plant Mol Biol **81:** 309–325

Ren G, An K, Liao Y, Zhou X, Cao Y, Zhao H, Ge X, Kuai B (2007) Identification of a novel chloroplast protein AtNYE1 regulating chlorophyll degradation during leaf senescence in Arabidopsis. Plant Physiol **144:** 1429–1441

Ren G, Zhou Q, Wu S, Zhang Y, Zhang L, Huang J, Sun Z, Kuai B (2010) Reverse genetic identification of CRN1 and its distinctive role in chlorophyll degradation in *Arabidopsis*. J Integr Plant Biol **52:** 496–504

Rodoni S, Mühlecker W, Anderl M, Kräutler B, Moser D, Thomas H, Matile P, Hörtensteiner S (1997) Chlorophyll breakdown in senescent chloroplasts: cleavage of pheophorbide *a* in two enzymic steps. Plant Physiol **115:** 669–676

Ruijter JM, Ramakers C, Hoogaars WM, Karlen Y, Bakker O, van den Hoff MJ, Moorman AFM (2009) Amplification efficiency: linking baseline and bias in the analysis of quantitative PCR data. Nucleic Acids Res **37:** e45

Sakuraba Y, Schelbert S, Park SY, Han SH, Lee BD, Andrès CB, Kessler F, Hörtensteiner S, Paek NC (2012) STAY-GREEN and chlorophyll catabolic enzymes interact at light-harvesting complex II for chlorophyll detoxification during leaf senescence in *Arabidopsis*. Plant Cell **24:** 507–518

Schelbert S, Aubry S, Burla B, Agne B, Kessler F, Krupinska K, Hörtensteiner S (2009) Pheophytin pheophorbide hydrolase (pheophytinase) is involved in chlorophyll breakdown during leaf senescence in *Arabidopsis*. Plant Cell **21:** 767–785

Schenk N, Schelbert S, Kanwischer M, Goldschmidt EE, Dörmann P, Hörtensteiner S (2007) The chlorophyllases AtCLH1 and AtCLH2 are not essential for senescence-related chlorophyll breakdown in *Arabidopsis thaliana*. FEBS Lett **581:** 5517–5525

Strain HH, Cope BT, Svec WA (1971) Analytical procedures for the isolation, identification, estimation and investigation of the chlorophylls. Methods Enzymol **23:** 452–476

Takamiya KI, Tsuchiya T, Ohta H (2000) Degradation pathway(s) of chlorophyll: what has gene cloning revealed? Trends Plant Sci **5:** 426–431

Tanaka A, Tanaka R (2006) Chlorophyll metabolism. Curr Opin Plant Biol **9:** 248–255

Tanaka R, Kobayashi K, Masuda T (2011) Tetrapyrrole metabolism in Arabidopsis thaliana. The Arabidopsis Book **9:** e0145, DOI: 10.1199/tab.0145

Trebitsh T, Goldschmidt EE, Riov J (1993) Ethylene induces *de novo* synthesis of chlorophyllase, a chlorophyll degrading enzyme, in *Citrus* fruit peel. Proc Natl Acad Sci USA **90:** 9441–9445

Tsuchiya T, Ohta H, Okawa K, Iwamatsu A, Shimada H, Masuda T, Takamiya K (1999) Cloning of chlorophyllase, the key enzyme in chlorophyll degradation: finding of a lipase motif and the induction by methyl jasmonate. Proc Natl Acad Sci USA **96:** 15362–15367

Tsuchiya T, Suzuki T, Yamada T, Shimada H, Masuda T, Ohta H, Takamiya K (2003) Chlorophyllase as a serine hydrolase: identification of a putative catalytic triad. Plant Cell Physiol **44:** 96–101

Valentin HE, Lincoln K, Moshiri F, Jensen PK, Qi Q, Venkatesh TV, Karunanandaa B, Baszis SR, Norris SR, Savidge B, et al (2006) The *Arabidopsis vitamin E pathway gene5-1* mutant reveals a critical role for phytol kinase in seed tocopherol biosynthesis. Plant Cell **18:** 212–224

Wang YQ, Yang Y, Fei Z, Yuan H, Fish T, Thannhauser TW, Mazourek M, Kochian LV, Wang X, Li L (2013) Proteomic analysis of chromoplasts from six crop species reveals insights into chromoplast function and development. J Exp Bot **64:** 949–961

Wesley SV, Helliwell CA, Smith NA, Wang M, Rouse DT, Liu Q, Gooding PS, Singh SP, Abbot D, Stoutjesdijk PA, et al (2001) Construct design for efficient, effective and high-throuput gene silencing in plants. Plant J **27:** 581–590

Willstätter R, Stoll A (1913) Die Wirkungen der Chlorophyllase. *In* R Willstätter, A Stoll, eds, Untersuchungen über Chlorophyll. Verlag Julius Springer, Berlin, pp 172–187

Winter D, Vinegar B, Nahal H, Ammar R, Wilson GV, Provart NJ (2007) An "Electronic Fluorescent Pictograph" browser for exploring and analyzing large-scale biological data sets. PLoS ONE **2:** e718

Zhang W, Liu TQ, Ren GD, Hörtensteiner S, Zhou YM, Cahoon EB, Zhang CY (2014) Chlorophyll degradation: the tocopherol biosynthesis related phytol hydrolase in Arabidopsis seeds is still missing. Plant Physiol (in press)

Zimmermann P, Hirsch-Hoffmann M, Hennig L, Gruissem W (2004) GENEVESTIGATOR: Arabidopsis microarray database and analysis toolbox. Plant Physiol **136:** 2621–2632

Zhou C, Han L, Pislariu C, Nakashima J, Fu C, Jiang Q, Quan L, Blancaflor EB, Tang Y, Bouton JH, et al (2011) From model to crop: functional analysis of a *STAY-GREEN* gene in the model legume *Medicago truncatula* and effective use of the gene for alfalfa improvement. Plant Physiol **157:** 1483–1496

Supplemental Table S1: *List of Primers*

Gene/construct	*Primer name*	*Sequence (5'-3')*
		RT-PCR
SlSGR	SlSGR_S	AACTCCCTGTGGTTCTCAAG
	SlSGR_AS	GGAAAGCAACAGGCACAAGC
SlPAO	SlPAO_S	GCATTCCGAAATTGGCTTAGAC
	SlPAO_AS	GCTAATCCAGCACTTATAATTGC
SlPPH	SlPPH_S	GTGTCGAATGAACAATGTACC
	SlPPH_AS	CCATTGAGAAGTCATTGATCC
SlCLH1	SlCLH1_S	GGTAGACTTGCTAGTGACCTG
	SlCLH1_AS	CAAGCTGGCTTGCAACATTCG
SlCLH2	SlCLH2_S	CTCTAAAATTCTCAGCACTCC
	SlCLH2_AS	GACCATAATCCTTAGCAAGG
SlCLH3	SlCLH3_S	CTCATGTTGGGCCAAATTTG
	SlCLH3_AS	ACCATAAGTTGCCTTTCCTC
SlCLH4	SlCLH4_S	GCTGAGTTTTTCAACGAGAG
	SlCLH4_AS	CAGGATCAAGTTTAATAGGAC
TIP41	TIP41_S	GCTGCGTTTCTGGCTTAGG
	TIP41_AS	ATGGAGTTTTTGAGTCTTCTGC
		qPCR
SlPPH	RT-PPH–F	TATGGAGGGAGCAAGTACGC
	RT-PPH-R	TGGAGGGCAGAGGAAAAGTAC
Expressed	Expressed F	GCTAAGAACGCTGGACCTAATG
	Expressed R	TGGGTGTGCCTTTCTGAATG
TIP41	TIP41 F	ATGGAGTTTTTGAGTCTTCTGC
	TIP41 R	GCTGCGTTTCTGGCTTAGG
		cloning SlPPH-GFP
SlPPH(long)	SlPPH(long)_XmaI_f	GGCCCGGGATGGAATTTTGTTCTTTCTATTCG
	SlPPH_XmaI_r	GGCCCGGGCTGGAGAGTAAACTCCATCTTG
SlPPH(short)	SlPPH(short)_XmaI_f	GGCCCGGGATGTTTTCTAGACTAAAAGAAAG
	SlPPH_XmaI_r	GGCCCGGGCTGGAGAGTAAACTCCATCTTG
		cloning MBP-ΔSlPPH
SlPPH	SlPPH_EcoRI_LP	GGAATTCGCTTCTGTTAAGGGGGTTGAC
	SlPPH_EcoRI_RP	GGAATTCTTATGGAGAGTAAACTCCATCTTG
		cloning 35S::SlPPH
SlPPH	SlPPH_Eco_RP	GGAATTCTTATGGAGAGTAAACTCCATCTTG
	SlPPH_LPNde	GTTCCATATGGAATTTTGTTCTTTCTATTCG
		cloning SlPPHi
SlPPH	SlPPH_XhoISacII_LP	CCCTCGAGCCGCGGACAACTAAATTTTAAAGAG
	SlPPH_KpnI_RP	GGGGTACCAGATTTTAGAAACATGGAAAG
	SlPPH_BamHI_LP	CGGGATCCGGACAACTAAATTTTAAAGAG
	SlPPH_ClaI_RP	CCATCGATAGATTTTAGAAACATGGAAAG

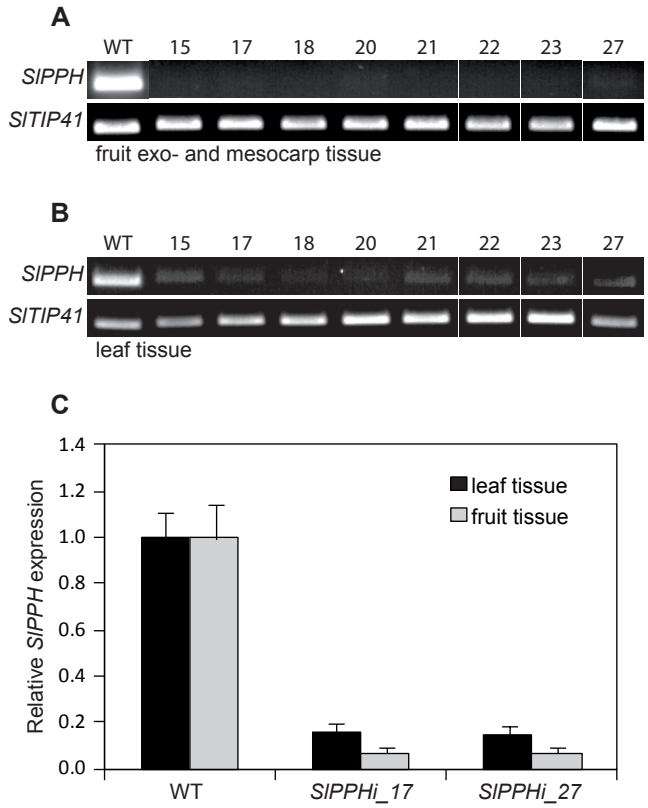

Supplemental Figure S1. Analysis of *SlPPH* expression of in SlPPH-silencing lines. A, Semi-quantitative gene expression analysis in fruits. B, Semi-quantitative gene expression analysis in leaves. *SlTIP41* was used as a control (Expósito-Rodríguez et al., 2008). PCR products were separated on agarose gels and visualized with ethidium bromide. Transgenic lines 17 and 27 were chosen for further investigations. C, Expression of *SlPPH* in lines 17 (*SlPPHi_17*) and 27 (*SlPPHi_27*), used in this study, was analyzed by qPCR in leaves and fruits at breaker + 1. Expression levels were normalized against two constitutively expressed genes *SlSIP41* and *Expressed* (Expósito-Rodríguez et al., 2008). Data are mean ± SE of at least three biological replicates with each two technical replicates.

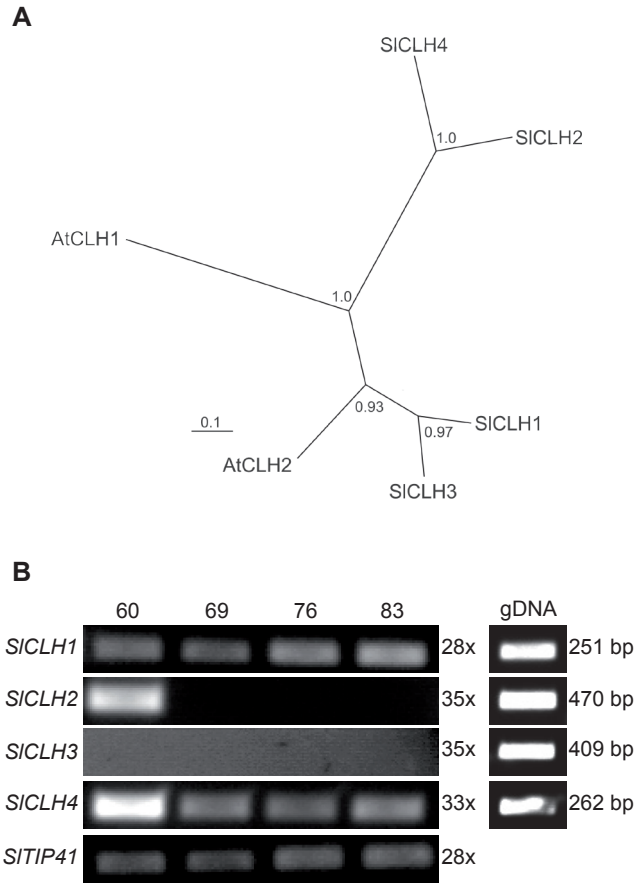

Supplemental Figure S2. Analysis of tomato chlorophyllases. A, Maximum likelihood phylogenetic tree of CLH proteins from Arabidopsis (AtCLHs) and tomato (SlCLHs). Branch support values are based on 100 bootstrap replicates. B, Analysis of gene expression of *SlCLH1-4* during natural leaf senescence in wild-type tomato starting from 60 days after germination. *SlTIP41* was used as a control (Expósito-Rodríguez et al., 2008). Expression was analyzed with the number of PCR cycles as indicated. PCR products were separated on agarose gels and visualized with ethidium bromide. PCR on genomic DNA (gDNA) isolated from tomato fruits was performed to test efficacy of the primers used for gene expression analyses. Size of the fragments amplified with gDNA is indicated on the right. Note that the results on gDNA shown here are identical to the ones shown in Figure 8.

3.2 Additional results: Dephytylation in siliques of *Arabidopsis thaliana*

3.2.1 PPH is not the sole dephytylating enzyme involved in chlorophyll breakdown in siliques of Arabidopsis

In order to investigate which dephytylating enzyme, PPH or CLH, is involved in chlorophyll breakdown in senescing siliques of Arabidopsis, siliques were incubated in the dark for up to 8 days. All siliques of the major shoots of 7 week-old plants (grown in a greenhouse with fluence rates of 100 to 200 µmol photons m^{-2} s^{-1}, 20 °C [day], 18 °C [night], 16 h light, 60% humidity) were cut and incubated on wet filter paper in the dark at room temperature. Siliques of *nye-1* served as a positive control for a stay-green phenotype in siliques (Ren et al., 2007). Pigments were extracted and analyzed as described (Das and Guyer et al., submitted). As shown in Figure A1 all investigated lines degraded chlorophyll over the time span of 8 days to the same level, except *nye-1* and *pph-1* which showed enhanced levels of chlorophyll after 8 days of dark incubation indicating delayed senescence. Strikingly, siliques of *pph-1* and of the triple knock-out line *pph-1/clh1-1/clh2-1* accumulated pheophytin *a* after 5 days in the dark. However,

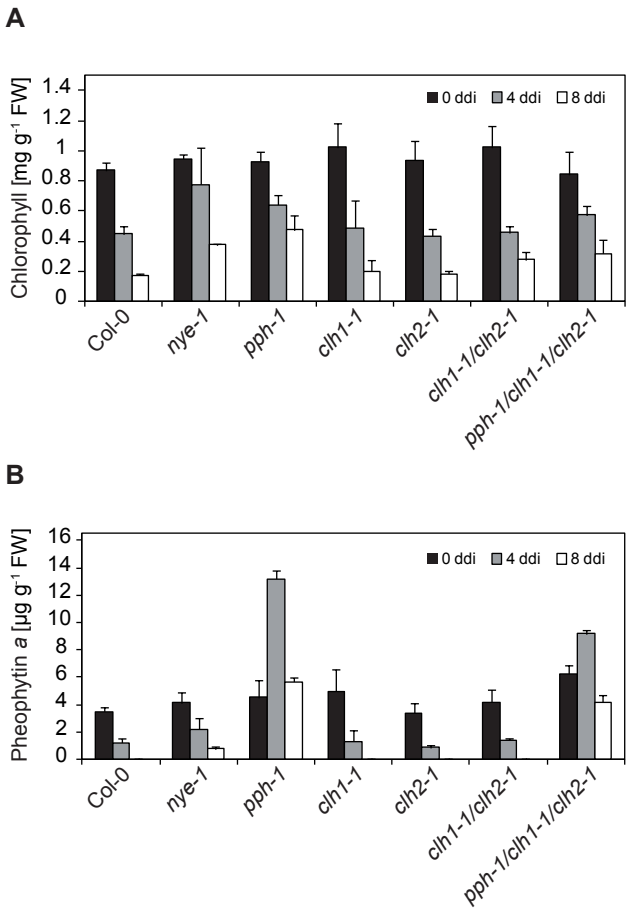

Figure A1. Chlorophyll and pheophytin *a* content in senescent siliques of different lines. A, Total chlorophyll content in detached siliques incubated in the dark (ddi) for up to 8 days. **B,** Pheophytin *a* content in dark incubated siliques. Data are mean values of three biological replicates, error bars indicate SD.

this effect was only transient and pheophytin *a* started to be degraded after 8 days (Figure A1). Lines that are deficient in CLH1 or CLH2 did not show any differences when compared to wild type (Figure A1), indicating that CLH1 and CLH2 are not involved in the dephytylation during chlorophyll breakdown in siliques.

3.2 2 Discussion

Data from Arabidopsis are very similar to the findings in tomato (Guyer et al., 2014). PPH is involved in the dephytylation of pheophytin during chlorophyll breakdown in senescing leaves, as it was described by Schelbert et al. (2009). In dark-incubated siliques which can be compared with tomato fruits, chlorophyll degradation was slightly delayed in *pph-1* when compared to wild type. However, the trend was similar to wild type which leads to the conclusion that chlorophyll is degraded normally. Also the absence of the two CHLOROPHYLLASES, CLH1 and CLH2, did not remarkably influence chlorophyll breakdown. Hence, CLHs are not involved in dephytylation during fruit ripening. Interestingly, pheophytin *a* accumulated in the absence of PPH, which indicates an involvement of PPH in the degradation of chlorophyll in senescing siliques. However, this effect was only of transient nature and finally pheophytin *a* was degraded. Taken together, these results are in good agreement with results from tomato fruits. I conclude that chlorophyll degradation during fruit ripening may generally be similar to leaf senescence, but differs in respect to dephytylation. In order to identify the hydrolytic activity accompanying PPH in fruits, Arabidopsis T-DNA insertion lines in genes encoding α/β-hydrolases will be analyzed in the future. By screening senescing siliques for altered pigment composition, candidate genes might be identified.

3.3 Acknowledgment and Contribution

My personal contribution to the publication Guyer et al. (2014) consisted of generating SlPPH-GFP fusions, the localization in protoplasts (with the help of Bastien Christ) and the complementation test in Arabidopsis. I carried out the experiments for determining the senescence phenotype of tomato leaves (with the support of Bastien Christ for phyllobilin analysis) and I measured hydrolytic activities in chromoplasts. Enzymatic activity of recombinant SlPPH was determined by Silvia Schelbert Hofstetter and me. I analyzed SlCLH gene expression by semiquantitative RT-PCR. The manuscript was written by Stefan Hörtensteiner and me.

Damian Menghini helped with the extraction and HPLC analysis of pigments of senescing Arabidopsis siliques.

4. Demetalation during Chlorophyll Breakdown

The changing of the color during senescence in leaves in autumn or in ripening fruits is one of the most eye-catching event in a plants life cycle. Nevertheless, a complex and not yet completely understood process underlies the phenomenon of chlorophyll breakdown. Nowadays it is widely accepted that the removal of the central Mg^{2+}-ion of chlorophyll is the first step in chlorophyll degradation. Yet, this mechanism remains to be characterized. In the past, many approaches have been undertaken in order to identify an involved metal-chelating substance (MCS) or metal-releasing protein (MRP). In this work I show that nicotianamine proposed by Kunieda et al. (2005) and the protein suggested by Lundquist et al. (2012), are most likely not the searched for MRP or MCS. In order to prove this, I investigated the phenotype of respective T-DNA insertion lines during leaf senescence. However, none of the lines showed differences in chlorophyll content when compared to wild type. Another promising approach which I followed relies on the fact that slight changes in pH trigger the spontaneous formation of pheophytin *a*, the substrate for downstream processes. Taking this into account, demetalation of chlorophyll might be a non-enzymatic process due to pH changes. Indeed, I could show that small changes in pH towards more acidic can be measured in senescing chloroplasts of Col-0. However, these findings need further confirmation. One approach which will be followed in the future is to further investigate plants with altered stromal pH. Results from these experiments may nail down the importance of pH changes in chlorophyll breakdown.

4.1 Introduction

Chlorophyll breakdown is an important natural process taking place during different steps of a plant‘s life cycle. In perennial and annual plants chlorophyll is broken down in order to enable retrieval and reallocation of nutrients, mainly nitrogen (Hörtensteiner and Feller, 2002). However, chlorophyll is not only broken down in leaves, but also in other organs such as fruits. In fleshy fruits, e.g. tomato, chlorophyll needs to be degraded in order to enable visibility of other pigments, mainly carotenoids (Egea et al., 2010). During the last years most of the steps of the chlorophyll breakdown pathway have been elucidated (reviewed in Christ and Hörtensteiner, 2014 and Hörtensteiner, 2013) and today we have a good understanding of the overall process, which is termed PAO/phyllobilin pathway (Hörtensteiner and Kräutler, 2011).

One of the first steps of chlorophyll degradation is the cleavage of the phytol moiety, an important reaction which releases the pigment from the thylakoid membrane and enables downstream processes. It has been shown for different plant species that this step is catalyzed by PHEOPHYTINASE (PPH), an esterase with high specificity for pheophytin, which is Mg-free chlorophyll (*Arabidopsis thaliana*: Schelbert et al., 2009; Ren et al., 2010, *Oryza sativa*: Morita et al., 2009, *Solanum lycopersicum*: Guyer et al., 2014). All these studies have shown that the removal of the central Mg^{2+}-ion of chlorophyll is crucial for the downstream PPH activity in order to prevent chlorophyll retention during senescence. Nevertheless, to date the process underlying Mg-dechelation remains to be identified.

Many approaches have been undertaken in the past. A first Mg-dechelating activity was detected in chloroplasts of oilseed rape. The activity was associated with the thylakoid membrane and it showed characteristics of an enzyme with pH optimum and high substrate affinity (Vicentini et al., 1995). By contrast, Shioi et al. (1996) isolated a Mg-dechelating activity from *Chenopodium album*. They found that the isolated activity remained intact after heat treatment and they claimed that the Mg-dechelatase activity is represented rather by a non-protein small-molecular-weight compound. Similar results were obtained from strawberries (*Fragaria* x *ananassa*) (Costa et al., 2002). The authors isolated a heat-stable small compound which showed high Mg-dechelating activity on the artificial substrate chlorophyllin (Costa et al., 2002). Besides the identified metal-chelating substances (MCS) from *Chenopodium* and strawberries, another Mg-dechelating activity was detected in *Chenopodium* by Suzuki and Shioi (2002). They isolated a small Mg-releasing protein (MRP) that had activity on chlorophyllin. Though, substrate comparison between MRP and MCS revealed that only MCS accepted chlorophyllide for Mg-dechelating activities. Therefore, the authors suggested MCS to be involved in dechelation of *Chenopodium* during senescence (Suzuki and Shioi, 2002; Kunieda et al., 2005). The same result was confirmed by Suzuki et al. (2005) in extracts from radish cotyledons.

Before the identification of PPH (Schelbert et al., 2009) it was thought that CHLOROPHYLLASE (CLH) catalyzes the cleavage of phytol (reviewed in Hörtensteiner, 2006). In this scenario Mg-dechelation would be the second step in chlorophyll breakdown

using chlorophyllide as substrate. However, since PPH is a highly specific enzyme, only accepting Mg-free chlorophyll, it is crucial that the central Mg^{2+}-ion is lost in a first step of chlorophyll breakdown (Schelbert et al., 2009). Therefore, the native substrate of MCS must be chlorophyll *a*. In all former studies (Vicentini et al., 1995; Shioi et al., 1996; Costa et al., 2002; Suzuki and Shioi, 2002; Kunieda et al., 2005; Suzuki et al., 2005) natural occurring chlorophyllide or artificial chlorophyllin were used as substrates for activity assays. Hence, it remains unclear if the identified MCS represents the active compound during chlorophyll breakdown.

In this work I followed three different approaches in order to identify the underlaying mechanism of Mg-removal. (i) In the work of Kunieda et al. (2005) the authors speculated that a putative nicotianamine could act as magnesium dechelator. In order to prove this assumption I investigated the phenotype of Arabidopsis mutants lacking one of the four nicotianamine synthases. (ii) A recent proteomics study in Arabidopsis plastoglobules identified a possible MRP candidate gene which contains a metal-binding domain (Lundquist et al., 2012). I looked at expression levels during leaf senescence, published on a free-access database, and checked for stay-green phenotypes in plants lacking the candidate gene. (iii) A third approach takes into account that chlorophyll reacts very sensitively against changes in pH and only slight acidic conditions can trigger the formation of pheophytin (Hirai et al., 2009; Saga et al., 2013). Here I investigated the effect of pH changes on chlorophyll and I measured pH changes in chloroplasts during senescence.

4.2 Results

4.2.1 Absence of MRP candidate genes does not reveal a stay-green phenotype during senescence

As speculated in the work of Kunieda et al. (2005) nicotianamine could putatively be involved in the removal of the central Mg^{2+}-ion of chlorophyll. Four nicotianamine synthases (*NAS1*, *-2*, *-3* and *-4*) are present in Arabidopsis. First, expression data for *NAS1*, *-2*, *-3* and *-4* published on GENEVESTIGATOR (Hruz et al., 2008) for green and senescent leaves were analyzed. As shown in Figure 1A, *NAS3* (At1g09240) showed high expression induction during senescence. The expression levels of *NAS1* (At5g04950), *NAS2* (At5g56080) and *NAS4* (At1g56430) remained unchanged in senescing leaves (Figure 1A). *NAS3* is therefore a good candidate gene for being involved in chlorophyll breakdown. As a follow-up experiment I looked at the phenotypic appearance of *nas3* mutants and analyzed their chlorophyll content in senescing leaves. Detached leaves of two T-DNA insertion lines (GK-010A10.01 and SAIL_224_G06) were incubated in the dark for up to 5 days. Though, leaves of the two *nas3* lines showed

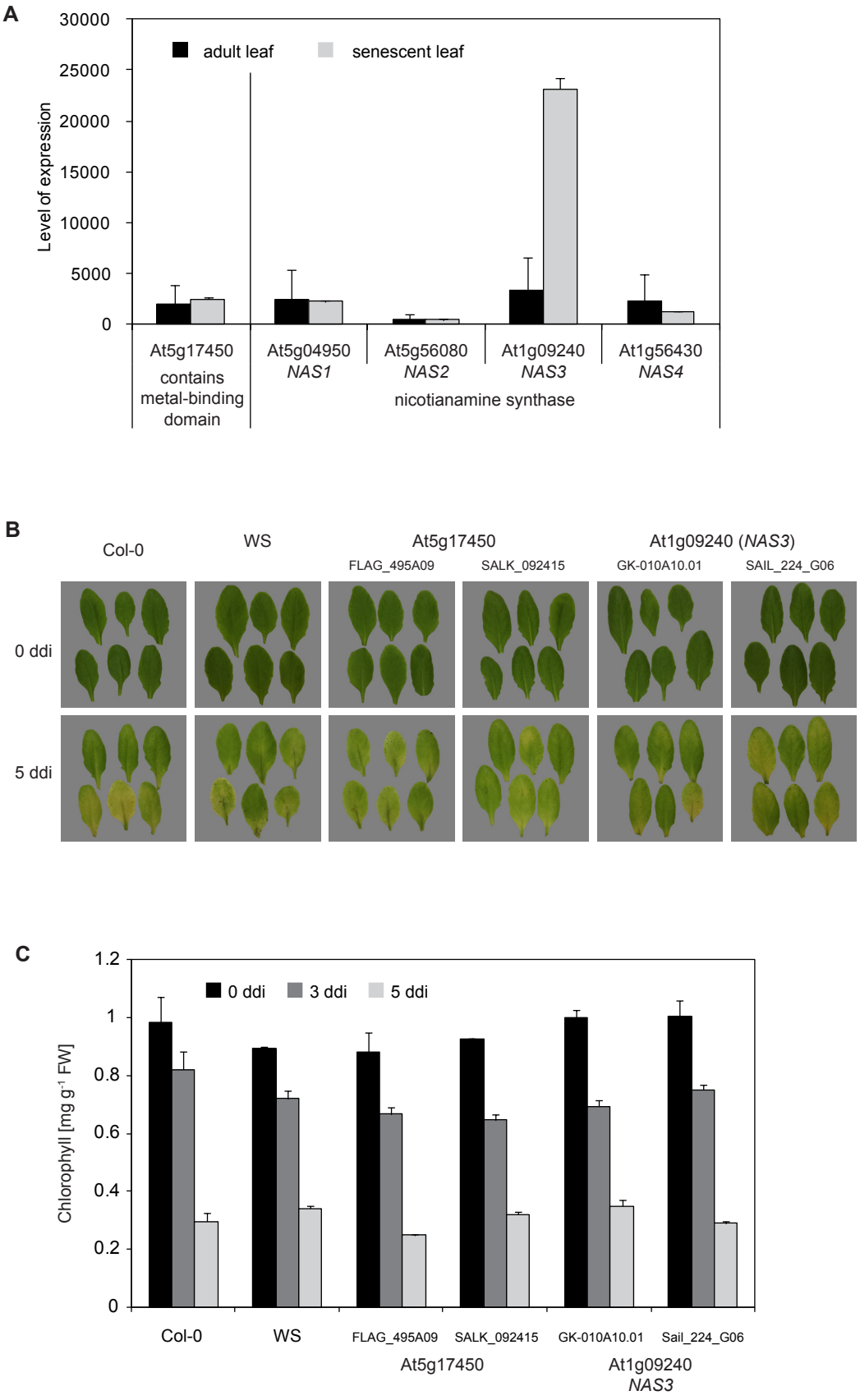
A
30000
25000
20000
15000
10000
5000
0
Level of expression
adult leaf
senescent leaf
At5g17450
contains metal-binding domain
At5g04950
NAS1
At5g56080
NAS2
At1g09240
NAS3
At1g56430
NAS4
nicotianamine synthase
B
Col-0
WS
At5g17450
FLAG_495A09
SALK_092415
At1g09240 (NAS3)
GK-010A10.01
SAIL_224_G06
0 ddi
5 ddi
C
1.2
1
0.8
0.6
0.4
0.2
0
Chlorophyll [mg g-1 FW]
0 ddi
3 ddi
5 ddi
Col-0
WS
FLAG_495A09
SALK_092415
GK-010A10.01
Sail_224_G06
At5g17450
At1g09240
NAS3

yellowing comparable to the two wild types Col-0 and WS (Figure 1B). Also the quantification of chlorophyll *a* and *b* contents did not reveal a stay-green phenotype of *nas3* (Figure 1C). Therefore, NAS3 is not considered to be involved in the dechelation process of chlorophyll.

As a second candidate the Arabidopsis gene At5g17450 was considered. As published by Lundquist et al. (2012) it might act as a MRP due to its metal-binding domain. However, data from GENEVESTIGATOR (Hruz et al., 2008) did not indicate any up-regulation of At5g17450 during leaf senescence (Figure 1A). Nevertheless, T-DNA insertion lines (FLAG_495A09 and SALK_092415) were analyzed for their phenotype during dark-induced senescence and chlorophyll contents were measured. The leaves of the two mutant lines resembled wild type in their phenotypic appearance (Figure 1B) and also chlorophyll contents did not differ (Figure 1C). Therefore, I did not continue the characterization of At5g17450.

4.2.2 Influence of pH on chlorophyll stability and its possible involvement in Mg^{2+}-dechelation

It has been published that chlorophyll, especially chlorophyll *a*, reacts very sensitively towards pH changes to an acidic environment. Under slight acidic conditions, the central Mg^{2+}-ion is released and pheophytin is formed spontaneously (Hirai et al., 2009; Saga et al., 2013). These findings need to be taken into account when investigating the demetalation of chlorophyll. Since experiments carried out by other researchers in the past (Vicentini et al., 1995; Shioi et al., 1996; Costa et al., 2002; Suzuki and Shioi, 2002; Kunieda et al., 2005; Suzuki et al., 2005) did not conclusively elucidate the process of Mg-dechelation, I followed a new approach based on the findings of Hirai et al. (2009) and Saga et al. (2013). I was interested whether small local pH changes might trigger the formation of pheophytin and therefore enable the subsequent dephytylation activity of PPH and other downstream chlorophyll breakdown processes.

Figure 1. Mutant screen does not reveal candidate genes for MCS or MRP. A, Comparison of expression levels of candidate genes in adult and senescent leaves (Data source: GENEVESTIGATOR). **B,** Leaf phenotype after 0 and 5 days senescence induction in the dark (ddi). **C,** Quantification of total chlorophyll in leaves after 0, 3 and 5 days senescence induction in the dark (ddi). Data are mean values of three technical replicates (At5g17450 Salk_092415 two replicates), error bars indicate SD.

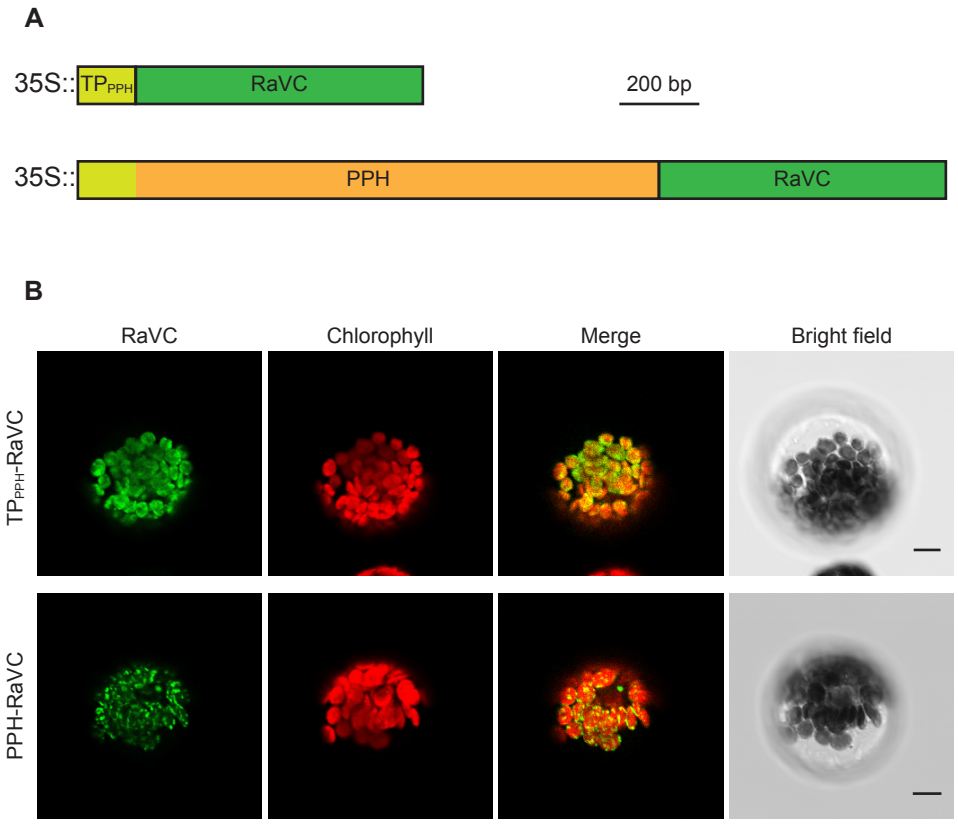

Figure 2. Subcellular localization of TP_{PPH}-RaVC and PPH-RaVC. A, Schematic overview of the fusions of RaVC to the transit peptide of PPH (TP_{PPH}-RaVC) and to the full length PPH (PPH-RaVC). Both constructs were expressed under the constitutive 35S promoter. **B,** Transient expression of TP_{PPH}-RaVC and PPH-RaVC in Arabidopsis (Col-0) protoplasts isolated from green leaves. RaVC fluorescence (RaVC) and chlorophyll autofluorescence (chlorophyll) were examined by confocal laser scanning microscopy. Merged images show overlay of RaVC and chlorophyll autofluorescence. Bars = 10 µm.

4.2.3 Senescent protoplasts of wild type show a slightly acidified internal chloroplastic pH while *pph-1* does not show any changes

In order to measure the pH in senescing protoplasts, the ratiometric fluorescing RaVC protein (Bagar et al., 2009) was targeted to the chloroplast. I obtained pEntr1a containing the full length RaVC from Nadine Paris (INRA, Montpellier, France). To target RaVC to the chloroplast, two constructs were designed (Figure 2A). For the first construct, TP_{PPH}-RaVC, the predicted chloroplast transit peptide of PPH (TP_{PPH}) plus the following two amino acids were cloned to the 5'-end of RaVC. The second construct, PPH-RaVC, consisted of full length PPH cloned to the 5'-end of RaVC. Both constructs were transiently expressed and localized in isolated mesophyll protoplasts of wild type Arabidopsis. Figure 2B shows that both constructs were targeted to the chloroplast. Images from confocal laser scanning microscopy indicated that RaVC fused to the transit peptide of PPH was present as free RaVC in the chloroplast, whereas the construct with

the full length PPH protein led to aggregated RaVC signals localized within chloroplasts (Figure 2B).

Changes in pH were identified by calculating the ratio of the fluorescence intensities of the emission signal of RaVC at 405 and 476 nm. As a control I used free RaVC expressed in *E. coli*. *E. coli* cells were lysed in buffers with different pH, ranging from pH 5 to pH 8.5. After a centrifugation step the soluble protein fraction was used for pH measurements. Emission signals at 405 and 476 nm of the free RaVC were detected between 500 and 530 nm and the ratio of the fluorescence intensity was calculated. Figure 3A shows that the ratio (F_{405nm} / F_{476nm}) was rising with increasing pH. In order to compare the pH in green and senescing protoplasts, TP_{PPH}-RaVC was expressed transiently in isolated protoplasts of green and dark-incubated leaves of Col-0 and *pph-1*. The ratio (F_{405nm} / F_{476nm}) was calculated for 12-20 protoplasts and the results are shown in Figure 3B. They show that the ratio was varying considerably among protoplasts; however, senescing protoplasts of Col-0 showed an overall lower F_{405nm} / F_{476nm} ratio which was not observed in senescing protoplasts of *pph-1*. As shown in Figure 3A, a lower F_{405nm} / F_{476nm} ratio indicates a lower pH, meaning that the pH in senescing chloroplasts of wild type is more acidic than in green leaves. In order to determine absolute pH values, further improvement of the calibration system is needed.

4.2.4 *kea* mutant lines could act as a model for plants with altered pH

KEA1, -2 and *-3* encode plastidial K^+/H^+ antiporters (Kunz et al., 2014). KEA1 and KEA2 are localized in the envelope, whereas KEA3 is localized in the thylakoid membrane. Plants deficient in KEA antiporters show changes of the pH in the chloroplasts. Knocking out KEA

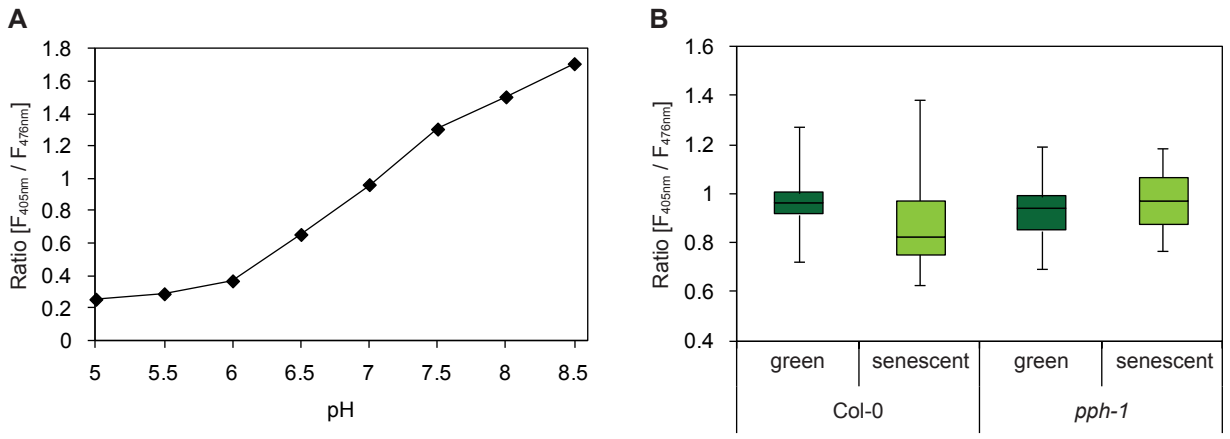

Figure 3. Ratiometric determination of pH changes in senescing chloroplasts. A, Reference curve for ratiometric pH measurement. For the reference curve free RaVC was expressed in *E. coli*. After lysing the cells in buffers with different pH, the fluorescence at 405 and 476 nm was measured and the ratio calculated. **B,** Ratio of the fluorescence at 405 and 476 nm in isolated protoplasts transiently expressing TP_{PPH}-RaVC. Blots represent values of 20 protoplasts (*pph-1* green 12 protoplasts).

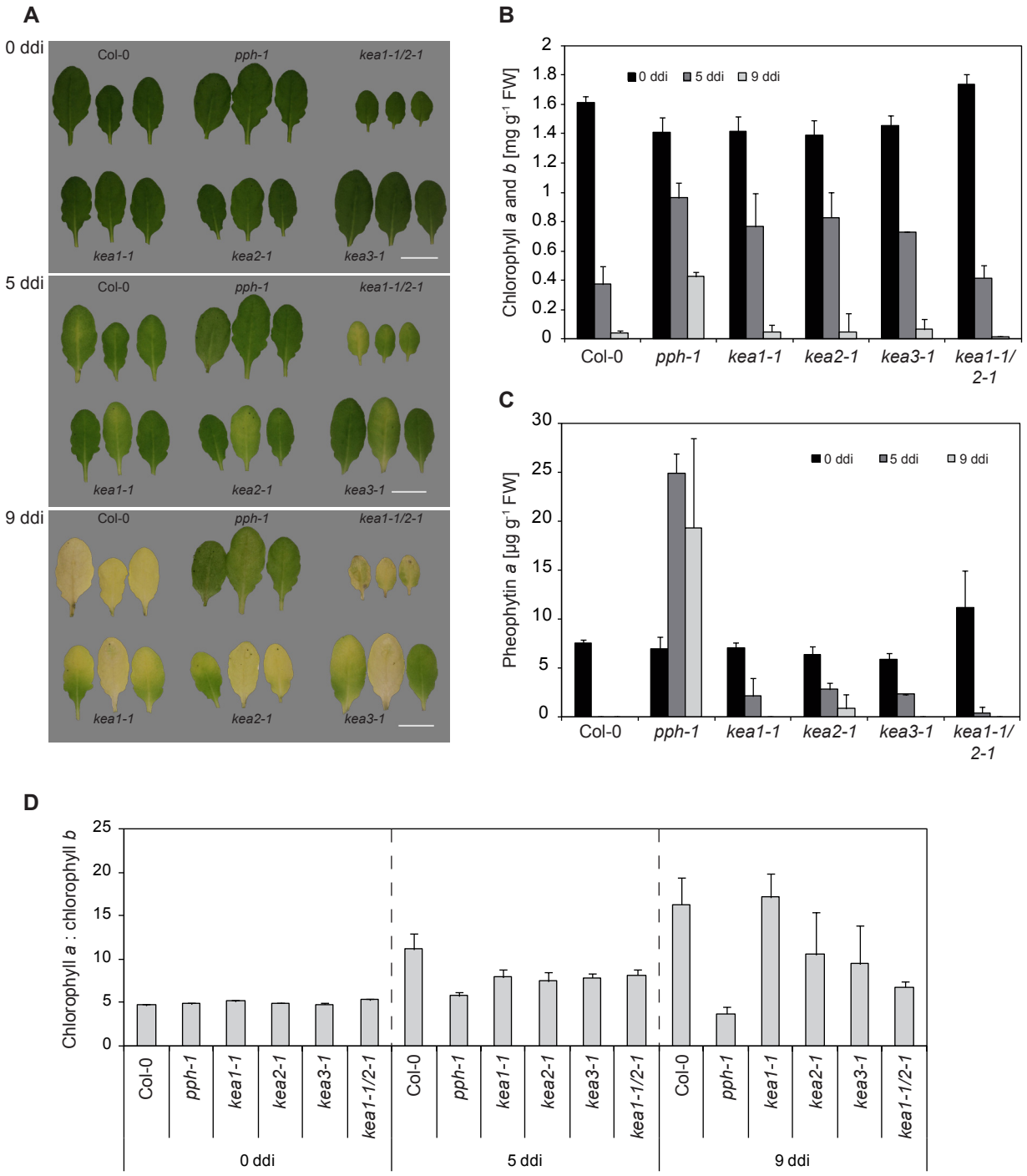

Figure 4. Phenotype and chlorophyll metabolite contents of kea-mutant lines during dark-induced senescence. A, Phenotypic appearance of *kea*-mutant lines. Detached leaves of wild type (Col-0), *pph-1*, *kea1-1*, *kea2-1*, *kea3-1* and the double mutant *kea1-1/2-1* were incubated in the dark for up to 9 days (ddi). Bars = 1 cm. **B,** Total chlorophyll and **C,** pheophytin *a* content in senescing leaves. **D,** Changes in chlorophyll *a* to chlorophyll *b* ratios during senescence. All data are mean values of three biological replicates, error bars indicate SD.

K^+/H^+ antiporters leads to a change in ΔpH across the thylakoid membrane (Kunz et al., 2014). I was interested if *kea*-mutant lines show a changed pattern of chlorophyll degradation due to pH changes in the chloroplasts. Single *kea* knock-out lines (*kea1-1*, *kea2-1* and *kea3-1*) as well as the double knock-out line *kea1-1/2-1* were incubated in the dark for up to 9 days. Col-0 and *pph-1* as a stay-green mutant were used as control plants. As shown in Figure 4A no changes in the phenotypic appearance of the *kea*-lines were observed when compared to wild type. After 9 days of dark-incubation (9 ddi) all leaves showed yellowing, except *pph-1* still appeared green (Figure 4A). Also the quantification of chlorophyll *a* and *b* by HPLC did not reveal changes in the degradation of chlorophyll. Chlorophyll contents were the same at 0 ddi for all lines, and Col-0 and the *kea*-lines degraded nearly 100% chlorophyll during the 9 days in the dark (Figure 4B). I was also interested in the pheophytin level, since it is Mg-free chlorophyll and its content might change with altered pH. However, no difference in pheophytin *a* levels between wild type and the *kea*-lines could be measured (Figure 4C). Pheophytin *b* was not detectable in any of the lines. Nevertheless, a closer look at the ratios of chlorophyll *a* : chlorophyll *b* revealed differences between *kea*-lines and Col-0 (Figure 4D). At 0 ddi the ratio was around 5 in all tested lines. In wild type the ratio increased continuously to around 15. By contrast, *pph-1* retained relatively more chlorophyll *b* than *a*, therefore the ratio dropped to almost 3.5. *kea1-1* showed a similar behavior as Col-0 with the ratio continuously increasing. For the two lines *kea2-1* and *kea3-1* the situation was not very conclusive. The ratio increased but to a lower extent than in wild type. However, the double mutant line *kea1-1/2-1* clearly showed a smaller increase of the ratio than Col-0. Yet, the ratio was still higher than that of *pph-1* (Figure 4D).

4.3 Discussion

Different approaches have been undertaken in the past in order to characterize the process of dechelation during chlorophyll breakdown in plants. However, the molecular identification of MCS (metal-chelating substance) and MRP (metal-releasing protein) remain unaccomplished. Studies in the past used chlorophyllin or chlorophyllide as substrates for activity measurements (Vicentini et al., 1995; Shioi et al., 1996; Costa et al., 2002; Suzuki and Shioi, 2002; Kunieda et al., 2005; Suzuki et al., 2005). Since PPH was identified as the dephytylating enzyme during chlorophyll breakdown (Schelbert et al., 2009), we know that demetalation involves the conversion of chlorophyll to pheophytin, hence, chlorophyll is the substrate for dechelating activities. Here I followed up on the proposed nicotianamine by Kunieda et al. (2005) as MCS. Nicotianamine is known to form stable complexes with several metals (Anderegg and Ripperger, 1989). However, plants lacking the *NAS3* gene, a nicotianamine synthase which is up-regulated in senescing leaves, did not reveal a stay-green phenotype in detached dark-incubated leaves. Also their chlorophyll content was comparable to wild type (Figure 1). From these data I conclude

that nicotianamine is not a magnesium-dechelating substance. However, the nicotianamine content is not different between *nas3* plants and wild type (Klatte et al., 2009). Analysis of a quadruple mutant that is deficient in all four NAS genes and which shows distinct changes in nicotianamine content (Klatte et al., 2009) should be analyzed in order to confirm these results. Also the candidate gene At5g17450, identified by Lundquist et al. (2012), is not considered to be an MRP. Its expression did not alter in senescing leaves and knocking-out the gene did not result in retained chlorophyll during degradation (Figure 1). From these findings I conclude that the central Mg^{2+}-ion of chlorophyll is not removed with the help of any of the investigated candidate proteins.

In this study I also followed a second approach in order to identify the mechanism which is responsible for Mg-dechelation. It has been shown that chlorophyll reacts very sensitively towards changes in pH and lowering the pH results in spontaneous formation of pheophytin (Hirai et al., 2009; Saga et al., 2013). Saga et al. (2013) speculated that this fact might also play an important role in the formation of pheophytin *a* as the primary electron acceptor in the reaction center of photosystem II. Chlorophyll degradation is a well organized process. Since it requires dismantling of the thylakoid membrane (Evans et al., 2010) , it is possible that this disintegration enables local changes in pH which might trigger removal of the central Mg^{2+}-ion. By investigating pH changes in the chloroplasts of senescing leaves of Col-0 and *pph-1*, I was able to show on the one hand, that the pH in senescing chloroplasts of wild type was slightly more acidic than in green leaves. On the other hand, the pH remained unchanged in *pph-1* chloroplasts (Figure 3).

Schelbert et al. (2009) showed that in *pph-1* grana thylakoids remained largely stacked during senescence. Supposing that small pH changes occur during senescence, they would probably not reach chlorophyll which remains strongly embedded into the thylakoid membranes in *pph-1*. If we assume that the unstacking of granas triggers or enables the effect of pH changes I would expect unchanged pH in plants which retain stacked granas during senescence. If so, the data would be in good agreement with this assumption. Anyhow, the data need to be confirmed in a second independent experiment, including other mutants having intact grana stacking during senescence. In the rice *stay green* (*sgr*) mutant altered grana stacking was observed (Park et al., 2007). Therefore, Arabidopsis *sgr* mutants are good candidates for a follow-up experiment. In order to confirm the observations from protoplasts also *in vitro* two Arabidopsis anti-silencing lines have been stably transformed with TP_{PPH}-RaVC and PPH-RaVC. Changes in pH will be investigated during the entire life cycle, including senescing leaves.

If pH changes play a role in chlorophyll breakdown, it is interesting to investigate plants which show alterations in the chloroplastic pH, because then an altered pattern of chlorophyll degradation could be expected. In a first experiment I looked at *kea*-lines, which are deficient in a K^+/H^+ antiporter and show altered ΔpH across the thylakoid membrane (Kunz et al., 2014). Yet, none of the investigated lines showed retarded chlorophyll breakdown, nor an altered pattern of pheophytin *a* content (Figure 4). Interestingly, the ratio of chlorophyll *a* to chlorophyll *b*

did not increase to the same extent in the double knock-out line *kea1-1/2-1* as it was observed in wild-type. The ratio was rather similar to *pph-1*. Altogether, these results are promising and future experiments might further prove the role of the plastidic pH for chlorophyll breakdown.

4.4 MATERIAL AND METHODS

4.4.1 Plant Material and Quantification of Metabolites

Arabidopsis T-DNA insertion lines were obtained as follows: the SALK line (Alonso et al., 2003) SALK_092415 (*At5g17450*), the GABI-Kat line (Kleinboelting et al., 2012) GK-010A10 (*At1g09240*) and the SAIL line (Sessions et al., 2002) SAIL_224_G06 (*At1g09240*) were obtained from the European Arabidopsis Stock Center, http://arabidopsis.info/; the FLAG line (Samson et al., 2002) FLAG_495A09 (*At5g17450*) was from the INRA Versailles Arabidopsis Stock Centre , http://publiclines.versailles.inra.fr/. Plants were screened for homozygosity with the primers listed in Table 1.

Table 1. List of primers.

At1g09240	**wild-type**	**knock-out**
Primers for GK-010A10.01 (5'-3')		
LP_N651 ATTAGGACCACCAACATTCCC	x	
RP_N651 CCAGGATAATTTTGAAAATGATTG	x	x
Gabi_LB CCCATTTGGACGTGAATGTAGACAC		x
Primers for SAIL_224_G06 (5'-3')		
LP_W863 TGATAAGGCATCAAACTTTTGTG	x	
RP_ W863 AACTCGAGCTTTCCGAGTTTC	x	x
Sail_LB2 GCTTCCTATTATATCTTCCCAAATTACCAATACA		x

At5g17450	**wild-type**	**knock-out**
Primers for FLAG_495A09 (5'-3')		
LP_Flag CATTGGTTGCTTAATTGGTCC	x	
RP_Flag GCATGAAAGGTTCTCTTTCCC	x	x
RB4 TCACGGGTTGGGGTTTCTACAGGAC		x
Primers for SALK_092415 (5'-3')		
LP_Salk CGGTCGGTTTCAACATTCAAG	x	
RP_Salk GAATCTTGAATGCATGTCACG	x	x
LBb1.3 ATTTTGCCGATTTCGGAAC		x

Columbia-0 (Col-0), Wassilewskija (Ws) and T-DNA insertion lines in *At1g09240* and *At1g17450* were grown in a greenhouse (20 °C [day], 18 °C [night], 16 h light, 60% humidity, fluence rate 100 to 200 µmol photons m^{-2} s^{-1}). For senescence induction detached leaves were incubated in a closed container on wet filter paper in the dark at room temperature. Chlorophyll was extracted by adding extraction buffer (10% [v/v] 10mM Tris-HCl pH 8, 90% [v/v] acetone) to the frozen leaf tissue (600 µl buffer 100 mg^{-1} plant material). The mixture was incubated for 20 min at -20 °C. After a centrifugation step the supernatant was measured in 80% (v/v) acetone with a spectrophotometer. Chlorophyll content was calculated as: chlorophyll *a* and *b* [µg ml^{-1}] = 6.45 A_{665} + 17.72 A_{649} (Strain et al., 1971).

Different homozygous *kea* T-DNA insertion lines were obtained from Julian Schroeder (University of California, San Diego, USA). Plants were grown for 5 weeks in a phytotron under short day conditions (20 °C, 8 h light, 60% humidity, fluence rate 150 µmol photons m^{-2} s^{-1}). For senescence induction detached leaves were incubated in a closed container on wet filter paper in the dark at room temperature. Extraction and analysis of chlorophyll and pheophytin was performed according to Das and Guyer et al. (submitted).

4.4.2 Cloning of RaVC Fusion Constructs

pEntr1a (Invitrogen) vector containing full length RaVC (pEntr1a-RaVC) was obtained from Nadine Paris (INRA, Montpellier, France). To generate the TP_{PPH}-RaVC construct, the PPH transit peptide was amplified using PCR Extender polymerase (5Prime) with the two primers PPH_{TP}-s (5'-ggggatccatggagataatctcactgaa-3') and PPH_{TP}-RaVC-as (5'-cgcccttgctcactccacttcgaatcacaagtc-3'), thereby adding the first 13 bp of RaVC at the 3'-end of the PPH transit peptide. In a second PCR reaction, RaVC was amplified using the two primers PPH_{TP}-RaVC-s (5'-gattcgaagtggagtgagcaagggcgaggagct-3') and RaVC-LP-Nde (5'-cccatatgatctgggtatcttg-3'), thereby adding the last 13 bp of the PPH transit peptide at the 5'-end of RaVC and a *Nde*I restriction site at the 3'-end. After gel purification (Wizard® SV Gel and PCR Clean-Up System, Promega) the PCR products were used as templates in a third PCR reaction and amplified with PPH_{TP}-s and RaVC-LP-Nde. The final PCR product was subsequently cloned into the *Nde*I restriction site of pEntr1a-RaVC and verified by sequencing. Finally, the construct was recombined into TCX341-pGWB502 (obtained from Nadine Paris, INRA, Montpellier, France) using Gateway LR Clonase II Enzyme Mix (Invitrogen). To generate the PPH-RaVC construct, the procedure was the same but with the primers PPH_{TP}-s and PPH-RaVC-as (5'-cgcccttgctcactgcagacttccctccaaaca-3') for the first PCR, PPH-RaVC-s (5'-agggaagtctgcagtgagcaagggcgaggagct-3') and RaVC-LP-Nde for the second PCR and PPH_{TP}-s and RaVC-LP-Nde for the final construct. TCX341-pGWB502, harboring TP_{PPH}-RaVC and PPH-RaVC, respectively, was transformed into NEB 10-beta competent *E. coli* (High Efficiency) cells (New England Biolabs) and positive colonies were selected with kanamycin.

4.4.3 Transient Transformation of Arabidopsis Protoplasts

TP_{PPH}-RaVC and PPH-RaVC fusion proteins were localized in mesophyll protoplasts from Arabidopsis grown under short-day conditions for 4-5 weeks (20 °C, 8 h light, 60% humidity, fluence rate 150 µmol photons m^{-2} s^{-1}). Isolation of mesophyll protoplasts was performed according to Endler et al. (2006). Transformation was performed with 20% (w/v) polyethylene glycol as described (Meyer et al., 2006). Transformed protoplasts were kept in the dark for 24 to 48 h prior to analysis by confocal laser-scanning microscopy (Leica TCS SP5; Leica Microsystems). RaVC fluorescence was imaged as described (Bagar et al., 2009). Excitation wavelengths were set to 405 nm (diode laser) and 476 nm (argon laser) and RaVC emission signals were detected between 500 and 530 nm. Chlorophyll autofluorescence was detected between 650 and 700 nm.

4.4.4 Internal Chloroplastic pH Measurement

Mesophyll protoplasts of Col-0 and *pph-1* were isolated and transformed as described above. For senescent protoplasts, detached leaves were incubated on wet filter paper in the dark for 4 days prior to isolation. Changes in pH were determined according to Bagar et al. (2009) by confocal laser-scanning microscopy (Leica TCS SP5; Leica Microsystems). Each protoplast was imaged twice for pH determination. For both images the gain was set to 60% to assure imaging in a non-saturating range. RaVC fluorescence was first excited at 405 nm (diode laser, 20% intensity) and the emission signal was detected between 500 and 530 nm. Subsequently, the same protoplast was excited at 476 nm (argon laser, 20% intensity) and the emission signal again detected between 500 and 530 nm. Chlorophyll autofluorescence was detected between 650 and 700 nm. Fluorescence intensities of emission signals after excitation at 405 and 476 nm were analyzed using Adobe Photoshop CS6 (Adobe Systems). For the calibration curve recombinant RaVC expressed in *E. coli* was used. For this, pRsetB (Invitrogen), containing RaVC (gift from Nadine Paris, INRA, Montpellier, France) was transformed into *E. coli* BL21(DE3). For protein expression cells were grown to an optical density at 600 nm of 0.5 and RaVC expression was induced by adding 1 mM isopropyl β-D-1-thiogalactopyranoside (IPTG). Protein expression was performed at 37 °C for 3 h. Subsequently, the cell pellet was resuspended in buffers with different pH ranging from pH 5 to pH 8.5 (50 mM acetate, 150 mM KCl, pH 5 and pH 5.5; 50 mM MES, 150 mM KCl, pH 6 and pH 6.5; 50 mM MOPS, 150 mM KCl, pH 7 and pH 7.5; 50 mM Tris-HCl, 150 mM KCl, pH 8 and pH 8.5) and lysed using a French Press (Constant Cell Disruption System; Constant Systems) at 150 MPa. Cell debris were separated by centrifugation. The supernatant was supplemented with 10% (v/v) glycerol, flash-frozen in liquid nitrogen and stored at -80 °C. For pH measurement by confocal laser-scanning microscopy one drop of protein extract (0.3 mg ml^{-1}) was imaged and analyzed as described above for protoplasts. The ratio of fluorescence intensities after excitation at 405 and 476 nm was calculated according to Bagar et al. (2009) using the equation $R = F_{405nm} / F_{476nm}$.

4.5 Acknowledgment and Contribution

I would like to thank Bastien Christ who helped me with the GENEVESTIGATOR expression data and with the confocal microscopy work and Damian Menghini who helped analyzing the *kea*-lines. I would also like to thank Nadine Paris (INRA, Montpellier, France) for providing me with vectors containing RaVC and for all her helpful inputs.

5. *Purification of PHEOPHYTINASE*

Phytol is hydrolyzed during chlorophyll degradation in leaves and other organs. Since phytol anchors chlorophyll in the thylakoid membrane, its cleavage is of great importance in order to enable downstream degradation processes. From different plants it is known that this specific hydrolysis is catalyzed by an enzyme termed PHEOPHYTINASE (PPH), which shows high substrate specificity for Mg-free chlorophyll (pheophytin). It has been shown that the specificity of PPH is determined by the molecular structure of the porphyrin ring. However, the binding mechanism remains unclear. In order to gain a better understanding of the mechanism of substrate binding and processing, and therefore to gain knowledge about the role and importance of the described tight specificity, I was interested to solve the crystal structure of PPH of Arabidopsis. Here, I tested different expression systems and suitable protein constructs to screen for conditions that allow production of high amounts of highly purified protein that can be used for protein crystallization. I show that a C-terminal affinity tag is essential in order to prevent co-purification of only partially translated protein fragments. I also observed that tag-free PPH aggregated to high molecular weight complexes which could not be separated by size-exclusion chromatography. Supplemenation with detergents or a special commercially available polymer partially prevented protein aggregation; however, the enzymatic activity was negatively influenced. Further improvements will be necessary in order to obtain high amounts of purified and tag-free PPH that is suitable for protein crystallization.

5.1 Introduction

PPH is a highly specific hydrolase that cleaves the ester bond between the porphyrin and the phytol side chain of pheophytin during chlorophyll breakdown (Schelbert et al., 2009; Guyer et al., 2014). It was shown that PPH is specific for the alcohol moiety and its activity is limited when the molecular structure of porphyrin is modified in the central or lower part (this work chapter II). It can be assumed that the described substrate specificity plays an important role in the regulation and coordination of chlorophyll breakdown. One approach to understand the importance of substrate specificity is to investigate the substrate binding mechanism of PPH. In order to understand this mechanism, resolving the crystal structure of PPH is of big importance. However, to be able to crystallize PPH, high amounts of pure recombinant protein are required.

In order to obtain high amounts of pure protein, the protein of interest is over-expressed in a heterologous expression system. Since the protein of interest needs to be separated from endogenous proteins prior to crystallization, a specific recognition site (tag) is fused to the protein of interest, which allows efficient purification from the crude extract (Lichty et al., 2005). Lichty et al. (2005) classified available protein and peptide tags into three groups. Class I-tags are tags that bind to small molecules immobilized on e.g. a column. Examples include the histidine-tag (His-tag) which binds to immobilized metals (e.g. nickel), the glutathione *S*-transferase (GST-tag) which binds glutathione, and maltose-binding protein (MBP-tag) which binds amylose. All three tags have in common that they can be released from the affinity column by out-competing the binding of the small molecule. Imidazole is used for the His-tag, reduced glutathione for the GST-tag and maltose for the MBP-tag. Class II-tags include peptide tags that specifically bind to a protein-binding partner. Class III-tags are similar to class II-tags, but the binding partner is an antibody, e.g. FLAG-tag (Lichty et al., 2005). Affinity tags can generally be fused to the N- or C-terminus of proteins. In order to remove the tag after protein purification, specific sequences are inserted between the protein of interest and the protein tag. These sequences are recognized by specific proteases (e.g. factor Xa [FXa], thrombin or tobacco etch virus protease [TEV]) (Young et al., 2012) resulting in tag-free protein.

In this study, the purification of Arabidopsis PPH was optimized. The MBP-tag was used as the main affinity tag and *Escherichia coli* (*E. coli*) was chosen as expression system. MBP encodes a 42 kDa protein that binds amylose and is released under non-denaturing conditions by adding low concentrations of maltose to the buffer. MBP can be fused to the C- or N-terminus of the protein of interest (Young et al., 2012). The advantage of using MBP is its ability to enhance production and solubility of the fusion partner (Lebendiker and Danieli, 2011). 70-90% pure fusion protein can be obtained by applying a single purification step using an affinity column. However, additional steps are normally required before any downstream applications. Ion-exchange is often used to separate MBP from the fusion partner and size-exclusion chromatography is applied as the final purification step (Lebendiker and Danieli, 2011). Here, I tried to optimize purification of a MBP-PPH fusion by additionally tagging PPH with a

6xHis-tag at its C-terminus. Proteolytic cleavage sites were present between PPH and both the MBP and the His-tag. However, challenges that were faced during protein purification and that could not all be solved, included protein fragmentation and loss of the enzymatic activity of PPH. Finally, the system of choice was a C-terminal MBP-tag with a TEV cleavage site between PPH and MBP. However, cleavage of the MBP-tag after protein purification was only partial. In addition, protein aggregates were observed which could not be separated by size-exclusion chromatography.

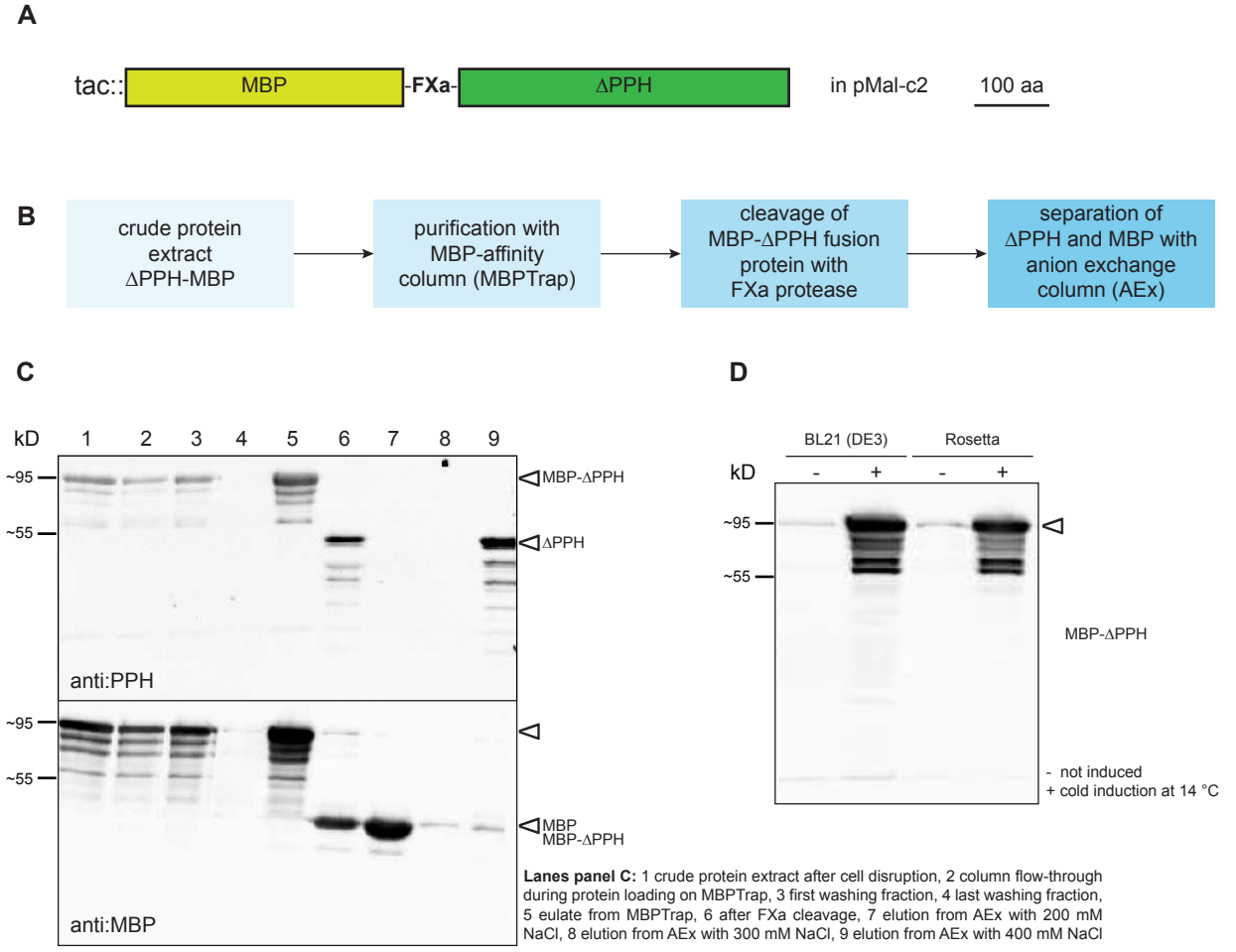

Figure 1. Expression of ΔPPH as MBP-ΔPPH fusion protein in pMal-c2. A, Schematic overview of the MBP-ΔPPH construct. Note that the factor Xa (FXa) site is not drawn in scale. **B,** Schematic overview of the purification process. The soluble protein fraction of the crude extract was purified with a MBP-affinity column (MBPTrap). MBP-ΔPPH fusion protein was subsequently cleaved with (FXa) protease. MBP and ΔPPH were separated with anion exchange chromatography (AEx). **C,** Western blot of samples during the purification process. The upper blot shows hybridization with anti PPH antibodies, the lower blot shows hybridization with anti MBP antibodies. MBP eluted with 200 mM NaCl (lane 7), ΔPPH eluted with 400 mM NaCl (lane 9). **D,** Western blot analysis using anti PPH antibodies of degradation products of ΔPPH after expression in *E. coli* BL21 (DE3) and in one of the available Rosetta strains at 14 °C.

5.2 Results

5.2.1 Expression of ΔPPH as MBP-ΔPPH fusion protein results in incompletely translated protein fragments

Schelbert et al. (2009) cloned a truncated version of Arabidopsis PPH (ΔPPH), lacking the predicted transit peptide, into pMal-c2 (New England Biolabs). The protein was expressed with an N-terminal maltose-binding protein fusion (ΔPPH-MBP) and a factor Xa (FXa) cleavage site (Figure 1A) in *Escherichia coli* (*E. coli*). The MBP-tag has a strong affinity towards MBP-binding columns and therefore it can be used to separate the fusion protein from endogenous *E. coli* proteins. Subsequent proteolytic cleavage with FXa enables the separation of the MBP-tag and ΔPPH. A schematic overview of the purification process is shown in Figure 1B. After protein expression in *E. coli* BL21(DE3) and cell disruption (see Material and Methods), the soluble protein fraction was loaded onto a MBP-affinity column. The fusion protein was eluted by adding 10 mM maltose to the buffer and subsequently cleaved with FXa. The resulting protein fragments, ΔPPH and MBP, were separated by anion exchange columns. For this, the protein solution was loaded on an anion exchange column and the two proteins were eluted by increasing the NaCl concentration to 400 mM. Figure 1C shows two Western blots with samples taken during different steps of the whole purification process. The Western blots, hybridized with antibodies against PPH or MBP, clearly show that the two proteins were separated and the overall purity was satisfying. However, it is apparent that the fusion protein fraction (lane 5) and the cleaved ΔPPH fraction (lane 6) contained several fragmented forms of the protein. Even after anion exchange (lane 9), fragmented PPH protein products, i.e. detectable with antibodies against PPH, were present. Two explanations are likely: (i) the proteins were partially degraded during expression in *E. coli* or during the purification process since PPH is located at the C-terminus. (ii) The fusion protein was not completely translated and different lengths of the fusion protein were present and subsequently co-purified. Fragmentation of overexpressed proteins in *E. coli* can be due to an inappropriate tRNA pool (Novy et al., 2001). To overcome this problem, I tested a different *E. coli* strain (Rosetta) and protein expression was induced at 14 °C in order to minimize protein degradation (Figure 1D). However, in both cases fragmented protein products of the fusion protein were still present. Apparently, it was not possible to overcome protein fragmentation by changing the bacterial strain and by reducing the induction temperature.

5.2.2 Introducing a C-terminal His-tag prevents protein fragmentation, but purified protein yield is very low

It can be assumed that the fragmented protein products resulting from MBP-ΔPPH expression (Figure 1C and D) were most likely due to the free C-terminus of ΔPPH. One the one hand, endonucleases had access to the protein and likely started to degrade the fusion protein. On the other hand, since the MBP-tag was fused to the N-terminus of ΔPPH, separation of complete fusion protein from un-completely translated protein was not possible. In order to overcome this limitation, an additional tag was introduced by fusing a 6xHis-tag to the C-terminus of

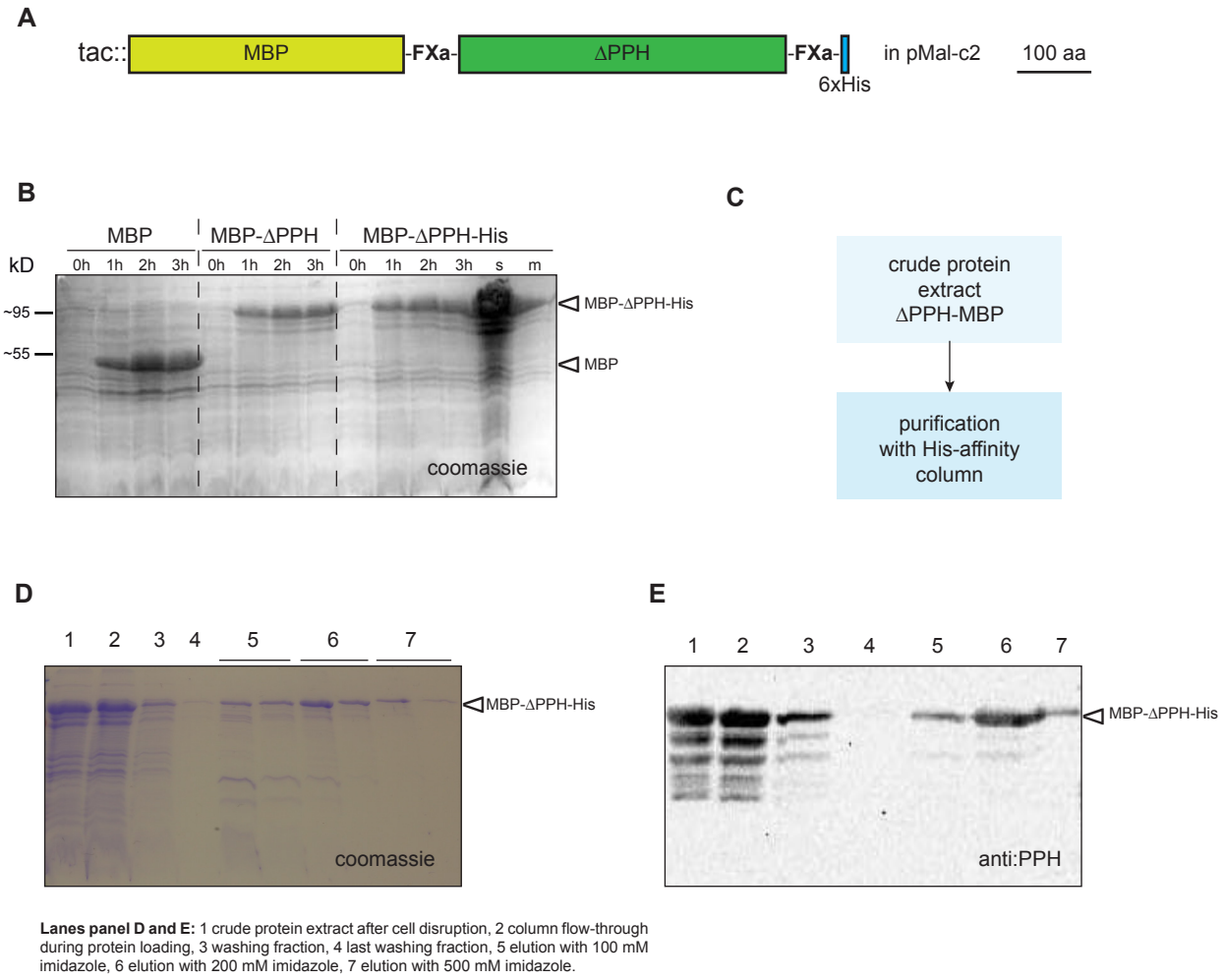

Lanes panel D and E: 1 crude protein extract after cell disruption, 2 column flow-through during protein loading, 3 washing fraction, 4 last washing fraction, 5 elution with 100 mM imidazole, 6 elution with 200 mM imidazole, 7 elution with 500 mM imidazole.

Figure 2. Expression and purification of ΔPPH as MBP-ΔPPH-His fusion protein in pMal-c2. A, Schematic overview of the ΔPPH construct with a N-terminal MBP tag and a C-terminal His tag. Note that FXa sites are not drawn to scale. **B,** Expression of MBP-ΔPPH-His fusion protein after 0 h, 1 h, 2 h and 3 h induction with 1 mM IPTG. After cell lysis, the fusion protein was found in the soluble fraction. SDS-PAGE gel after coomassie staining. s, soluble fraction; m, membrane fraction. **C,** Schematic overview of the first purification process. MBP-ΔPPH-His was purified from the soluble protein fraction of crude extracts with a His-affinity column (HisTrap). Protein was eluted with increasing imidazole concentrations. **D,** Coomassie-stained SDS-PAGE gel and **E,** Western blot analysis with anti PPH antibodies after protein purification with a His-affinity column.

MBP-ΔPPH together with a second FXa cleavage site (MBP-ΔPPH-His) (Figure 2A). The construct was expressed in *E. coli* BL21(DE3). Expression of the fusion protein was comparable to the MBP control and the first construct, MBP-ΔPPH (Figure 2B), and after cell lysis the major part of the fusion protein was present in the soluble protein fraction. A first purification procedure was performed as schematically described in Figure 2C. For this, the crude protein fraction was loaded onto a His-affinity column. The loading buffer contained 20 mM Tris-HCl pH 7.4, 0.5 M NaCl and 20 mM imidazole. The bound protein was eluted from the column by stepwise increasing the imidazole concentration to 500 mM. Most of the fusion protein eluted at an imidazole concentration of 200 mM (Figure 2D). When probing the different fractions in a Western blot with antibodies against PPH, it became evident that expression of MBP-ΔPPH-His also led to the formation of fragmented fusion protein, comparable to MBP-ΔPPH (Figure 1). However, tagging ΔPPH at its C-terminus allowed separation of degraded and incompletely translated protein fragments. The fusion protein was well purified from endogenous *E. coli* proteins (Figure 2D) and fragmented proteins were not anymore present after purification with a His-affinity column (Figure 2E). Nevertheless, although the protein quality was good, the obtained yield was very low. Since the goal of the protein purification was protein crystallization, a higher yield was required.

5.2.3 NP-40 enhances the yield of purified protein, but cleavage and enzyme activity are negatively influenced

With the strategy described above (Figure 2), purity of MBP-ΔPPH-His was good and fragmented fusion proteins could be removed. However, the yield was very low. From Figure 2D it is evident that the major part of expressed fusion protein was found in the flow-through after loading on a His-affinity column. Since the His-tag was fused to the C-terminus of MBP-ΔPPH without a spacer between the tag and the protein, it is possible that the 6 His residues were not freely accessible and therefore efficient binding to the His-affinity column was not possible. I tried to solve this problem by supplementing the soluble protein fraction with nonidet-40 (NP-40). NP-40 is a weak non-ionic, non-denaturing detergent that slightly solubilizes proteins (Labeta et al., 1988), and accessibility of the His-tag might be improved. In a first purification test the binding efficiency of MBP-ΔPPH-His to a His-affinity column was compared in samples with and without NP-40. The buffer of the sample without NP-40 contained 20 mM Tris-HCl pH 8, 0.5 M NaCl and 20 mM imidazole and the buffer with NP-40 contained 20 mM Tris-HCl pH 8, 1 M NaCl, 20 mM imidazole and 0.5% NP-40. The NaCl concentration was increased to 1 M to prevent ion-exchange (GE Healthcare, 2012), thus unspecific protein binding. For both samples 10 mg of crude protein were loaded on a His-affinity column. The columns were washed with buffer containing 40 mM imidazole and the proteins were eluted by stepwise increasing the imidazole concentration to 500 mM. Figure 3A shows a Western blot hybridized with antibodies against PPH of protein samples taken during the purification process. Indeed, less fusion protein

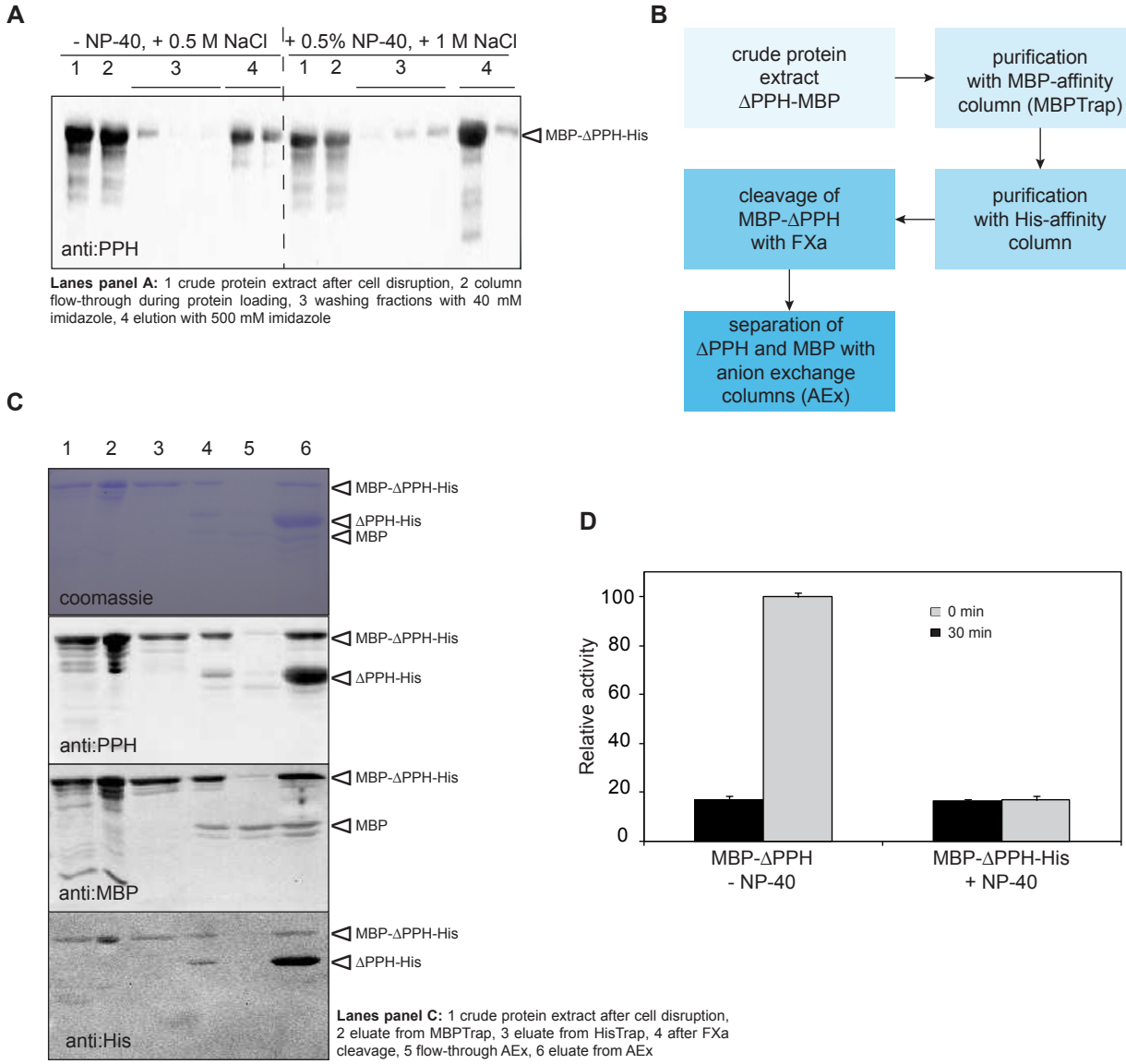

Figure 3. Purification of ΔPPH with the addition of NP-40. A, NP-40 enhances protein yield during purification. Western blot with antibodies against PPH is shown. Two samples of crude protein extract were purified with His affinity column, either not containing NP-40 or containing 0.5% NP-40 and increased NaCl concentration. **B,** Schematic overview of the final purification process. **C,** Coomassie-stained SDS-PAGE gel and Western blots probed with different antibodies as indicated. The fusion protein was pre-purified with a MBP-affinity column and subsequently purified with a His-affinity column. The eluted fusion protein was cleaved with FXa and separated with an anion exchange column (AEx). MBP was found in the flow through after AEx and ΔPPH-His eluted with 500 mM NaCl. **D,** Activity measurement of MBP-ΔPPH and MBP-ΔPPH-His supplemented with NP-40. Enzymatic conversion of pheophytin *a* to pheophorbide *a* was measured by HPLC. Data are mean values of 2-3 replicates, error bars indicate SD.

was detected in the flow-through and more protein eluted from the His-affinity column when the protein sample was supplemented with 0.5% NP-40 and increased NaCl concentration. In a next step an entire purification process, including proteolytic cleavage of the fusion protein, was performed. Figure 3B shows a schematic overview of the purification process. The crude protein extract was first loaded on a MBP-affinity column. The buffer contained 20 mM Tris-HCl pH 8 and 200 mM NaCl. Bound protein was eluted by adding 10 mM maltose to the buffer. Subsequently, the eluted protein fraction was supplemented with 0.1% (v/v) NP-40 and 40 mM imidazole. NaCl concentration was adjusted to 1 M. After protein purification with a His-affinity column the eluted protein was cleaved with 1% (w/w) FXa. Finally, MBP and ΔPPH were separated by anion exchange chromatography. For this, 5 volumes of 20 mM Tris-HCl pH 8 were added to lower the NaCl concentration to 200 mM. MBP was found in the flow-through and ΔPPH eluted by raising the NaCl concentration to 500 mM. Different samples of the purification process were analyzed by coomassie staining on a SDS-PAGE and by Western blots with antibodies against PPH, MBP and His (Figure 3C). The obtained protein yield was high; however, cleavage of the fusion protein was incomplete and a remarkable amount of protein remained intact as MBP-ΔPPH-His fusion protein. In addition, as seen from the Western blots with antibodies against PPH and His, cleavage of the His-tag seemed not to be possible (Figure 3C). Since the goal of the protein purification was to obtain pure protein for crystallization, it was of high importance that the enzymatic function of PPH remained intact. Therefore activity assays

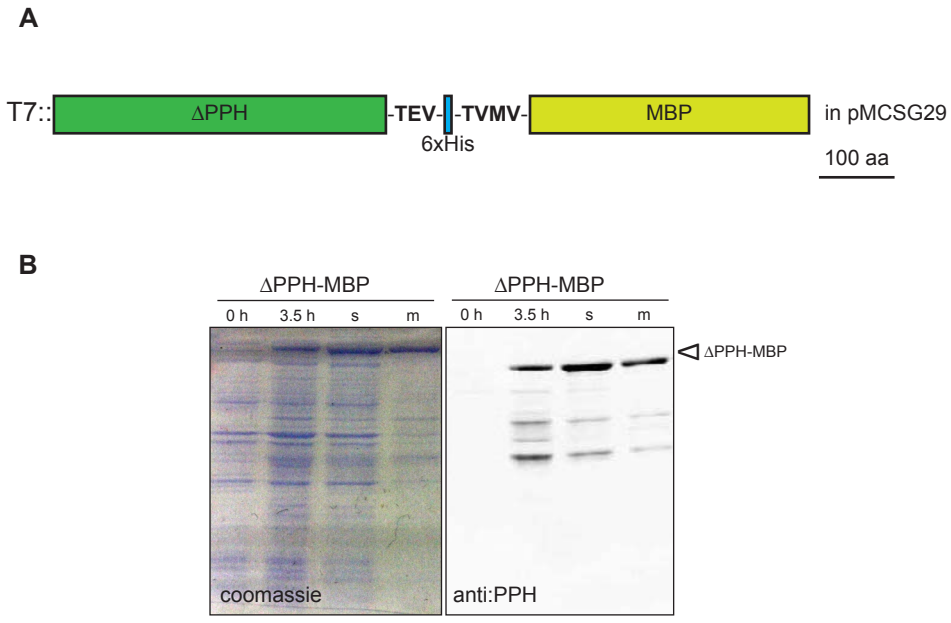

Figure 4. Expression of ΔPPH as ΔPPH-MBP fusion protein in pMCSG29. **A,** Schematic overview of the ΔPPH-MBP construct in pMCSG29. Note that TEV and TVMV sites are not drawn to scale. **B,** Protein expression in *E. coli* BL21(DE3). Left, coomassie-stained SDS-PAGE gel; right, Western blot after hybridization with antibodies against PPH. s, soluble fraction; m, membrane fraction.

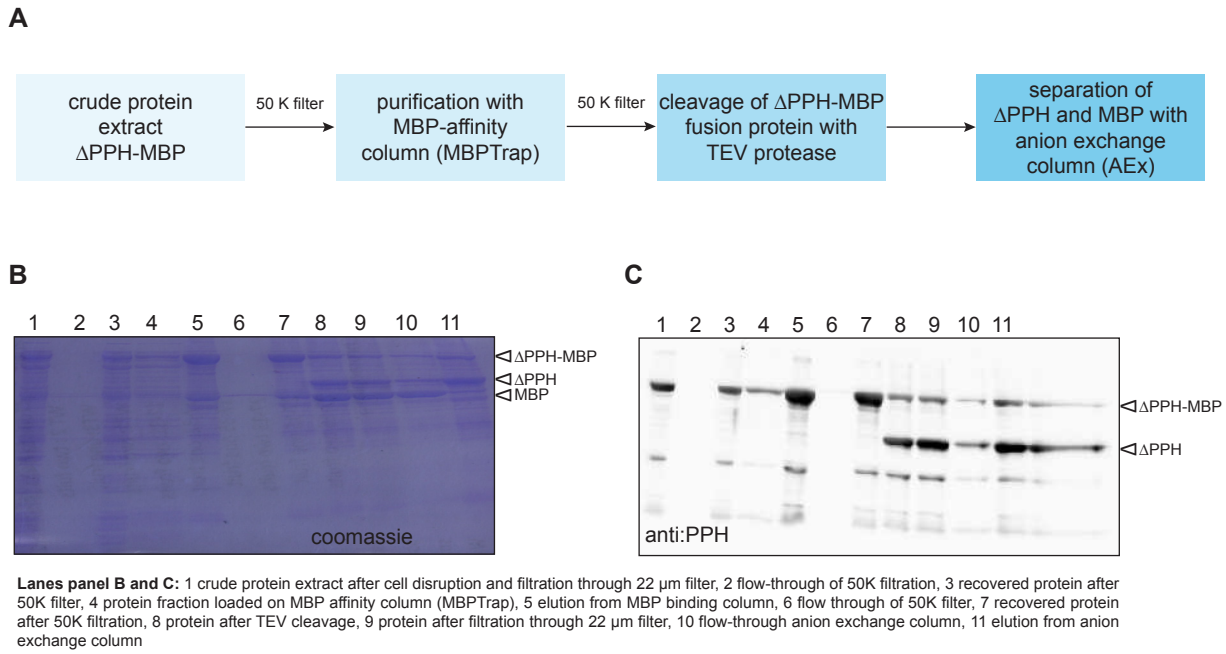

Figure 5. Purification and cleavage of ΔPPH-MBP. A, Schematic overview of the purification process. ΔPPH-MBP was first purified with a MBP-affinity column. After TEV cleavage of the fusion protein, MBP and ΔPPH were separated with an anion exchange column. **B,** Coomassie-stained SDS-PAGE gel. **C,** Western blot with anti PPH antibodies.

were performed using ΔPPH purified from MBP-ΔPPH (Figure 1A) and ΔPPH purified from MBP-ΔPPH-His (Figure 2A). Conversion of pheophytin *a* into pheophorbide *a* was monitored by HPLC (Figure 3D). ΔPPH purified from MBP-ΔPPH showed high enzymatic activity and was able to convert pheophytin *a*, while ΔPPH purified from MBP-ΔPPH-His did not show any enzymatic activity. Most likely the loss of activity was due to the addition of NP-40; however it would be necessary to compare the activity with crude MBP-ΔPPH-His fusion protein not supplemented with NP-40.

5.2.4 Expression of ΔPPH as N-terminal MBP fusion protein (ΔPPH-MBP)

Although the purity of ΔPPH, which was expressed as MBP-ΔPPH-His fusion protein, was high, the protein was not suitable for protein crystallization due to the activity loss (Figure 3). Therefore, ΔPPH was cloned into pMCSG29 (Eschenfeldt et al., 2010) thereby adding a C-terminal MBP-tag with a TEV cleavage site (ΔPPH-MBP) (Figure 4A). The fusion protein was expressed in *E. coli* BL21(DE3) and the major part of the protein was found in the soluble fraction after cell lysis (Figure 4B). Western blot analysis using antibodies against PPH indicated that ΔPPH was well expressed without protein fragmentation (Figure 4B). Figure 5A shows a schematic overview of a first purification test of ΔPPH-MBP. The crude protein extract in MBP buffer (20 mM Tris-HCl pH 8, 200 mM NaCl) was filtered through a 50 K cut-off membrane,

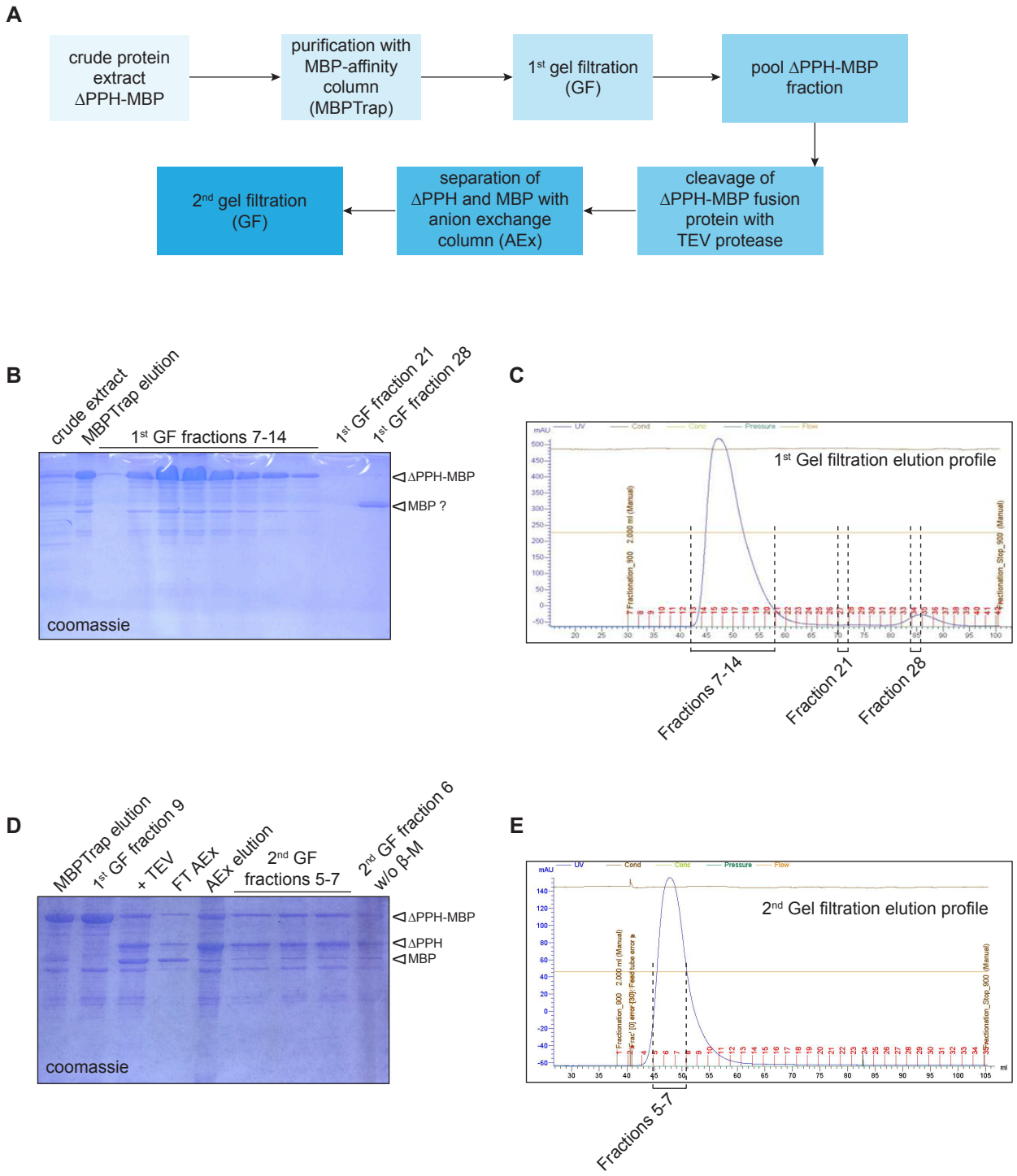

Figure 6. Separation of cleaved and un-cleaved protein by gel filtration. A, Schematic overview of the purification process. The fusion protein ΔPPH-MBP was first purified with a MBP-affinity column (MBPTrap) and subsequently loaded on a gel filtration (GF) column. Eluted ΔPPH-MBP was pooled and cleaved with TEV. MBP and ΔPPH were separated with an anion exchange column (AEx). As final purification step a second GF purification was performed. **B,** Coomassie-stained SDS-PAGE gel with samples of the purification process until the 1st GF step. GF fractions 7-14 (see panel C) represent the first, high molecular weight, peak. Fraction 28 (see panel C) represents the second peak with a clearly lower molecular weight. Probably this peak contained cleaved MBP protein. **C,** Chromatogram (A_{280}) of the 1st gel filtration. Two protein peaks eluted that were analyzed on SDS-PAGE (panel B).

loaded onto a MBP-affinity column and eluted by adding 10 mM maltose to the MBP buffer. The eluted protein, containing ΔPPH-MBP, was again filtered through a 50 K cut-off membrane. After TEV cleavage, ΔPPH and MBP were separated by anion exchange chromatography. For that, the protein sample was supplemented with 1 mM EDTA (anion exchange loading buffer: 20 mM Tris-HCl pH 8, 200 mM NaCl, 1 mM EDTA) and ΔPPH eluted by increasing the NaCl concentration to 500 mM. A coomassie-stained SDS-PAGE gel (Figure 5B) and a corresponding Western blot with PPH antibodies (Figure 5C) of different protein fractions during the purification process, clearly showed that the protein purity was satisfying; however, cleavage of the fusion protein with TEV was only partial. A remarkable fraction of the protein remained intact as fusion protein and co-eluted together with ΔPPH from the anion exchange column. Thus, the separation of the two protein forms by anion exchange was not possible.

5.2.4 Purified ΔPPH aggregates to high molecular weight complexes after MBP-tag cleavage

Size-exclusion chromatography (gel filtration) was included in the purification process (Figure 6A) in order to separate cleaved and un-cleaved protein forms (ΔPPH and ΔPPH-MBP). ΔPPH-MBP was purified with a MBP-affinity column (protein was present in 20 mM Tris-HCl pH 8, 200 mM NaCl), by eluting with 10 mM maltose in the buffer. Subsequently, the fusion protein was loaded on a gel filtration column. The eluted ΔPPH-MBP fusion protein was pooled and cleaved with TEV protease. The cleaved protein was supplemented with 1 mM EDTA and separated by anion exchange chromatography. MBP was found in the flow-through, while ΔPPH eluted together with the un-cleaved fusion protein by increasing the NaCl concentration to 500 mM. Finally the protein was again loaded on a gel filtration column (Figure 6A). Figures 6B and D show a SDS-PAGE gel after coomassie staining of protein fractions collected from the first part and second part, respectively, of the purification process. Two peaks eluted from the first gel filtration column (Figure 6C), one contained ΔPPH-MBP (fractions 7-14) with a high molecular weight and a second peak eluted with fraction 28. This fraction contained most likely free MBP. Fractions 5-7 of the 2nd gel filtration purification contained proteins of high molecular weight (Figure 6E). Analysis by SDS-PAGE (Figure 6D) revealed that this protein peak contained both, ΔPPH and un-cleaved ΔPPH-MBP. Apparently it was not possible to separate ΔPPH-MBP from cleaved ΔPPH by gel filtration although the size of the fusion protein is around 99 kDa while the cleaved ΔPPH has a size of around 47 kDa. It seemed that the cleaved protein aggregated to dimers or even higher molecular weight complexes and, therefore,

D, Coomassie-stained SDS-PAGE gel. The first two samples are the same as loaded on the blot of panel B. GF fractions 5-7 represent the eluted protein peak (see panel E). The last sample represents one fraction which was prepared without β-mercaptoethanol (w/o β-M) prior to loading on SDS-PAGE. **E,** Chromatogram (A_{280}) of the 2nd gel filtration. Only one protein peak eluted which contained cleaved ΔPPH but also un-cleaved ΔPPH-MBP fusion protein. FT, flow-through.

co-eluted with ΔPPH-MBP. Those aggregates were likely denatured during preparation for SDS-PAGE and even in the absence of β-mercaptoethanol (last lane of the blot shown in Figure 6D) the aggregates or dimers were not stable and were present in a denatured form.

In order to verify if ΔPPP forms oligomers in its native conformation or whether it aggregates when cleaved from MBP, the protein was analyzed on native PAGE gels. For this, the crude protein extract was first purified with a MBP-affinity column and eluted protein was cleaved with TEV. MBP and ΔPPH were separated by anion exchange. The eluted protein fraction was diluted until a NaCl concentration of 200 mM was reached. In order to remove un-cleaved protein, the eluted protein was loaded for a second time on a MBP-affinity column. It was expected that un-cleaved protein that still had the MBP-tag would bind to the column and therefore could be separated from ΔPPH. The eluted protein was finally loaded on a gel filtration column.

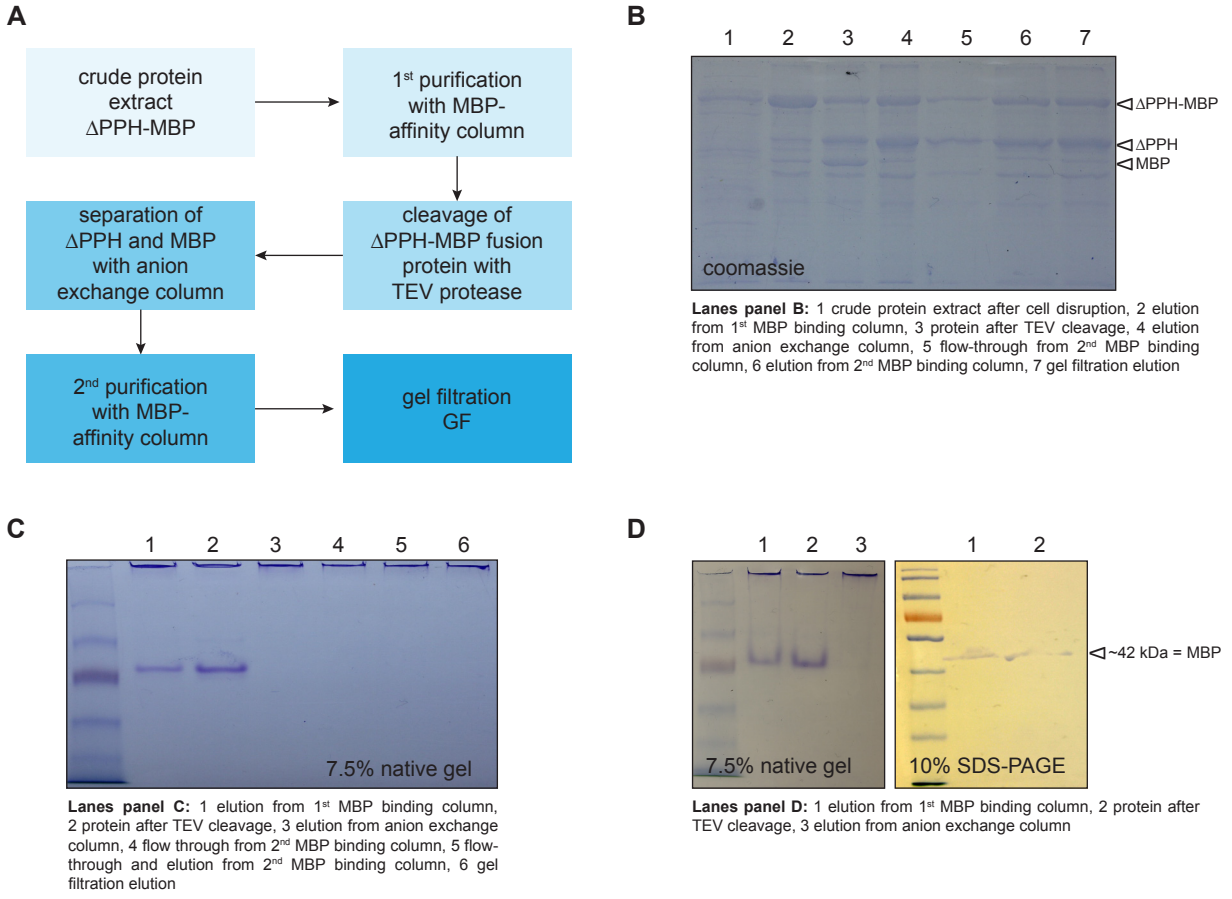

Figure 7. ΔPPH aggregates to high molecular weight complexes. A, Schematic overview of the purification process. The ΔPPH-MBP fusion protein was first purified with a MBP-affinity column and subsequently cleaved with TEV. MBP and ΔPPH were separated with an anion exchange column (AEx). The eluted protein fraction was purified for a second time with a MBP-affinity column and finally loaded onto a gel filtration column (GF). **B,** Coomassie-stained SDS-PAGE gel with samples of the whole purification process. **C,** Native gel with samples of the purification process. **D,** The bands which were detectable on the native PAGE were excised and inserted into the pockets of a SDS-PAGE gel and analyzed under denaturating conditions.

A schematic overview of this purification process is shown in Figure 7A. However, it was not possible to remove un-cleaved protein by the second MBP-affinity column (Figure 7B). In order to determine if ΔPPH is present as dimer in its native conformation, protein samples were loaded on a native PAGE gel. Interestingly, only a single band was detected for the first two samples, i.e. the eluted protein from the MBP-affinity column and the protein fraction after TEV cleavage (Figure 7C). Three bands with different sizes were although expected after TEV cleavage: the ΔPPH-MBP fusion protein with ~99 kDa, ΔPPH with 47 kDa and MBP with 42 kDa. If ΔPPH were present as a dimer in its native conformation, two bands would have been expected: ΔPPH-MBP and ΔPPH both with ~99 kDa and MBP with 47 kDa. Remarkably, large amounts of protein did not enter the gel and were retained in the pockets of the gel and it was assumed that highly aggregated protein was present, which could not enter the gel under native conditions. In order to investigate the composition and exact size of the bands, before and after TEV cleavage, detectable in the native PAGE gel (Figure 7C), they were excised and gel slices were placed into the pockets of a SDS-PAGE gel and run under denaturing conditions. As shown in Figure 7D the bands of the native gel resulted in a single band on the SDS-PAGE with a size of ~42 kDa, corresponding to the size of free MBP. From these results it can be concluded that cleaved ΔPPH aggregated to high molecular weight complexes which could not be separated by gel filtration and which were not detectable under native conditions because they did not enter the native gel.

5.2.5 Detergents partially prevent protein aggregation, but enzymatic activity is affected

If free ΔPPH aggregates to high molecular weight complexes it might be possible to separate the different protein units by supplementing the protein buffer with weak detergents that slightly solubilize the protein aggregates. As a consequence it should be possible to separate cleaved and un-cleaved ΔPPH-MBP fusion proteins by gel filtration. Here, different detergents were tested. ΔPPH-MBP fusion protein was purified on a MBP-affinity column. The eluate was supplemented with 1% (w/v) n-docecyl β-D-maltoside (DDM), 1% (w/v) N,N-dimethyldodecylamine N-oxide (DDAO) or 1% (v/v) octaethylene glycol monododecyl ether (C12E8) and subsequently cleaved with TEV protease. Cleaved proteins were analyzed by native PAGE (Figure 8A). When compared to Figure 7C the protein fraction after elution from the MBP-affinity column did not enter the gel this time. However, an explanation for this observation is difficult. A single band was detected for the sample after TEV cleavage without detergents (Figure 8A) as already observed in Figure 7C. Interestingly, a second band appeared in the samples with detergents (Figure 8A), but it remained unclear what the composition of the second band was. It is possible that cleaved ΔPPH aggregated with un-cleaved ΔPPH-MBP fusion protein thereby forming high molecular weight complexes and that these aggregates were separated by adding one of the tested detergents. In this case, the lower band probably represents ΔPPH and MBP (42-47 kDa) and the higher band contains the un-cleaved fusion protein (~99 kDa). However, comparable to the sample without detergents, a large amount of protein did not enter the gel and remained in the gel pockets.

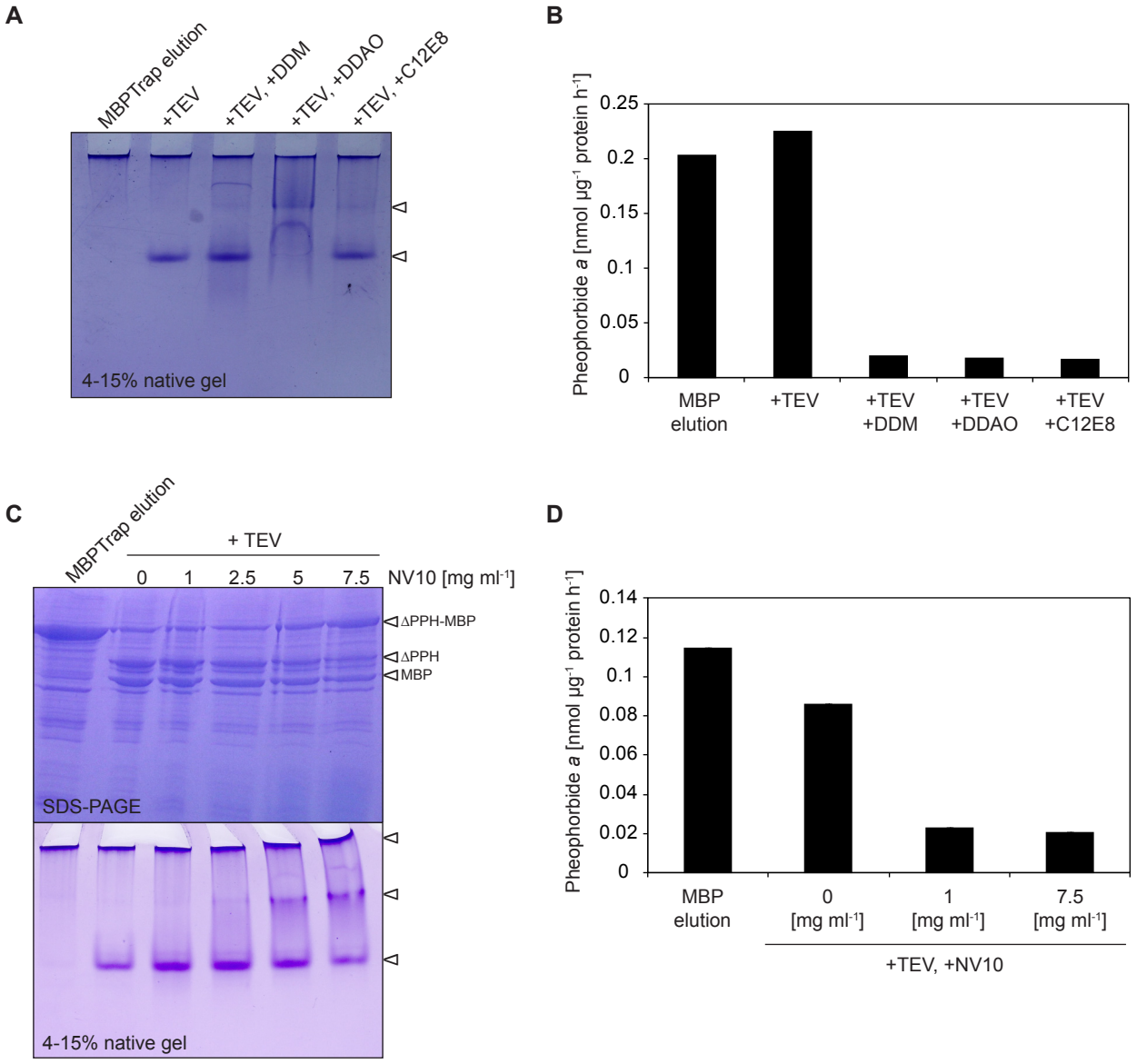

Figure 8. Influence of detergents and NV10 polymer on protein aggregation. A, Protein samples after MBP-affinity column (MBPTrap) elution and after TEV cleavage with different detergents were analyzed under native conditions. **B,** Influence of detergents on enzymatic activity. Conversion of pheophytin *a* to pheophorbide *a* was analyzed by HPLC. Data are single replicates. **C,** Protein samples after MBP-affinity column (MBPTrap) elution and after TEV cleavage with different concentrations of NV10 were analyzed by SDS-PAGE and under native conditions. **D,** Influence of NV10 on enzymatic activity. Conversion of pheophytin *a* to pheophorbide a was analyzed by HPLC. Data are single replicates. DDM, n-dodecyl β-D-maltoside; DDAO, N,N-dimethyldodecylamine N-oxide; C12E8, octaethylene glycol monododecyl ether.

An alternative additive which was analyzed, was the commercially available NVoy Polymer, NV10 (Expedeon). NV10 is described by the producer to prevent protein aggregation after tag-cleavage. Here, different NV10 concentrations, ranging from 0–7.5 mg ml^{-1}, were tested. Protein samples eluted from the MBP-affinity column were supplemented with NV10, cleaved with TEV and the cleavage efficiency analyzed by SDS-PAGE (Figure 8C). The shown blot indicated

that cleavage of the fusion protein occurred in the presence of NV10 but 7.5 mg ml^{-1} NV10 partially inhibited cleavage of the fusion protein. Native PAGE shows that NV10 might prevent protein aggregation (Figure 8D), thus, with a NV10 concentration higher than 2.5 mg ml^{-1} a second band appeared. However, the composition of the second band remains to be identified.

Although the results of detergent and NV10 treatment (Figure 8A and C) looked promising, the enzymatic activity of ΔPPH was affected (Figure 8B and D) as deduced from activity assays of different protein samples collected after the MBP-affinity purification or after TEV-cleavage. Thus, none of the samples containing detergents or NV10 was anymore able to convert pheophytin *a* to pheophorbide *a*, indicating that the hydrolytic activity of PPH was completely inhibited by the detergents (Figure 8B) and by NV10 (Figure 8D). Since the goal of the project was to purify functional protein, it will not be possible to continue with these additives. However, it remains to be tested if the substances can be removed and protein activity may recover.

5.3 Discussion

Protein purification is essential for protein crystallization. Different affinity tags with broad application have been developed during the past years (reviewed in: Lichty et al., 2005; Young et al., 2012). By optimizing protein purification of Arabidopsis PPH I found that first of all a C-terminal affinity tag is essential in order to prevent co-purification of incompletely translated or partially digested protein fragments. However, adding a short 6xHis-tag to the 3'-end was not sufficient. It was observed that the His-tag was not freely accessible and therefore the obtained yield of purified protein was very low. By changing the expression vector to pMCSG29 (Eschenfeldt et al., 2010) good results in yield and purity were obtained. Nevertheless, cleavage of the MBP-tag with the TEV protease was only partial. However, the biggest challenge I faced in this study was aggregation of PPH after tag-cleavage. High molecular weight complexes were observed which could not be separated by size-exclusion chromatography. It remains to be shown what the composition of the aggregates was. It is unclear if PPH forms oligomers in its native conformation or whether PPH aggregated with un-cleaved PPH-MBP fusion protein to high molecular weight complexes. Adding weak detergents or a special commercially available polymer could partially prevent protein aggregation. However, enzymatic activity was lost during the purification process in the presence of these compounds.

From this study I concluded that purification of PPH with the chosen system is difficult and very challenging. Since cleavage of the MBP-tag led to protein aggregation, an alternative would be to crystallize PPH as fusion protein. Since the fusion protein exhibited enzymatic activity, the protein was properly folded. It is known that co-crystallization of MBP with its fusion partner is difficult since the formation of well-organized crystals is challenged due to the

flexible linker region between the tag and the protein of interest (Smyth et al., 2003). However, co-crystallization can also be an advantage. The crystal structure of MBP has been resolved and therefore it can be used to solve the structure of the fusion partner by applying molecular replacement methods (Smyth et al., 2003). A first co-crystallization approach of ΔPPH-MBP has been performed and showed first promising results (this work chapter II).

Nevertheless, in order to obtain protein of good quality that can be used for protein crystallization, it is of big advantage to start the purification process with a broad screen of different tags and expression systems. Every tag has its advantages and disadvantages which have to be analyzed at the beginning. Also screening different expression conditions could rapidly lead to better results. For example it has been shown for MBP fusion proteins, that a shift of an oligomeric to a monomeric form can be achieved by applying a heat-shock treatment of the bacterial cells prior to protein expression (Lebendiker and Danieli, 2011). Therefore, for the construct used in this study, ΔPPH-MBP, changes in the expression procedure could have potentially improved the problem of protein aggregation. Last but not least, screening protein crystallization conditions is time consuming; nevertheless, it is worth trying to co-crystallize the protein of interest together with the affinity tag. As shown in chapter II of this work, first crystallization conditions could be identified for ΔPPH-MBP fusion protein.

5.4 Material and Methods

5.4.1 Cloning of fusion proteins

pMal-c2_PPH-His

A His-tag was added at the 3'-end of PPH by PCR amplification using Advantage polymerase (Clontech) and the primers PPH_BamHI-f (5'-gggatccagtggaaattccgatggttatg-3') and PPH-His_SalI_r (5'-cccgtcgactagtgatggtgatggtgatgcgatcctctccttccctcgattgcagacttccctccaaacac-3'). The resulting PCR product was subcloned into pGem-T easy (Promega) and transformed into NEB 10-beta competent *Escherichia coli* (*E. coli*) (High Efficiency) cells (New England Biolabs). Sequence accuracy was verified by sequencing. The PPH-His fragment in pGem-T-easy was excised by *Bam*HI and *Sal*I and ligated to the linearized pMal-c2 (New England Biolabs) vector. The Construct was transformed into *E. coli* DH5α. The construct was again verified by sequencing and finally transferred into *E. coli* BL21(DE3).

pMCSG29-PPH

See Material and Methods chapter II.

5.4.2 Protein expression

All proteins used in this study were expressed in *E. coli*. Cell cultures with respective antibiotics were grown at 37 °C to an optical density at 600 nm of 0.5–0.6. Protein expression was induced by adding 0.3–1 mM isopropyl β-D-1-thiogalactopyranoside (IPTG). pMal-c2-PPH (MBP-ΔPPH) and pMal-c2-PPH-His (MBP-ΔPPH-His) were expressed at 37 °C during 3 h. pMCSG29-PPH (ΔPPH-MBP) was expressed at 20 °C over night according to Stols et al. (2007). An initial expression test of pMCSG29-PPH was performed at 37 °C during 3.5 h. After protein expression bacterial cells were harvested by centrifugation and the cell pellet was resuspended in respective buffers (details see under results). Cell lysis was performed by using a French Press (Constant Cell Disruption System; Constant Systems) at 150 MPa and subsequent centrifugation was applied in order to separate soluble and membrane fractions. For the initial expression test of pMal-c2-PPH-His, the bacterial cells were harvested and treated with lysozyme and subsequently lysed by sonication (Schelbert et al., 2009).

5.4.3 Protein purification and proteolytic cleavage

Purification with MBP-affinity columns was performed by using MBPTrap HP columns (GE Healthcare). For protein purification with His-affinity columns, HisTrap HP columns (GE Healthcare) or Ni Sepharose 6 Fast Flow (GE Healthcare) were used. Anion exchange was performed with HiTrap Q HP columns (GE Healthcare). For gel filtration a HiLoad 16/600 Superdex 200 pg column (GE Healthcare) was used. The flow-rate was set to < 1 ml min^{-1} and all purification steps were carried out on ice or at 4 °C. For passing protein through 50 K cut-off filters, Amicon Ultra-15 centrifugal filter units with ultracel-50 membrane (Merck Millipore) were used.

For proteolytic cleavage with factor Xa (FXa), the fusion protein was supplemented with 0.5–1% (w/w) FXa (New England Biolabs) and incubated up to 72 h at 4 °C. For proteolytic cleavage with TEV, the protein sample was diluted to 1 mg ml^{-1} and supplemented with ProTEV plus (Promega) (30-75 U mg^{-1} protein). TEV cleavage was performed over night at room temperature.

5.4.4 Protein analysis: quantification, SDS-PAGE, native gels, Western blot

Protein quantification

Protein quantification was performed by using Bradford dye (BioRad). A standard curve was generated by measuring different concentrations of bovine serum albumin.

SDS-PAGE

10 ml of a 12.5% running gel consisted of 4.2 ml acrylamide (30% [w/v] acrylamide/Bis solution, BioRad), 2.5 ml 1.5 M Tris-HCl pH 8.8, 100 µl 10% (w/v) sodium dodecyl sulfate (SDS) 5 µl TEMED, 50 µl 10% (w/v) ammonium persulfate (APS) and 3.2 ml H_2O. For a 10% running gel, acrylamide and H_20 were adjusted accordingly. 5 ml of a 4% stacking gel contained of 666 µl acrylamide (30% [w/v] acrylamide/Bis solution, BioRad), 1.25 ml 0.5 M Tris-HCl pH 6.8, 50 µl 10% (w/v) SDS 2.5 µl TEMED, 50 µl 10% (w/v) APS and 3 ml H_2O. Gels were in 1x Lämmli-buffer (10x Lämmli-buffer: 14.14 g l^{-1} Tris base, 0.5% [w/v] SDS, 72 g l^{-1} glycine). Protein samples were prepared for gel-loading by mixing with sample buffer (5x sample buffer: 125 mM Tris pH 6.8, 5% [w/v] SDS, 25% [w/v] glycerol, 0.15% [w/v] bromphenol blue, 20% [v/v] β-mercaptoethanol) and boiling for 5 min.

Native PAGE

For native PAGE, pre-casted gels were used (4–15% Mini-PROTEAN TGX Gel, BioRad) or they were prepared according to Arndt et al. (2012). 15 ml of a 7.5% native gel consisted of 2.5 ml acrylamide (30% [w/v] acrylamide/Bis solution, BioRad), 2.5 ml 1.5 M Tris-HCl pH 8.8, 5 ml H_2O, 50 µl 10% (w/v) APS and 10 µl TEMED. Protein samples were mixed with an equal volume of sample buffer (30% [w/v] glycerol, 187 mM Tris-HCl pH 6.8 and 0.15% [w/v] bromphenol blue). The running buffer for native gels contained 3 g l^{-1} Tris base and 14.4 g l^{-1} glycine.

Western blot

After protein separation by SDS-PAGE, the gels were equilibrated in transfer buffer (25 mM Tris pH 8.3, 192 mM glycine, 20% [v/v] methanol) and the proteins were transferred onto nitrocellulose membrane (Whatman). The membrane was blocked with 5% (w/v) milk powder and washed with TTBS (50 mM Tris pH 7.5, 200 mM NaCl, 0.05% [v/v] Tween20). Membranes were hybridized with the primary antibody (anti-PPH: AgriSera, J. Parankiewicz-Aspulan, anti-MBP: New England Biolabs, anti-poly-His: Sigma-Aldrich), diluted in TTBS (anit-PPH and anti-MBP: 1:10’000 [v/v], anti-poly-His: 1:5‘000 [v/v]), over night at 4 °C. After washing the membranes with TTBS the secondary antibody (1:40’000 [v/v] in TTBS), conjugated with horseradish peroxidase (HRP), was applied (anti-rabbit and anti-mouse: Sigma-Aldrich) during 1.5–2 h at room temperature. Blots were developed by incubation with Immun-Star WesternC Kit (BioRad) and imaged with a gel Chemidoc XRS System (BioRad).

5.4.5 Activity assays

Comparison of ΔPPH purified from MBP-ΔPPH and from MBP-ΔPPH-His

5 µg of the purified protein (~0.4 µg µl^{-1}) were incubated for 30 min at 34 °C with ~7 µg pheophytin (~1 µg µl^{-1} dissolved in acetone) in assay buffer (0.1 M Hepes-KOH, 1 mM EDTA, pH 8). The total volume of the assays was 70 µl. Reactions were stopped by adding 2 volumes of acetone. The mixture was centrifuged and analyzed by HPLC according to Das and Guyer et al. (submitted).

Activity of ΔPPH with detergents or NV10

5 µg of protein (1 µg µl^{-1}) were incubated for 60-75 min at 34 °C with ~6 µg pheophytin (~2 µg µl^{-1} dissolved in acetone) in assay buffer (0.1 M Hepes-KOH, 1 mM EDTA, pH 8). Total volumes of the assays were 100 µl for assays testing NV10 and 50 µl for testing detergents. Reactions were stopped by adding 2 volumes of acetone. The mixture was centrifuged and analyzed by HPLC according to Das and Guyer et al. (submitted). Conversion of pheophytin *b* was not analyzed.

5.5 Acknowledgment and contribution

All experimental work was carried out by myself. I would like to thank Silvia Schelbert Hofstetter for cloning the pMal-c2-PPH (MBP-ΔPPH) construct and for instructing me to the procedures of protein purification. I also would like to thank Undine Krügel (Institute of Plant Biology, University of Zurich) for all her methodological inputs and for her great help and patience.

Conclusion and Outlook

Chlorophyll breakdown is of high relevance for plants. The detoxification associated with its degradation is a requisite for nutrient reallocation from source to sink organs. Thus, chlorophyll breakdown is one important step in achieving high-value crop plants.

Pheophytinase (PPH) has been described for being responsible for dephytylating pheophytin during leaf senescence in Arabidopsis (Schelbert et al., 2009). Here, the substrate specificity has been further defined to be determined by the acid moiety of the ester bond. Changes in the molecular structure of the porphyrin ring inhibit enzymatic activity. Solving the crystal structure of PPH would enlighten the binding mechanism of PPH and could give some insights into the relevance of this tight substrate specificity. In the future, the final elucidation of the crystal structure of PPH is of big interest. Due to the inhibitory effect of chlorophyll, we know that PPH binds chlorophyll but does not convert it to chlorophyllide. Therefore, it might be possible to use chlorophyll to crystallize PPH as an enzyme-pigment complex. Another approach to understand the binding is the use of a PPH variety that is mutated in the active site serine residue (PPH_{S221A}) impairing its enzymatic function (Schelbert et al., 2009). However, it has not yet been shown if PPH_{S221A} binds pheophytin at all. If so, co-crystallization of PPH_{S221A} with pheophytin and of wild-type PPH with chlorophyll would give insight into structural characteristics responsible for proper substrate binding and enzymatic activity. It would be interesting to see if PPH could be mutated in a way that the tight substrate specificity is lost and to elucidate what the biological effect of such a protein would be. However, the first next step is to find appropriate crystallization conditions which lead to protein crystals usable for structure solving.

The results of the comparison study of dephytylating activities in senescing tomato leaves and ripening fruits open up new questions. The stay-green phenotype of leaves of tomato plants that are impaired in PPH activity is a strong proof that PPH is the core hydrolase in leaf senescence in different plant species. However, the picture seems to be more complex in fruits. PPH is involved, but is accompanied by other hydrolases. CLH expression data from tomato and the analysis of chlorophyll degradation in Arabidopsis siliques are in good agreement with each other. Hence, it can be assumed that CLHs are not the hydrolases accompanying PPH activity in ripening fruits. In order to identify the responsible hydrolase in fruits, two approaches could be followed in the future. The access to a tomato EMS-mutant collection will be useful in order to screen for tomato fruits that show alterations in fruit color break. We expect mutants with

altered pigment composition that accumulate pheophytin or retain chlorophyll, which can be easily scored by HPLC and would allow selecting candidates for further analysis. If mutants can be identified that show differences in fruit ripening, whole genome sequencing could identify the involved genes. The other approach is the use of Arabidopsis T-DNA insertion lines in genes encoding α/β-hydrolases. However, the Arabidopsis genome encodes hundreds of such proteins which could be considered as candidates. Nevertheless, HPLC analysis of mutants is facile and gives immediate results. Identifying a second dephytylating enzyme in chlorophyll degradation is definitively a major goal in the near future.

To date, the process underlying magnesium (Mg) dechelation remains unclear. As already discussed in the literature, slight pH changes lead to spontaneous formation of pheophytin *in vitro* (Hirai et al., 2009; Saga et al., 2013). We now have first promising indications that local plastidic pH changes might trigger the loss of Mg. However, this assumption only derives from observations of chloroplastic pH in transiently transformed protoplasts. An observation *in planta* is still required. For this, the ratiometric pH probe used here was stably transformed into Arabidopsis. Hopefully, this will enable pH tracking during the entire development including senescence. Assuming that stromal pH changes are involved and that dismantling of the thylakoid membrane is a prerequisite for such pH-derived effect, the analysis of different stay-green mutants will be helpful. In my preliminary experiments I observed pH differences between wild type and *pph-1*. The most interesting would be the analysis of plants deficient in SGR. These plants show, comparable to *pph-1*, retention of stacking of the grana thylakoids during senescence. Therefore, it could be possible that pH changes do not occur and chlorophyll is not demetalated. Maybe these findings will also give an answer to the observation that *pph-1* plants mostly retain chlorophyll and only partially accumulate pheophytin (Schelbert et al., 2009). An additional proof will possibly derive from the analysis of plants that have an altered pH homeostasis in chloroplasts. These mutants will be crossed with *pph-1* and other stay-green plants to further investigate the effect of the chloroplastic pH.

List of Abbreviations

ACD	ACCELERATED CELL DEATH
Arabidopsis	*Arabidopsis thaliana*
C12E8	octaethylene glycol monododecyl ether
CCE	chlorophyll catabolic enzyme
CLH	CHLOROPHYLLASE
Col-0	*Arabidopsis thaliana* ecotype Columbia-0
DDAO	N,N-dimethyldodecylamine N-oxide
Ddi	days after dark incubation
DDM	n-dococyl β-D-maltoside
DNCC	dioxobilin-type nonfluorescent chlorophyll catabolite
ER	endoplasmic reticulum
FXa	factor Xa
GFP	green fluorescent protein
HCAR	7-hydroxymethyl chlorophyll *a* reductase
His	histidin
hmFCC	*hypermodified* FCCs
HPLC	high-pressure liquid chromatography
HR	hypersensitive response
IPTG	isopropyl β-D-1-thiogalactopyranoside
KEA	K^+-efflux antiporter
LHCII	light-harvesting complex II
MBP	maltose-binding protein
MCS	metal chelating substance
MES16	METHYL ESTERASE 16
MPD	2-methyl-2,4-pentanediol
MRP	metal-releasing protein
NAS	NICOTIANAMINE SYNTHASE
NCC	nonfluorescent chlorophyll catabolite
NOL	NYC-like
NP-40	nonidet-40
NYC	NON-YELLOW COLORING

NYE	NONYELLOWING
PAO	PHEOPHORBIDE A OXYGENASE
PCR	polymerase chain reaction
PEG	polyethylene glycol
pFCC	*primary* fluorescent chlorophyll catabolite
PPH	PHEOPHORBIDE PHEOPHYTIN HYDROLASE
RaVC	ratiometric pH probe
RCC	red chlorophyll catabolite
RCCR	RED CHLOROPHYLL CATABOLITE REDUCTASE
ROS	reactive oxygen species
SDS-PAGE	sodium dodecyl sulfate polyacrylamide gel electrophoresis
SGR	STAY GREEN
T-DNA	transfer DNA
TEV	tobacco etch virus protease
TP	transit peptide
UGT	UDP-DEPENDENT GLYCOSYLTRANSFERASE
Ws	*Arabidopsis thaliana* ecotype Wassilewskija
YCC	yellow chlorophyll catabolites

Literature

Alonso JM, Stepanova AN, Leisse TJ, Kim CJ, Chen H, Shinn P, Stevenson DK, Zimmermann J, Barajas P, Cheuk R, et al (2003) Genome-wide insertional mutagenesis of *Arabidopsis thaliana*. Science **301:** 653–657

Anderegg G, Ripperger H (1989) Correlation between metal complex formation and biological activity of nicotianamine analogues. J Chem Soc, Chem Commun 647–650

Arndt C, Koristka S, Bartsch H, Bachmann M (2012) Native polyacrylamide gels. *In:* BT Kurien, HR Scofield, eds, Methods in Molecular Biology: Protein Electrophoresis: Methods and Protocols, **869:** pp. 49–53

Aubry S, Mani J, Hörtensteiner S (2008) Stay-green protein, defective in Mendel's green cotyledon mutant, acts independent and upstream of pheophorbide *a* oxygenase in the chlorophyll catabolic pathway. Plant Mol Biol **67:** 243–256

Azoulay Shemer T, Harpaz-Saad S, Belausov E, Lovat N, Krokhin O, Spicer V, Standing KG, Goldschmidt EE, Eyal Y (2008) Citrus chlorophyllase dynamics at ethylene-induced fruit color-break; a study of chlorophyllase expression, post-translational processing kinetics and in-situ intracellular localization. Plant Physiol **148:** 108–118

Azoulay-Shemer T, Harpaz-Saad S, Cohen-Peer R, Mett A, Spicer V, Lovat N, Krokhin O, Brand A, Gidoni D, Standing KG, et al (2011) Dual N- and C-terminal processing of citrus chlorophyllase precursor within the plastid membranes leads to the mature enzyme. Plant Cell Physiol **52:** 70–83

Badgaa A, Jia A, Ploss K, Boland W (2014) Chlorophyll degradation in the gut of generalist and specialist Lepidopteran caterpillars. J Chem Ecol **40:** 1232–1240

Bagar T, Altenbach K, Read ND, Benčina M (2009) Live-cell imaging and measurement of intracellular pH in filamentous fungi using a genetically encoded ratiometric probe. Eukaryot Cell **8:** 703–712

Barry CS, McQuinn RP, Chung MY, Besuden A, Giovannoni JJ (2008) Amino acid substitutions in homologs of the STAY-GREEN protein are responsible for the *green-flesh* and *chlorophyll retainer* mutations of tomato and pepper. Plant Physiol **147:** 179–187

Barsan C, Sanchez-Bel P, Rombaldi C, Egea I, Rossignol M, Kuntz M, Zouine M, Latche A, Bouzayen M, Pech JC (2010) Characteristics of the tomato chromoplast revealed by proteomic analysis. J Exp Bot **61:** 2413–2431

Barsan C, Zouine M, Maza E, Bian W, Egea I, Rossignol M, Bouyssie D, Pichereaux C, Purgatto E, Bouzayen M, et al (2012) Proteomic analysis of chloroplast-to-chromoplast transition in tomato reveals metabolic shifts coupled with disrupted thylakoid biogenesis machinery and elevated energy-production components. Plant Physiol **160:** 708–725

Christ B, Hörtensteiner S (2014) Mechanism and Significance of Chlorophyll Breakdown. J Plant Growth Regul **33:** 1–17

Christ B, Schelbert S, Aubry S, Süssenbacher I, Müller T, Kräutler B, Hörtensteiner S (2012) MES16, a member of the methylesterase protein family, specifically demethylates fluorescent chlorophyll catabolites during chlorophyll breakdown in Arabidopsis. Plant Physiol **158:** 628–641

Christ B, Süssenbacher I, Moser S, Bichsel N, Egert A, Müller T, Kräutler B, Hörtensteiner S (2013) Cytochrome P450 CYP89A9 is involved in the formation of major chlorophyll catabolites during leaf senescence in Arabidopsis. Plant Cell **25:** 1868–1880

Costa ML, Civello PM, Chaves AR, Martinez GA (2002) Characterization of Mg-dechelatase activity obtained from *Fragaria* x *ananassa* fruit. Plant Physiol Biochem **40:** 111–118

Das A, Guyer L, Hörtensteiner S (submitted) Chlorophyll and chlorophyll catabolite analysis by HPLC. Springer protocols

De Rybel B, van den Berg W, Lokerse AS, Liao C-Y, van Mourik H, Möller B, Llavata-Peris CI, Weijers D (2011) A versatile set of ligation-independent cloning vectors for functional studies in plants. Plant Physiol **156:** 1292–1299

Egea I, Barsan C, Bian W, Purgatto E, Latché A, Chervin C, Bouzayen M, Pech J-C (2010) Chromoplast differentiation: current status and perspectives. Plant Cell Physiol **51:** 1601–1611

Endler A, Meyer S, Schelbert S, Schneider T, Weschke W, Peters SW, Keller F, Baginsky S, Martinoia E, Schmidt UG (2006) Identification of a vacuolar sucrose transporter in barley and Arabidopsis mesophyll cells by a tonoplast proteomic approach. Plant Physiol **141:** 196–207

Eschenfeldt W, Lucy S, Millard C, Joachimiak A, Mark ID (2009) A family of LIC vectors for high-throughput cloning and purification of proteins. *In:* Doyle SA, ed, Methods in Molecular Biology: High throughput protein expression and purification **498:** pp. 105–115

Eschenfeldt W, Maltseva N, Stols L, Donnelly M, Gu M, Nocek B, Tan K, Kim Y, Joachimiak A (2010) Cleavable C-terminal His-tag vectors for structure determination. J Struct Funct Genomics **11:** 31–39

Evans IM, Rus AM, Belanger EM, Kimoto M, Brusslan JA (2010) Dismantling of *Arabidopsis thaliana* mesophyll cell chloroplasts during natural leaf senescence. Plant Biol **12:** 1–12

Fojan P, Jonson PH, Petersen MTN, Petersen SB (2000) What distinguishes an esterase from a lipase: A novel structural approach. Biochimie **82:** 1033–1041

GE Healthcare (2012) Recombinant protein purification. Principles and methods. Downloaded from www.gelifesciences.com/protein-purification

Goldschmidt EE (2001) Chlorophyll decomposition in senescing leaves and ripening fruits: functional and evolutionary perspectives. *In:* Ben-Arie R, Philosoph-Hadas S, eds, Proc 4th Int Conf on Postharvest. Acta Hort **553:** 331–335

Guyer L, Hofstetter Schelbert S, Christ B, Lira BS, Rossi M, Hörtensteiner S (2014) Different mechanisms are responsible for chlorophyll dephytylation during fruit ripening and leaf senescence in tomato. Plant Physiol **166:** 44–56

Hendry GAF, Houghton JD, Brown SB (1987) The degradation of chlorophyll - A biological enigma. New Phytol **107:** 255–302

Hirai Y, Tamiaki H, Kashimura S, Saga Y (2009) Demetalation kinetics of natural chlorophylls purified from oxygenic photosynthetic organisms: effect of the formyl groups conjugated directly to the chlorin pi-macrocycle. Photochem Photobiol Sci **8:** 1701–1707

Horie Y, Ito H, Kusaba M, Tanaka R, Tanaka A (2009) Participation of chlorophyll *b* reductase in the initial step of the degradation of light-harvesting chlorophyll *a*/*b*-protein complexes in Arabidopsis. J Biol Chem **284:** 17449–17456

Hörtensteiner S (1999) Chlorophyll breakdown in higher plants and algae. Cell Mol Life Sci **56:** 330–347

Hörtensteiner S (2006) Chlorophyll degradation during senescence. Annu Rev Plant Biol **57:** 55–77

Hörtensteiner S (2013) Update on the biochemistry of chlorophyll breakdown. Plant Mol Biol **82:** 505–517

Hörtensteiner S, Feller U (2002) Nitrogen metabolism and remobilization during senescence. J Exp Bot **53:** 927–937

Hörtensteiner S, Kräutler B (2011a) Chlorophyll breakdown in higher plants. Biochem Biophys Acta **1807:** 977–988

Hörtensteiner S, Vicentini F, Matile P (1995) Chlorophyll breakdown in senescent cotyledons of rape, *Brassica napus* L.: enzymatic cleavage of phaeophorbide *a* in vitro. New Phytol **129:** 237–246

Hruz T, Laule O, Szabo G, Wessendorp F, Bleuler S, Oertle L, Widmayer P, Gruissem W, Zimmermann P (2008) Genevestigator V3: a reference expression database for the meta-analysis of transcriptomes. Advances in Bioinformatics **2008:** 5

Hu X, Makita S, Schelbert S, Sano S, Ochiai M, Tsuchiya T, Hasegawa SF, Hortensteiner S, Tanaka A, Tanaka R (2015) Re-examination of chlorophyllase function implies its involvement in defense against chewing herbivores. Plant Physiol **167:** 660-670

Ischebeck T, Zbierzak AM, Kanwischer M, Dörmann P (2006) A salvage pathway for phytol metabolism in Arabidopsis. J Biol Chem **281:** 2470–2477

Ito H, Tanaka Y, Tsuji H, Tanaka A (1993) Conversion of chlorophyll *b* to chlorophyll *a* by isolated cucumber etioplasts. Arch Biochem Biophys **306:** 148–151

Kariola T, Brader G, Li J, Palva ET (2005) Chlorophyllase 1, a damage control enzyme, affects the balance between defense pathways in plants. Plant Cell **17:** 282–294

Klatte M, Schuler M, Wirtz M, Fink-Straube C, Hell R, Bauer P (2009) The analysis of Arabidopsis nicotianamine synthase mutants reveals functions for nicotianamine in seed iron loading and iron deficiency responses. Plant Physiol **150:** 257–271

Kleinboelting N, Huep G, Kloetgen A, Viehoever P, Weisshaar B (2012) GABI-Kat SimpleSearch: new features of the *Arabidopsis thaliana* T-DNA mutant database. Nucleic Acids Res **40:** D1211–D1215.

Kräutler B, Hörtensteiner S (2013) Chlorophyll breakdown: chemistry, biochemistry and biology. *In*: Ferreira GC, Kadish KM, Smith KM, Guilard R, eds, Handbook of Porphyrin Science, vol. **28**. World Scientific Publishing, USA, pp 117–185

Kräutler B, Matile P (1999) Solving the riddle of chlorophyll breakdown. Accounts Chem Res **32:** 35–43

Kunieda T, Amano T, Shioi Y (2005) Search for chlorophyll degradation enzyme, Mg-dechelatase, from extracts of *Chenopodium album* with native and artificial substrates. Plant Sci **169:** 177–183

Kunz H-H, Gierth M, Herdean A, Satoh-Cruz M, Kramer DM, Spetea C, Schroeder JI (2014) Plastidial transporters KEA1, -2, and -3 are essential for chloroplast osmoregulation, integrity, and pH regulation in Arabidopsis. Proc Natl Acad Sci USA **111:** 7480–7485

Kusaba M, Ito H, Morita R, Iida S, Sato Y, Fujimoto M, Kawasaki, S, Tanaka R, Hirochika H, Nishimura M, et al (2007) Rice NON-YELLOW COLORING1 is involved in light-harvesting complex II and grana degradation during leaf senescence. Plant Cell **19:** 1362–1375

Kusaba M, Tanaka A, Tanaka R (2013) Stay-green plants: what do they tell us about the molecular mechanism of leaf senescence. Photosynth Res **117:** 221–234

Labeta MO, Fernandez N, Festenstein H (1988) Solubilisation effect of Nonidet P-40, Triton X-100 and CHAPS in the detection of MHC-like glycoproteins. J Immunol Methods **112:** 133–138

Lebendiker M, Danieli T (2011) Purification of proteins fused to maltose-binding protein. *In:* Walls D, Loughran ST, eds, Methods in Molecular Biology: Protein Chromatography **681**: pp. 281–293

Lichty JJ, Malecki JL, Agnew HD, Michelson-Horowitz DJ, Tan S (2005) Comparison of affinity tags for protein purification. Protein Expres Purif **41:** 98–105

Lineweaver H, Burk D (1934) The determination of enzyme dissociation constants. J Am Chem Soc **56:** 658–666

Lippold F, vom Dorp K, Abraham M, Hölzl G, Wewer V, Yilmaz, JL, Lager I, Montandon C, Besagni C, Kessler F, et al (2012) Fatty acid phytyl ester synthesis in chloroplasts of Arabidopsis. Plant Cell **24:** 2001–2014

Lu Y-P, Li Z-S, Drozdowicz Y-M, Hörtensteiner S, Martinoia E, Rea PA (1998) AtMRP2, an Arabidopsis ATP binding cassette transporter able to transport glutathione S-conjugates and chlorophyll catabolites: functional comparisons with AtMRP1. Plant Cell **10:** 267–282

Lundquist PK, Poliakov A, Bhuiyan NH, Zybailov B, Sun Q, van Wijk KJ (2012) The functional network of the Arabidopsis plastoglobule proteome based on quantitative proteomics and genome-wide coexpression analysis. Plant Physiol **158:** 1172–1192

Mach JM, Castillo AR, Hoogstraten R, Greenberg JT (2001) The *Arabidopsis*-accelerated cell death gene *ACD2* encodes red chlorophyll catabolite reductase and suppresses the spread of disease symptoms. Proc Natl Acad Sci USA **98:** 771–776

Matile P, Ginsburg S, Schellenberg M, Thomas H (1988) Catabolites of chlorophyll in senescing barley leaves are localized in the vacuoles of mesophyll cells. Proc Natl Acad Sci USA **85:** 9529–9532

Matile P, Hörtensteiner S, Thomas H, Kräutler B (1996) Chlorophyll breakdown in senescent leaves. Plant Physiol **112:** 1403–1409

Meguro M, Ito H, Takabayashi A, Tanaka R, Tanaka A (2011) Identification of the 7-hydroxymethyl chlorophyll *a* reductase of the chlorophyll cycle in Arabidopsis. Plant Cell **23:** 3442–3453

Meyer A, Eskandari S, Grallath S, Rentsch D (2006) AtGAT1, a high affinity transporter for g-aminobutyric acid in *Arabidopsis thaliana*. J Biol Chem **281:** 7197–7204

Morita R, Sato Y, Masuda Y, Nishimura M, Kusaba M (2009) Defect in non-yellow coloring 3, an α/β hydrolase-fold family protein, causes a stay-green phenotype during leaf senescence in rice. Plant J **59:** 940–952

Müller T, Moser S, Ongania K-H, Pružinská A, Hörtensteiner S, Kräutler B (2006) A divergent path of chlorophyll breakdown in the model plant *Arabidopsis thaliana*. Chem Bio Chem **7:** 40–42

Mur LAJ, Aubry S, Mondhe M, Kingston-Smith A, Gallagher J, Timms-Taravella E, James C, Papp I, Hörtensteiner S, Thomas H, et al (2010) Accumulation of chlorophyll catabolites photosensitizes the hypersensitive response elicited by *Pseudomonas syringae* in Arabidopsis. New Phytol **188:** 161–174

Novy R, Drott D, Yaeger K Mierenhof R (2001) Overcoming the codon bias of *E. coli* for enhanced protein expression. inNovations newsletter of novagen, inc **12:** 1-3

Oberhuber M, Berghold J, Breuker K, Hörtensteiner S, Kräutler B (2003) Breakdown of chlorophyll: a nonenzymatic reaction accounts for the formation of the colorless "nonfluorescent" chlorophyll catabolites. Proc Natl Acad Sci USA **100:** 6910–6915

Park S-Y, Yu J-W, Park J-S, Li J, Yoo S-C, Lee N-Y, Lee S-K, Jeong S-W, Seo HS, Koh H-J, et al (2007) The senescence-induced staygreen protein regulates chlorophyll degradation. Plant Cell **19:** 1649–1664

Pattanayak GK, Venkataramani S, Hörtensteiner S, Kunz L, Christ B, Moulin M, Smith AG, Okamoto Y, Tamiaki H, Sugishima M, et al (2012) ACCELERATED CELL DEATH 2 suppresses mitochondrial oxidative bursts and modulates cell death in Arabidopsis. Plant J **69:** 589–600.

Pružinská A, Anders I, Tanner G, Roca M, Hörtensteiner S (2003) Chlorophyll breakdown: pheophorbide *a* oxygenase is a Rieske-type iron-sulfur protein, encoded by the *accelerated cell death 1* gene. Proc Natl Acad Sci USA **100:** 15259–15264

Pružinská A, Tanner G, Aubry S, Anders I, Moser S, Müller T, Ongania K-H, Kräutler B, Youn J-Y, Liljegren SJ, et al (2005) Chlorophyll breakdown in senescent Arabidopsis leaves: characterization of chlorophyll catabolites and of chlorophyll catabolic enzymes involved in the degreening reaction. Plant Physiol **139:** 52–63

Ren G, An K, Liao Y, Zhou X, Cao Y, Zhao H, Ge X, Kuai B (2007) Identification of a novel chloroplast protein AtNYE1 regulating chlorophyll degradation during leaf senescence in Arabidopsis. Plant Physiol **144:** 1429–1441

Ren GD, Zhou Q, Wu SX, Zhang YF, Zhang LG, Huang JR, Sun ZF, Kuai BK (2010) Reverse genetic identification of CRN1 and its distinctive role in chlorophyll degradation in Arabidopsis. J Integr Plant Biol **52:** 496–504

Rodoni S, Mühlecker W, Anderl M, Kräutler B, Moser D, Thomas H, Matile P, Hörtensteiner S (1997a) Chlorophyll breakdown in senescent chloroplasts. Cleavage of pheophorbide *a* in two enzymic steps. Plant Physiol **115:** 669–676

Rodoni S, Vicentini F, Schellenberg M, Matile P, Hörtensteiner S (1997b) Partial purification and characterization of red chlorophyll catabolite reductase, a stroma protein involved in chlorophyll breakdown. Plant Physiol **115:** 677–682

Rüdiger W (2002) Biosynthesis of chlorophyll *b* and the chlorophyll cycle. Photosynth Res **74:** 187–193

Saga Y, Hirai Y, Sadaoka K, Isaji M, Tamiaki H (2013) Structure-dependent demetalation kinetics of chlorophyll *a* analogs under acidic conditions. Photochem Photobiol **89:** 68–73

Sakuraba Y, Schelbert S, Park S-Y, Han S-H, Lee B-D, Besagni Andrès C, Kessler F, Hörtensteiner S, Paek N-C (2012) STAY-GREEN and chlorophyll catabolic enzymes interact at light-harvesting complex II for chlorophyll detoxification during leaf senescence in Arabidopsis. Plant Cell **24:** 507–518

Samson F, Brunaud V, Balzergue S, Dubreucq B, Lepiniec L, Pelletier G, Caboche M, Lecharny A (2002) FLAGdb/FST: a database of mapped flanking insertion sites (FSTs) of *Arabidopsis thaliana* T-DNA transformants. Nucleic Acids Res **30:** 94–97

Sato Y, Moria R, Katsuma S, Nishimura M, Tanaka A, Kusaba M (2009) Two short-chain dehydrogenase/reductases, NON-YELLOW COLORING 1 and NYC1-LIKE, are required for chlorophyll *b* and light-harvesting complex II degradation during senescence in rice. Plant J **57:** 120–131.

Schelbert Hofstetter S (2010) Biochemical and molecular identification of pheophytinase, an important esterase of chlorophyll breakdown during leaf senescence and fruit ripening. Dissertation, Universität Zürich, Zürich

Schelbert S, Aubry S, Burla B, Agne B, Kessler F, Krupinska K, Hörtensteiner S (2009) Pheophytin pheophorbide hydrolase (pheophytinase) is involved in chlorophyll breakdown during leaf senescence in Arabidopsis. Plant Cell **21:** 767–785

Schenk N, Schelbert S, Kanwischer M, Goldschmidt EE, Dormann P, Hortensteiner S (2007) The chlorophyllases AtCLH1 and AtCLH2 are not essential for senescence-related chlorophyll breakdown in *Arabidopsis thaliana*. FEBS Lett **581:** 5517–5525

Schrag JD, Cygler M (1997) Lipase and α/β hydrolase fold. *In:* Abelson JN, Simon MI, eds, Methods in Enzymology: Lipases **284:** 85-107

Sessions A, Burke E, Presting G, Aux G, McElver J, Patton D, Dietrich B, Ho P, Bacwaden J, Ko C, et al (2002) A high-throughput Arabidopsis reverse genetics system. Plant Cell **14:** 2985–2994

Shioi Y, Tomita N, Tsuchiya T, Takamiya K (1996a) Conversion of chlorophyllide to pheophorbide by Mg-dechelating substance in extracts of *Chenopodium album*. Plant Physiol Bioch **34:** 41–47

Shioi Y, Watanabe K, Takamiya K (1996b) Enzymatic conversion of pheophorbide *a* to a precursor of pyropheophorbide *a* in leaves of *Chenopodium album*. Plant Cell Physiol **37:** 1143–1149

Smyth DR, Mrozkiewicz MK, McGrath WJ, Listwan P, Kobe B (2003) Crystal structures of fusion proteins with large-affinity tags. Protein Sci **12:** 1313–1322

Stols L, Zhou M, Eschenfeldt WH, Millard CS, Abdullah J, Collart FR, Kim Y, Donnelly M.I. (2007) New vectors for co-expression of proteins: Structure of *Bacillus subtilis* ScoAB obtained by high-throughput protocols. Protein Expres Puri **53:** 396–403

Strain HH, Cope BT, Svec WA (1971) Analytical procedures for the isolation, identification, estimation and investigation of the chlorophylls. Methods Enzymol **23:** 452–476

Sugishima M, Kitamori Y, Noguchi M, Kohchi T, Fukuyama K (2009) Crystal structure of red chlorophyll catabolite reductase: enlargement of the ferredoxin-dependent bilin reductase family. J Mol Biol **389:** 376–387

Suzuki T, Shioi Y (2002) Re-examination of Mg-dechelation reaction in the degradation of chlorophylls using chlorophyllin *a* as substrate. Photosynth Res **74:** 217–223.

Suzuki T, Kunieda T, Murai F, Morioka S, Shioi Y (2005) Mg-dechelation activity in radish cotyledons with artificial and native substrates, Mg-chlorophyllin *a* and chlorophyllide *a*. Plant Physiol Biochem **43:** 459–464

Takamiya K, Tsuchiya T, Ohta H (2000) Degradation pathway(s) of chlorophyll: what has gene cloning revealed? Trends Plant Sci **5,** 426–431

Thomas H. Howarth CJ (2000) Five ways to stay green. J Exp Bot **51:** 329–337

Thomas H, Bortlik K-H, Rentsch D, Schellenberg M, Matile P (1989) Catabolism of chlorophyll in vivo: significance of polar chlorophyll catabolites in a non-yellowing senescence mutant of Festuca pratensis Huds. New Phytol **111:** 3–8

Thomas H, Ougham H, Canter P, Donnison I (2002) What stay-green mutants tell us about nitrogen remobilization in leaf senescence. J Exp Bot **53:** 801–808

Tommasini R, Vogt E, Fromenteau M, Hörtensteiner S, Matile P, Amrhein N, Martinoia E (1998). An ABC transporter of *Arabidopsis thaliana* has both glutathione-conjugate and chlorophyll catabolite transport activity. Plant J **13:** 773–780

United Nations (2014) The Millenium Development Goals Report 2014. Too-Kong T ,ed, United Nations New York. Downloaded from http://www.un.org/millenniumgoals/news.shtml

Valentin HE, Lincoln K, Moshiri F, Jensen PK, Qi Q, Venkatesh TV, Karunanandaa B, Baszis SR, Norris SR, Savidge B et al (2006) The *Arabidopsis vitamin E pathway gene5-1* mutant reveals a critical role for phytol kinase in seed tocopherol biosynthesis. Plant Cell **18:** 212–224

Vencl F, Gómez N, Ploss K, Boland W (2009) The chlorophyll catabolite, pheophorbide *a*, confers predation resistance in a larval tortoise beetle shield defense. J Chem Ecol **35:** 281–288

Vicentini F, Iten F, Matile P (1995) Development of an assay for Mg-dechelatase of oilseed rape cotyledons, using chlorophyllin as the substrate. Physiol Plant **94:** 57–63

Wüthrich KL, Bovet L, Hunziker PE, Donnison IS, Hörtensteiner S (2000) Molecular cloning, functional expression and characterisation of RCC reductase involved in chlorophyll catabolism. Plant J **21:** 189–198

Young CL, Britton ZT, Robinson AS (2012) Recombinant protein expression and purification: A comprehensive review of affinity tags and microbial applications. Biotechnology Journal **7:** 620–634

Zhang W, Liu T, Ren G, Hörtensteiner S, Zhou Y, Cahoon EB, Zhang C (2014) Chlorophyll degradation: the tocopherol biosynthesis-related phytol hydrolase in Arabidopsis seeds is still missing. Plant Physiol **166:** 70–79

Acknowledgment

I would like to thank Stefan Hörtensteiner for letting me work on this interesting and challenging topic. I enjoyed his trust in my self-dependent work but I appreciated his open door and his helpful and supportive guidance. Thank you.

I would like to thank Enrico Martinoia, Magdalena Rossi and Christoph Ringli, for being part of my PhD committee.

I would like to thank Silvia Schelbert Hofstetter for introducing me to the protein lab work and for trusting me to take over her "tomato-story". I also would like to thank Bastien Christ for all his support in the daily lab work, for methodological inputs and critical discussions of my results. Undine Krügel was a very big help for all protein purification related work. I would like to thank her for her time and for her patience.

Thank you Aditi, Aurélie, Bastien, Damian, Kathrin, Lukas, Mareike, Noemi, Sandro, Shinya, Silvia, Song and Sylvain for creating such a stimulating and amicable working atmosphere.

I would like to thank the whole P1-floor for creating a very pleasant environment. I enjoyed the coffee breaks and all the discussions, not related to chlorophyll breakdown.

I would like to thank my family and friends for all their support during my PhD. I appreciated their honest interest in my work. Many thanks go to Reto for his graphical inputs. I specially would like to thank Marco for reading my thesis. He was very supportive and always believed in my goals.